

Electronic Supplementary Information

Phosphorus ring expansion at cobalt: targeted synthesis of P₄, P₅ and P₇ ligands

Karolina Trabitsch,^a Sebastian Hauer,^a Kai Schwedtmann,^b Philipp Royla,^b Jan J. Weigand,^{*b} and Robert Wolf^{*a}

^a University of Regensburg, Institute of Inorganic Chemistry, 93040 Regensburg (Germany)

^b Technische Universität Dresden, Department of Chemistry and Food Chemistry, 01062 Dresden (Germany)

Table of Contents

1. Experimental Procedures	2
General Procedures	2
NMR Simulations	2
Preparation of [(PHDI)Co(CN)(η ³ -P ₄ Cy ₂)] (1a-Cy)	3
Preparation of [(PHDI)Co(CN)(η ³ -P ₄ Ph ₂)] (1a-Ph)	6
Preparation of [(Ar*BIAN)Co(CN)(η ³ -P ₄ Cy ₂)] (1b-Cy)	9
Preparation of [(Ar*BIAN)Co(CN)(η ³ -P ₄ (N(<i>i</i> Pr) ₂) ₂)] (1b-N(<i>i</i>Pr)₂)	12
Preparation of [(Ar*BIAN)Co(η ⁴ -P ₅ tBu ₂)] (2b-tBu)	14
Preparation of [(Ar*BIAN)Co(η ⁴ -P ₅ (N(<i>i</i> Pr) ₂) ₂)] (2b-N(<i>i</i>Pr)₂)	17
Preparation of [(PHDI)Co(CN)(η ³ -P ₄ Lc)] (3a)	20
Preparation of [(PHDI)Co(CN)(η ³ -P ₅ (Lc) ₂)] [OTf] (4a[OTf])	24
Preparation of [(PHDI)Co(μ:η ⁴ ,κ ¹ -P ₅ Lc){W(CO) ₅ }] (5a-W(CO)₅) and [(PHDI)Co(μ ₃ :η ⁴ ,η ¹ ,η ¹ -P ₇ Lc){W(CO) ₅ }] (6a-{W(CO)₅})	29
Preparation of [(Ar*BIAN)Co(η ² :η ² -P ₇ Lc)] (6b)	37
2. VT ³¹ P{ ¹ H} NMR reaction monitoring	40
[K(18c-6)][(PHDI)Co(η ⁴ -P ₄)] (J) + 0.5 [(Lc) ₄ P ₄][OTf] ₄ (G[OTf]₄)	40
[K(18c-6)][(Ar*BIAN)Co(η ⁴ -P ₄)] (K) + 0.5 [(Lc) ₄ P ₄][OTf] ₄ (G[OTf]₄)	44
[K(18c-6)][(Ar*BIAN)Co(CN)(η ³ -P ₃)] (I) + 0.5 [(Lc) ₄ P ₄][OTf] ₄ (G[OTf]₄)	47
3. Additional experiments	49
Reduction of [(Lc) ₄ P ₄][OTf] ₄ : Reaction screening	49
Reaction of [K(18c-6)][(PHDI)Co(η ⁴ -P ₄)] (J) with 0.25, 0.5 and 1.0 equivalents [(Lc) ₄ P ₄][OTf] ₄ (G[OTf]₄)	51
Reaction of [{(PHDI)Co} ₂ (μ,η ⁴ :η ⁴ -P ₄)] and G[OTf]₄ or 7[OTf]₂	53
Reaction of [(PHDI)Co(μ:η ⁴ ,κ ¹ -P ₅ Lc){W(CO) ₅ }] (5a-W(CO)₅) with excess [W(CO) ₅ (THF)]	55
4. UV/Vis spectra	57
5. IR spectra	62
6. X-ray Crystallography	66
7. References	77

1. Experimental Procedures

General Procedures

All reactions were carried out under an inert atmosphere of argon using standard Schlenk-line or glovebox techniques (maintained at <0.1 ppm H₂O and <0.1 ppm O₂). Solvents were dried and degassed with a MBraun SPS800 solvent purification system unless otherwise stated. Methylcyclohexane and benzene were stirred over sodium/benzophenone and distilled. All dry solvents except *n*-hexane and *n*-pentane were stored under argon over activated 3 Å molecular sieves in gas-tight ampules. *n*-Hexane and *n*-pentane were stored over a potassium mirror.

NMR spectra were recorded on Bruker Avance III HD 400 spectrometers [¹H (400.03 MHz), ¹³C{¹H} (100.59 MHz), ³¹P{¹H} (161.94 MHz)] or a Bruker Avance III HDX, 500 MHz Ascend spectrometer equipped with a BBO Prodigy Cryo probe [¹H (500.13 MHz), ¹³C{¹H} (125.75 MHz), ³¹P{¹H} (202.45 MHz)] or a Bruker Avance III HD 600 spectrometer equipped with a TCI Cryo probe [¹H (600.25 MHz), ¹³C{¹H} (150.93 MHz)] at 300 K unless otherwise noted. ¹H and ¹³C{¹H} spectra were referenced internally to residual solvent resonances (¹H NMR: THF-*d*₈: 1.72 ppm, C₆D₆: 7.16 ppm; ¹³C{¹H} NMR: THF-*d*₈: 25.31 ppm, C₆D₆: 128.06 ppm). Chemical shifts (δ) are given in ppm referring to external standards of tetramethylsilane (¹H, ¹³C{¹H}), 85% H₃PO_{4(aq.)} (³¹P and ³¹P{¹H} spectra). The assignment of the ¹H and ¹³C NMR signals was confirmed by two-dimensional (¹H,¹H-COSY, ³¹P,³¹P-COSY, ¹H,¹³C-HSQC, ¹H,¹³C-HMBC and ¹H,¹H-NOESY) experiments. Coupling constants (*J*) are reported in Hz.

UV/vis spectra were recorded on an Ocean Optics DH-2000-BAL Spectrometer. Mass spectra were recorded by the Central Analytical Department at the University of Regensburg using a Jeol AccuTOF GCX. Elemental analyses were performed by the Central Analytical Department of the University of Regensburg using a Vario micro cube. IR spectra were recorded with a Bruker ALPHA spectrometer equipped with a diamond ATR unit.

The starting materials [K(18c-6)][(PHDI)Co(η⁴-P₄)],^[1] [nBu₄N][(PHDI)Co(η³-P₃)(CN)],^[1] [K(18c-6)][(Ar*BIAN)Co(η⁴-P₄)],^[2] [K(18c-6)][(Ar*BIAN)Co(CN)(η³-P₃)],^[2] [K(THF)][^{Mes}BIANCo(COD)],^[3] [K(18c-6)][Fe(anthracene)₂],^[4] [K(DME)₂][Co(anthracene)₂]^[5] and Cy₂PCl,^[6] were prepared according to literature procedures. The literature protocol was slightly modified for [(PHDI)Co(η⁴-P₅tBu₂)] (instead of crystallization, the solvent was removed and the resulting powder was used for further synthesis). [(Lc)₄P₄][OTf]₄ was prepared and kindly provided by the group of Jan J. Weigand.^[7] 18c-6, tBu₂PCl, Ph₂PCl, [nBu₄N]CN were purchased from Sigma Aldrich; [W(CO)₆] from Merck; (iPr₂N)₂PCl from Acros and all were used as received.

NMR Simulations

For compounds which give rise to a higher order spin system in the ³¹P{¹H} NMR spectrum, the resolution enhanced ³¹P{¹H} NMR spectrum was transferred to the software gNMR, version 5.0.6.0, by Cherwell Scientific.^[8] The full line shape iteration procedure of gNMR was applied to obtain the best match of the fitted to the experimental spectrum. ¹J(³¹P³¹P) coupling constants were set to negative values and all other signs of the coupling constants were obtained accordingly.^[9-14]

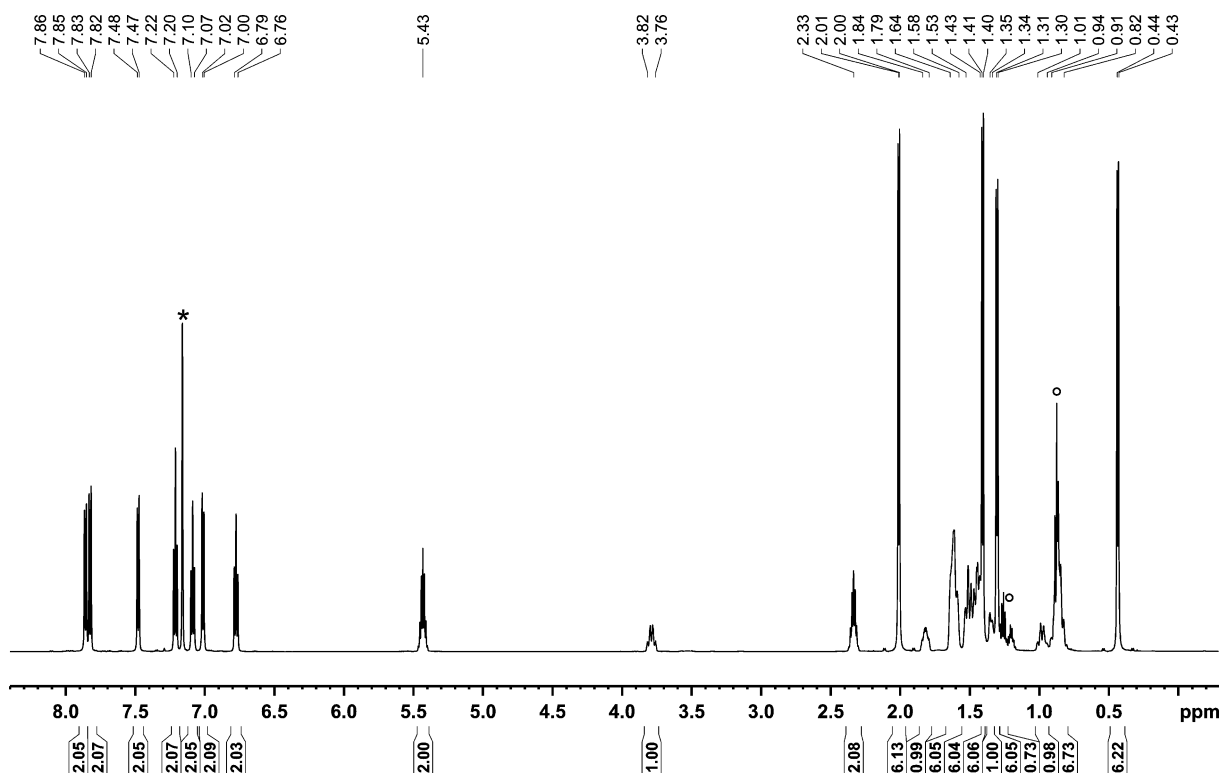


Figure S1. ^1H NMR spectrum (600.24 MHz, 300 K, C_6D_6) of $[(\text{PHDI})\text{Co}(\text{CN})(\eta^3\text{-P}_4\text{Cy}_2)] (\mathbf{1a}\text{-Cy}) \cdot (n\text{-pentane})_{0.1}$; * C_6D_6 , o $n\text{-pentane}$.

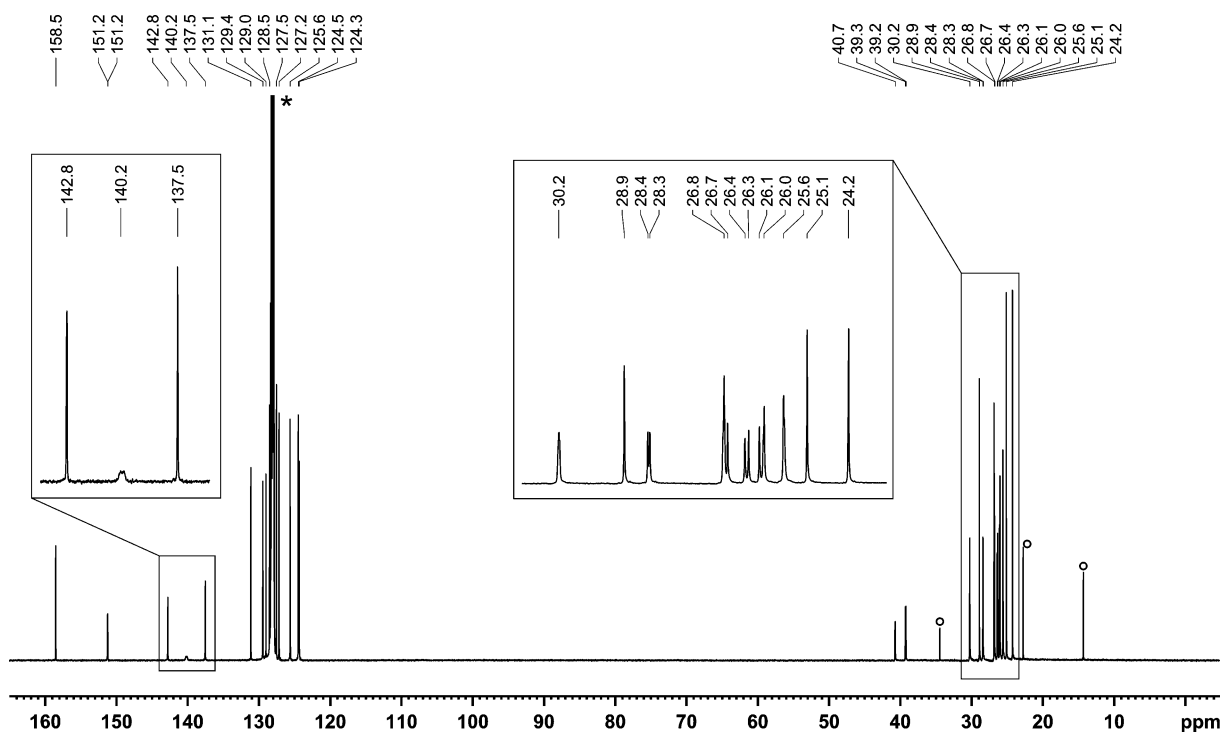


Figure S2. $^{13}\text{C}\{^1\text{H}\}$ NMR spectrum (150.93 MHz, 300 K, C_6D_6) of $[(\text{PHDI})\text{Co}(\text{CN})(\eta^3\text{-P}_4\text{Cy}_2)] (\mathbf{1a}\text{-Cy}) \cdot (n\text{-pentane})_{0.1}$; * C_6D_6 , o $n\text{-pentane}$.

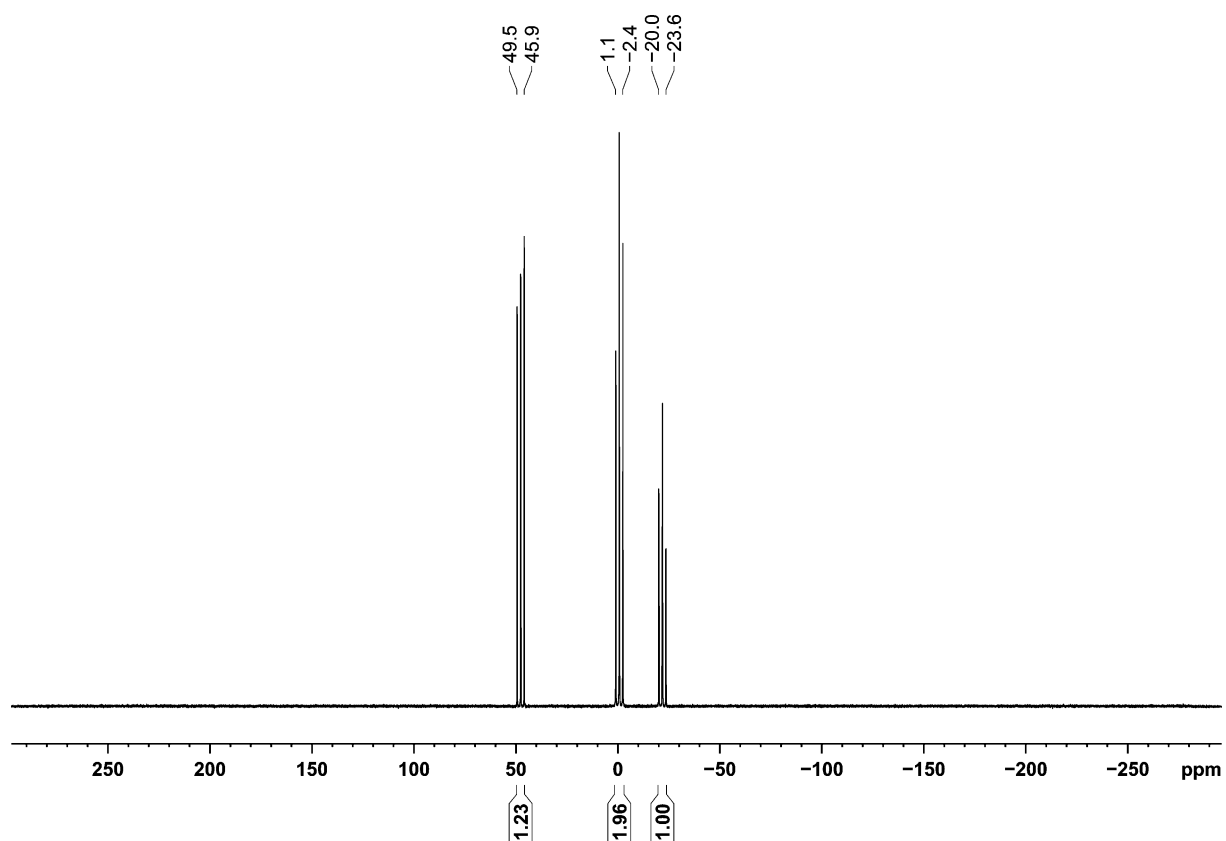


Figure S3. $^{31}\text{P}\{^1\text{H}\}$ NMR spectrum (162.04 MHz, 300 K, C_6D_6) of $[(\text{PHDI})\text{Co}(\text{CN})(\eta^3\text{-P}_4\text{Cy}_2)]$ (**1a-Cy**)·(*n*-pentane) $_{0.1}$.

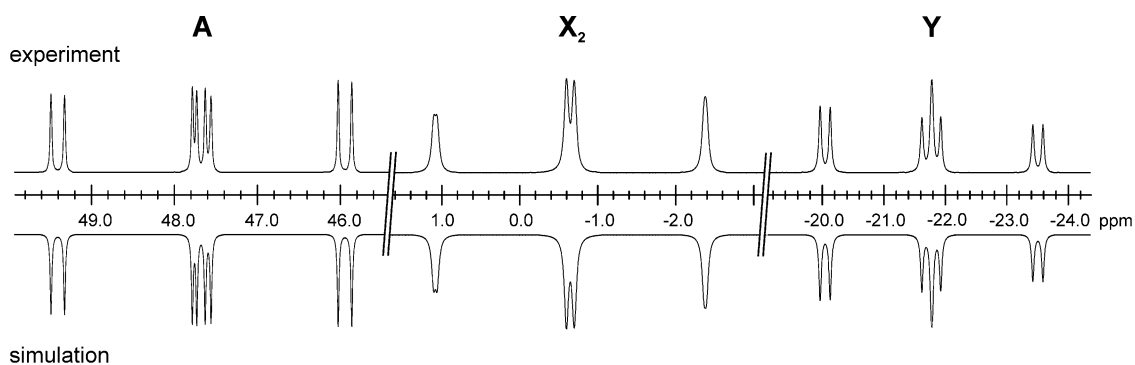
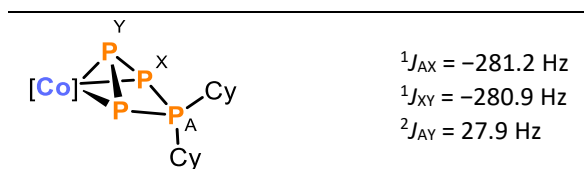
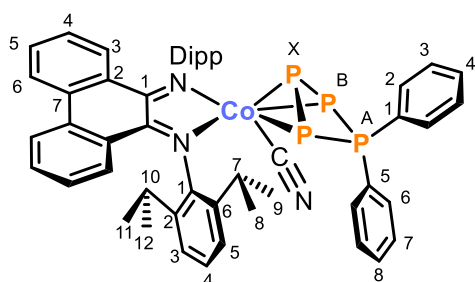


Figure S4. Section of the $^{31}\text{P}\{^1\text{H}\}$ NMR spectrum (162.04 MHz, 300 K, C_6D_6) of $[(\text{PHDI})\text{Co}(\text{CN})(\eta^3\text{-P}_4\text{Cy}_2)]$ (**1a-Cy**); experimental (upwards) and simulation (downwards).

Table S1. Coupling constants from the iterative fit of the AX_2Y spin system and schematic representation of the CoP_4Cy_2 core of $[(\text{PHDI})\text{Co}(\text{CN})(\eta^3\text{-P}_4\text{Cy}_2)]$ (**1a-Cy**); $\delta(\text{P}_\text{A}) = 47.6$ ppm, $\delta(\text{P}_\text{Y}) = -0.67$ ppm, $\delta(\text{P}_\text{X}) = -21.7$ ppm.



Preparation of [(PHDI)Co(CN)(η^3 -P₄Ph₂)] (1a-Ph)



To a suspension of $[n\text{Bu}_4\text{N}][(\text{PHDI})\text{Co}(\text{CN})(\eta^3\text{-P}_3)] \cdot (\text{toluene})_{0.2}$ (103.0 mg, 0.107 mmol, 1.0 equiv.) in toluene (4 mL) was added dropwise a stock solution of Ph_2PCl (0.08 M, 1.33 mL, 0.107 mmol, 1.0 equiv.) in toluene during which a slow colour change from purple to dark blue was observed. The reaction mixture was stirred at room temperature for 42 h. The solution was filtered over a pad of silica (1.5 × 0.8 cm), washed with toluene (3 mL) and the solvent was removed *in vacuo*. The dark blue residue was

washed with *n*-hexane (6 × 0.5 mL) and dried *in vacuo*. The crystalline solid contains 0.8 molecules of toluene per molecule of compound after drying as indicated by the $^1\text{H}/^{13}\text{C}\{^1\text{H}\}$ NMR spectra and elemental analysis. Yield: 52.1 mg (50% based on the maximum theoretical yield of 0.107 mmol).

UV/vis (THF, λ_{max} / nm, ϵ_{max} / $\text{L} \cdot \text{mol}^{-1} \cdot \text{cm}^{-1}$): 320sh (33000), 340 (36000), 360sh (29000), 385sh (19000), 620 (35800).

^1H NMR (400.30 MHz, 300 K, C_6D_6): δ / ppm = 0.43 (d, $^3J_{\text{HH}} = 6.8$ Hz, 6H, $-\text{CH}(\text{C}^8\text{H}_3)_2$ of Dipp), 1.25 (d, $^3J_{\text{HH}} = 6.8$ Hz, 6H, $-\text{CH}(\text{C}^9\text{H}_3)_2$ of Dipp), 1.34 (d, $^3J_{\text{HH}} = 6.8$ Hz, 6H, $-\text{CH}(\text{C}^{11}\text{H}_3)_2$ of Dipp), 1.95 (d, $^3J_{\text{HH}} = 6.8$ Hz, 6H, $-\text{CH}(\text{C}^{12}\text{H}_3)_2$ of Dipp), 2.37 (sept., $^3J_{\text{HH}} = 6.8$ Hz, 6H, $-\text{C}^7\text{H}(\text{CH}_3)_2$ of Dipp), 5.31 (sept., $^3J_{\text{HH}} = 6.5$ Hz, 6H, $-\text{C}^{10}\text{H}(\text{CH}_3)_2$ of Dipp), 6.74-6.78 (m, 2H, $-\text{C}^4\text{H}$ of PHDI), 6.80-6.91 (m, 5H, $-\text{C}^3\text{H}$ of Ph overlapping with $-\text{C}^4\text{H}$ of Ph), 6.95-6.99 (m, 1H, $-\text{C}^8\text{H}$ of Ph), 7.01-7.08 (m, 6H, $-\text{C}^5\text{H}$ of Dipp overlapping with $-\text{C}^5\text{H}$ of PHDI overlapping with $-\text{C}^7\text{H}$ of Ph), 7.22-7.26 (m, 2H, $-\text{C}^4\text{H}$ of Dipp), 7.31-7.36 (m, 2H, $-\text{C}^6\text{H}$ of Ph), 7.49-7.55 (m, 4H, $-\text{C}^3\text{H}$ of Dipp overlapping with $-\text{C}^2\text{H}$ of Ph), 7.79-7.84 (m, 4H, $-\text{C}^3\text{H}$ of PHDI overlapping with $-\text{C}^6\text{H}$ of PHDI).

$^{13}\text{C}\{^1\text{H}\}$ NMR (100.61 MHz, 300 K, C_6D_6): δ / ppm = 24.3 (s, $-\text{CH}(\text{C}^8\text{H}_3)_2$ of Dipp), 25.1 (s, $-\text{CH}(\text{C}^{11}\text{H}_3)_2$ of Dipp), 25.9 (s, $-\text{CH}(\text{C}^9\text{H}_3)_2$ of Dipp), 26.0 (s, $-\text{CH}(\text{C}^9\text{H}_3)_2$ of Dipp), 27.0 (s, $-\text{CH}(\text{C}^{12}\text{H}_3)_2$ of Dipp), 28.4 (s, $-\text{C}^7\text{H}(\text{CH}_3)_2$ of Dipp), 28.5 (s, $-\text{C}^7\text{H}(\text{CH}_3)_2$ of Dipp), 28.9 (s, $-\text{C}^{10}\text{H}(\text{CH}_3)_2$ of Dipp), 124.3 (s, $-\text{C}^3\text{H}$ or $-\text{C}^6\text{H}$ of PHDI), 124.5 (s, $-\text{C}^5\text{H}$ of Dipp), 125.8 (s, $-\text{C}^3\text{H}$ of Dipp), 127.3 (s, $-\text{C}^4\text{H}$ of Dipp), 127.6 (s, $-\text{C}^4\text{H}$ of PHDI), 128.4 (s, $-\text{C}^5\text{H}$ of PHDI or $-\text{C}^7\text{H}$ of Ph), 128.6 (s, $-\text{C}^5\text{H}$ of PHDI or $-\text{C}^7\text{H}$ of Ph), 128.7 (s, $-\text{C}^3\text{H}$ of Ph), 128.8 (s, $-\text{C}^2$ of PHDI), 129.5 (s, $-\text{C}^3\text{H}$ or $-\text{C}^6\text{H}$ of PHDI), 130.9 (s, $-\text{C}^4\text{H}$ of Ph), 131.3 (s, $-\text{C}^7$ of PHDI), 131.4 (s, s, $-\text{C}^5$ of Ph), 131.4 (s, $-\text{C}^1$ of Ph), 131.5 (s, $-\text{C}^6\text{H}$ of Ph), 131.8 (s, $-\text{C}^8\text{H}$ of Ph), 131.9 (s, $-\text{C}^2\text{H}$ of Ph), 132.0 (s, $-\text{C}^2\text{H}$ of Ph), 137.7 (s, $-\text{C}^6$ of Dipp), 142.9 (s, $-\text{C}^2$ of Dipp), 150.9 (s, $-\text{C}^1$ of Dipp), 158.6 (s, $-\text{C}^1$ of PHDI), $\text{C}\equiv\text{N}$: not detected.

$^{31}\text{P}\{^1\text{H}\}$ NMR (161.98 MHz, 300 K, C_6D_6 , AB_2X spin system): δ / ppm = -35.5 - -27.0 (m, 1P, P_X), 14.5 - 21.1 (m, 3P, $\text{P}_\text{A}/\text{P}_\text{B}$), for parameters obtained by simulation, see Table S2.

IR (solid state): ν / cm^{-1} = 3054w (C-H), 2955m (C-H), 2922m (C-H), 2862m (C-H), 2104m ($\text{C}\equiv\text{N}$), 1493m, 1464m, 1436m, 1382m, 1356m, 1315m, 1254m, 1237m, 1098m, 1053m, 999m, 794m, 756s, 723s, 687s.

Elemental analysis calcd. for $\text{C}_{51}\text{H}_{52}\text{CoN}_3\text{P}_4 \cdot (\text{C}_7\text{H}_8)_{0.8}$ (Mw = 963.54 $\text{g} \cdot \text{mol}^{-1}$) C 70.55, H 6.11, N 4.36; found C 70.20, H 6.17, N 4.48.

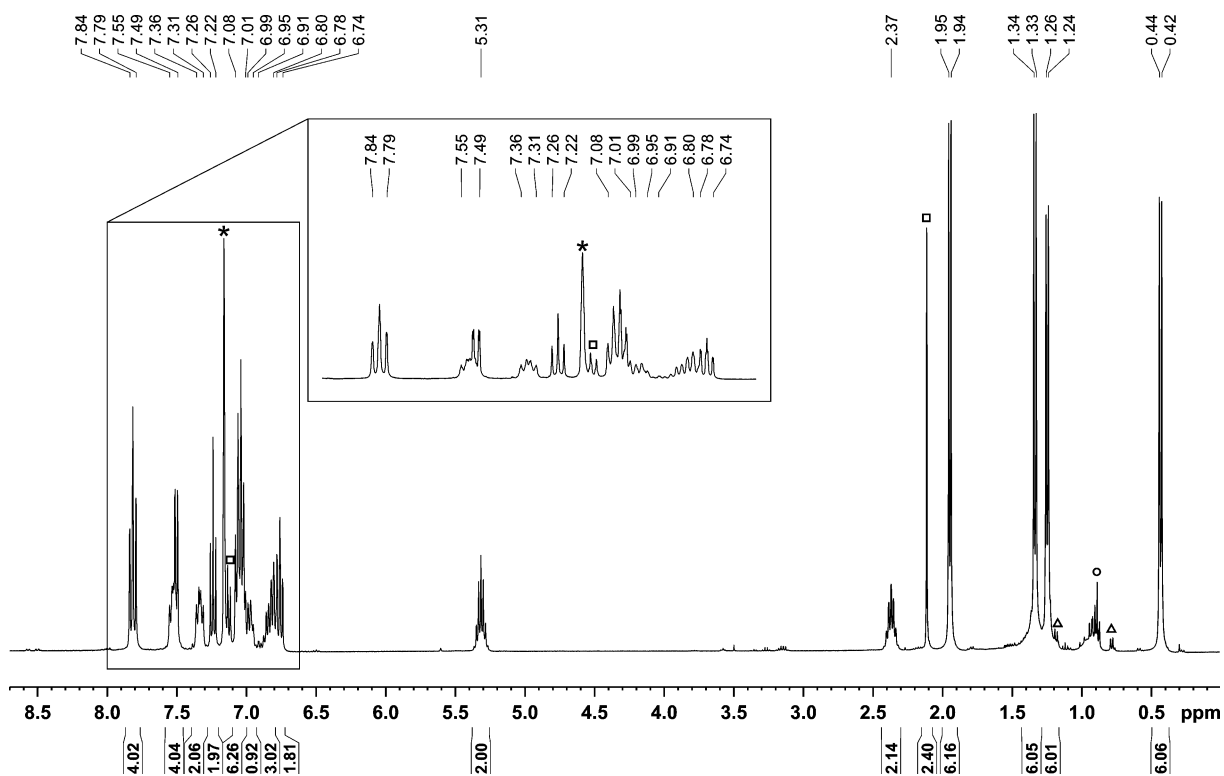


Figure S5. ^1H NMR spectrum (400.30 MHz, 300 K, C_6D_6) of $[(\text{PHDI})\text{Co}(\text{CN})(\eta^3\text{-P}_4\text{Ph}_2)] (\mathbf{1a-Ph}) \cdot (\text{toluene})_{0.8}$; * C_6D_6 , \square toluene, \circ n -hexane, \triangle minor unknown impurity.

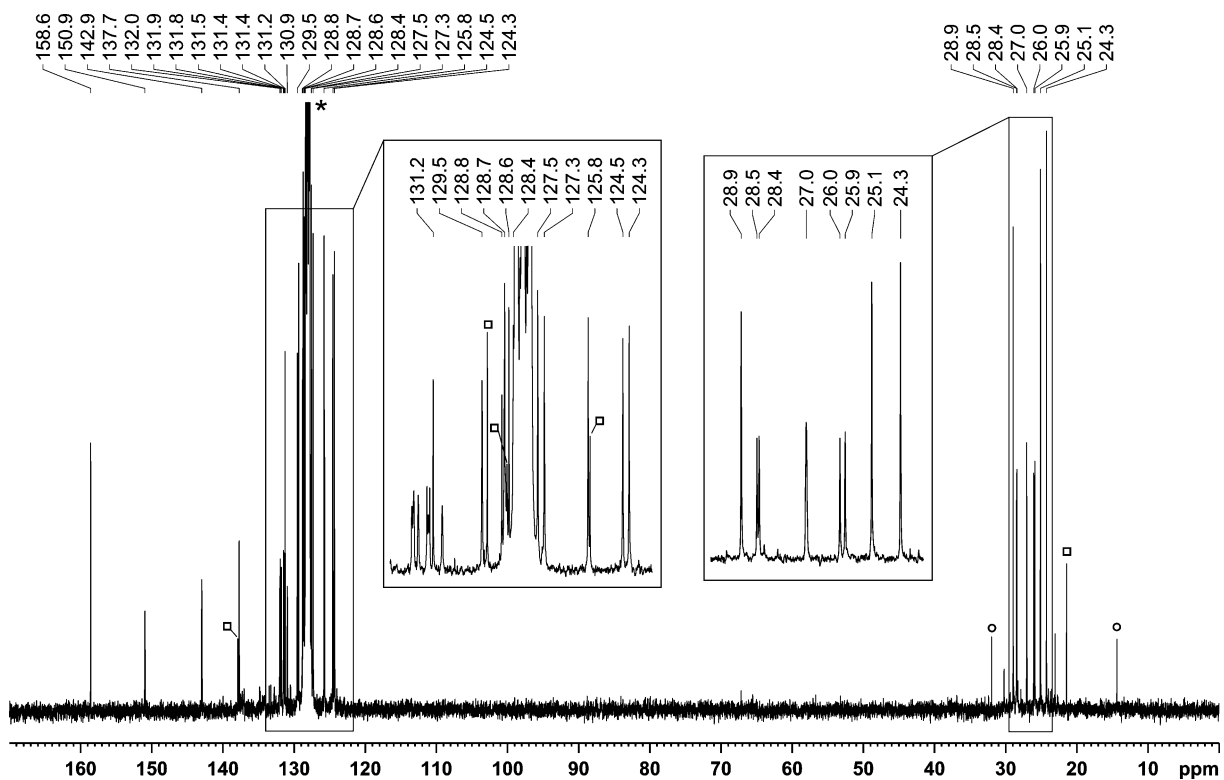


Figure S6. $^{13}\text{C}\{^1\text{H}\}$ NMR spectrum (100.61 MHz, 300 K, C_6D_6) of $[(\text{PHDI})\text{Co}(\text{CN})(\eta^3\text{-P}_4\text{Ph}_2)] (\mathbf{1a-Ph}) \cdot (\text{toluene})_{0.8}$; * C_6D_6 , \square toluene, \circ n -hexane.

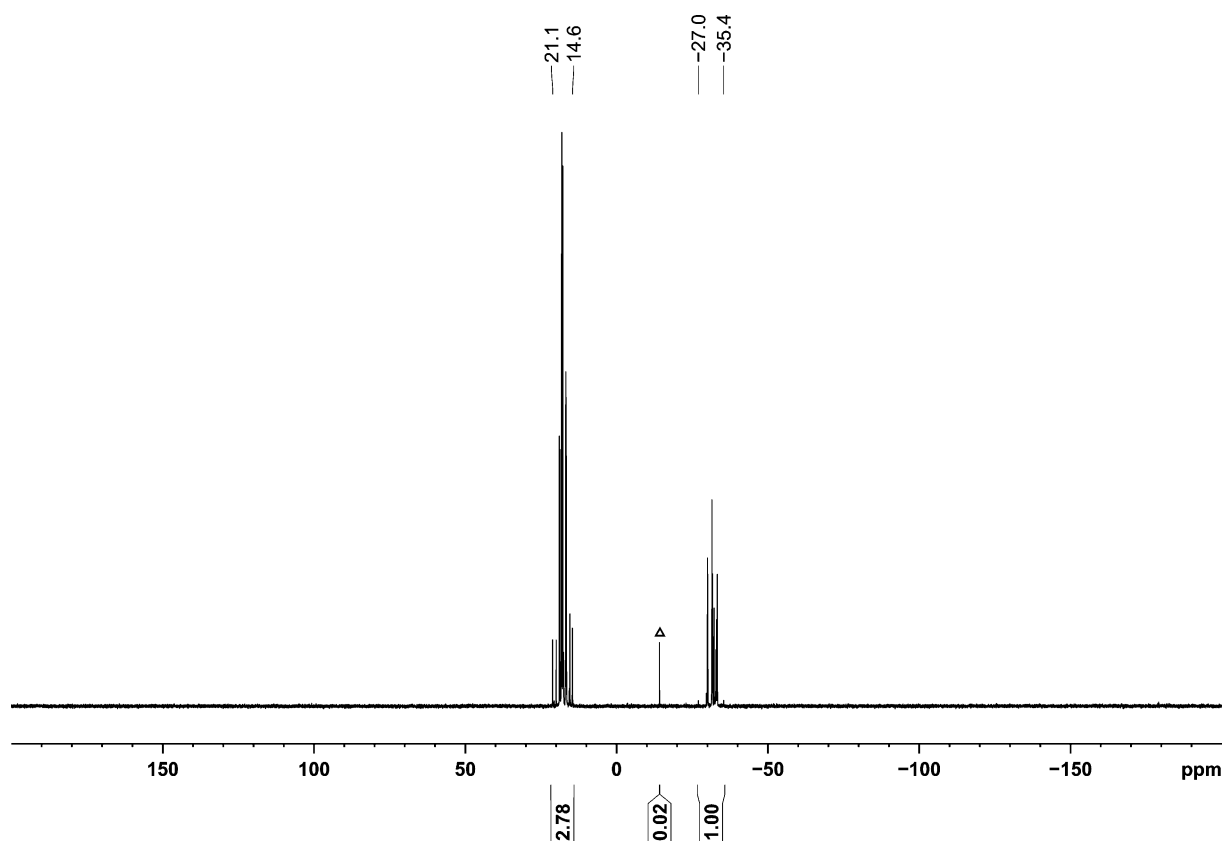


Figure S7. $^{31}\text{P}\{^1\text{H}\}$ NMR spectrum (161.98 MHz, 300 K, C_6D_6) of $[(\text{PHDI})\text{Co}(\text{CN})(\eta^3\text{-P}_4\text{Ph}_2)]$ (**1a-Ph**)- $(\text{toluene})_{0.8}$; Δ minor unknown impurity.

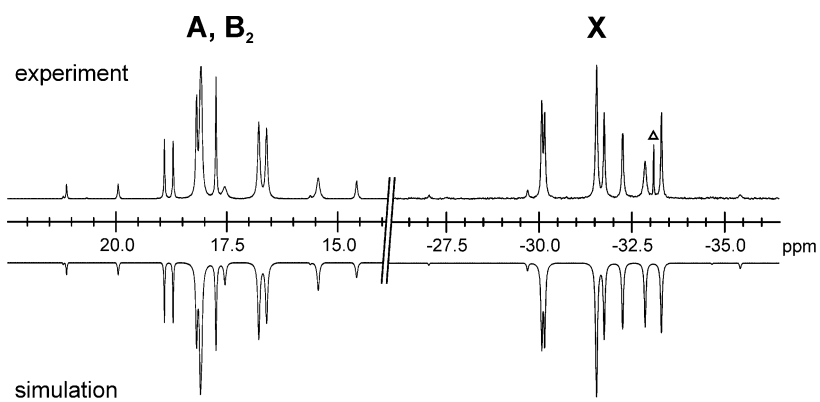
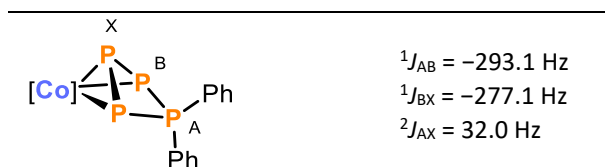
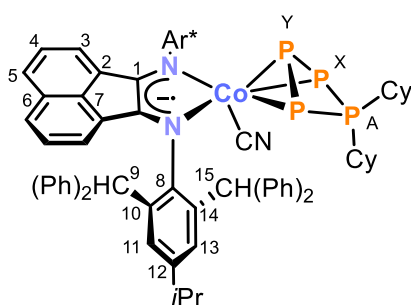


Figure S8. Section of the $^{31}\text{P}\{^1\text{H}\}$ NMR spectrum (161.98 MHz, 300 K, C_6D_6) of $[(\text{PHDI})\text{Co}(\text{CN})(\eta^3\text{-P}_4\text{Ph}_2)]$ (**1a-Ph**); experimental (upwards) and simulation (downwards); Δ minor unknown impurity.

Table S2. Coupling constants from the iterative fit of the AB_2X spin system and schematic representation of the CoP_5Ph_2 core of $[(\text{PHDI})\text{Co}(\text{CN})(\eta^3\text{-P}_4\text{Ph}_2)]$ (**1a-Ph**); $\delta(\text{P}_\text{A}) = 18.8$ ppm, $\delta(\text{P}_\text{B}) = 17.0$ ppm, $\delta(\text{P}_\text{X}) = -31.7$ ppm.



Preparation of $[(\text{Ar}^*\text{BIAN})\text{Co}(\text{CN})(\eta^3\text{-P}_4\text{Cy}_2)]$ (**1b-Cy**)



A stock solution of Cy_2PCL (0.112 M, 273 μL , 0.031 mmol, 1.1 equiv.) in *n*-hexane was added to a deep purple solution of $[\text{K}(18\text{c}-6)][(\text{Ar}^*\text{BIAN})\text{Co}(\text{CN})(\eta^3\text{-P}_3)]$ (50 mg, 0.031 mmol, 1.0 equiv.) in toluene (1.5 mL). The reaction mixture was stirred for two weeks at 40 °C. The color slowly changed to cyan during that period. The solid was removed by filtration over a pad of silica (1 \times 0.5 cm) and the residue was washed with toluene (2 \times 0.5 mL). The combined filtrates were concentrated to approx. 1 mL and layered with *n*-hexane (3.5 mL). Storage of the

solution at room temperature for five days and one day at -35 °C gave shimmering cyan crystals, which were isolated by decantation of the mother liquor, washed with *n*-hexane (2 \times 1 mL) and drying *in vacuo*. Yield: 15.0 mg (34% based on the maximum theoretical yield of 0.031 mmol).

$^1\text{H NMR}$ (400.13 MHz, 300 K, C_6D_6): δ / ppm = 0.79-0.91 (m, 4H, $-\text{CH}_2$ of Cy), 0.97-1.01 (m, 12H, $-\text{CH}(\text{CH}_3)_2$ of *iPr*), 1.05-1.35 (m, 6H, $-\text{CH}_2$ of Cy), 1.48-1.63 (m, 6H, $-\text{CH}_2$ of Cy), 1.71-1.78 (m, 5H, $-\text{CH}$ of Cy overlapping with $-\text{CH}_2$ of Cy), 2.55 (sept, $^3J_{\text{HH}} = 6.9$ Hz, 2H, $-\text{CH}(\text{CH}_3)_2$ of *iPr*), 3.72-3.81 (m, 1H, $-\text{CH}$ of Cy), 5.71 (s, 2H, $-\text{C}^9\text{H}(\text{Ph})_2$), 5.89 (d, $^3J_{\text{HH}} = 7.1$ Hz, 2H, $-\text{C}^3\text{H}$ of BIAN), 6.25-6.29 (m, 2H, $-\text{C}^4\text{H}$ of BIAN), 6.60-6.66 (m, 8H, $-\text{CH}_{\text{Ar}}$ of Ph), 6.81-6.85 (m, 8H, $-\text{CH}_{\text{Ar}}$ of Ph), 7.02-7.23 (m, 14H, $-\text{C}^5\text{H}$ of BIAN) overlapping with $-\text{CH}_{\text{Ar}}$ of Ph overlapping with C_6D_6 solvent signal), 7.27-7.27 (m, 2H, $-\text{C}^{11}\text{H}$), 7.31-7.35 (m, 4H, $-\text{CH}_{\text{Ar}}$ of Ph), 7.55-7.56 (m, 2H, $-\text{C}^{13}\text{H}$), 7.93-7.97 (m, 8H, $-\text{CH}_{\text{Ar}}$ of Ph), 9.02 (s, 2H, $-\text{C}^{15}\text{H}(\text{Ph})_2$).

$^{13}\text{C}\{^1\text{H}\}$ NMR (100.61 MHz, 300 K, C_6D_6): δ / ppm = 23.7 (s, $-\text{CH}(\text{CH}_3)_2$ of *iPr*), 23.9 (s, $-\text{CH}(\text{CH}_3)_2$ of *iPr*), 25.4 (d, $^2J_{\text{PC}} = 3.5$ Hz, $-\text{CH}_2$ of Cy), 25.9 (s, $-\text{CH}_2$ of Cy), 26.2 (s, $-\text{CH}_2$ of Cy), 26.3 (s, $-\text{CH}_2$ of Cy), 27.0 (d, $^2J_{\text{PC}} = 11.3$ Hz, $-\text{CH}_2$ of Cy), 30.8 (s, $-\text{CH}_2$ of Cy), 33.6 (s, $-\text{CH}(\text{CH}_3)_2$ of *iPr*), 37.6 (d, $^1J_{\text{PC}} = 13.4$ Hz, $-\text{CH}$ of Cy), 40.9 (d, $^1J_{\text{PC}} = 7.1$ Hz, $-\text{CH}$ of Cy), 51.0 (s, $-\text{C}^9\text{H}(\text{Ph})_2$), 51.2 (d, $J_{\text{PC}} = 4.7$ Hz through space, $-\text{C}^{15}\text{H}(\text{Ph})_2$), 123.3 (s, $-\text{C}^3\text{H}$ of BIAN), 125.7 (s, $-\text{C}_{\text{Ar}}\text{H}$ of Ph), 125.9 (s, $-\text{C}_{\text{Ar}}\text{H}$ of Ph), 126.2 (s, $-\text{C}_{\text{Ar}}\text{H}$ of Ph), 126.2 (s, $-\text{C}_{\text{Ar}}\text{H}$ of Ph), 126.4 (s, $-\text{C}^5\text{H}$ of BIAN), 127.4 (s, $-\text{C}^4\text{H}$ of BIAN), 127.7 (s, $-\text{C}_{\text{Ar}}\text{H}$ of Ph overlapping with C_6D_6 solvent signal), 127.9 (s, $-\text{C}_{\text{Ar}}\text{H}$ of Ph overlapping with C_6D_6 solvent signal), 127.9 (s, $-\text{C}^{11}\text{H}$ overlapping with C_6D_6 solvent signal), 128.1 (s, $-\text{C}_{\text{Ar}}\text{H}$ of Ph overlapping with C_6D_6 solvent signal), 128.2 (s, $-\text{C}_{\text{Ar}}\text{H}$ of Ph), 128.3 (s, $-\text{C}_{\text{Ar}}\text{H}$ of Ph), 128.8 (s, $-\text{C}^{13}\text{H}$), 129.4 (s, $-\text{C}^2$ of BIAN), 129.8 (s, $-\text{C}^6$ of BIAN), 130.4 (s, $-\text{C}_{\text{Ar}}\text{H}$ of Ph), 130.6 (s, $-\text{C}_{\text{Ar}}\text{H}$ of Ph), 131.1 (s, $-\text{C}_{\text{Ar}}\text{H}$ of Ph), 134.4 (s, $-\text{C}^{10}$), 138.1 (s, $-\text{C}^7$ of BIAN), 139.8 (s, $-\text{C}^{14}$), 143.3 (s, $-\text{C}_{\text{Ar}}$ of Ph), 144.4 (s, $-\text{C}_{\text{Ar}}$ of Ph), 145.1 (m, $-\text{C}_{\text{Ar}}$ of Ph), 146.2 (s, $-\text{C}^{12}$), 146.6 (s, $-\text{C}^8\text{-N}$), 147.2 (s, $-\text{C}_{\text{Ar}}$ of Ph), 168.6 (s, $-\text{C}^1\text{=N}$ of BIAN); $\text{C}\equiv\text{N}$: not detected.

$^{31}\text{P}\{^1\text{H}\}$ NMR (162.04 MHz, 300 K, C_6D_6 , AX_2Y spin system): δ / ppm = -47.0 - -43.5 (m, 1P, P_Y), -26.4 - -22.9 (m, 2P, P_X), 58.1 - 61.8 (m, 1P, P_A), for parameters obtained by simulation, see Table S3.

UV/Vis (THF, λ_{max} / nm, ϵ_{max} / $\text{L}\cdot\text{mol}^{-1}\cdot\text{cm}^{-1}$): 240 (60000), 310sh (15000), 390 (6000), 490 (6000), 680 (15000).

IR (solid state): ν / cm^{-1} = 3058w (C-H), 3023w (C-H), 2923m (C-H), 2850m (C-H), 2090m ($\text{C}\equiv\text{N}$), 1600w, 1567w, 1492s (C-N), 1439m, 1417m, 1297w, 1193w, 1031w, 694vs, 604s, 540s.

Elemental Analysis calcd. for $\text{C}_{95}\text{H}_{90}\text{CoN}_3\text{P}_4$ (Mw = 1456.61 $\text{g}\cdot\text{mol}^{-1}$): C 78.34, H 6.23, N 2.88; found C 78.24, H 6.62, N 2.43.

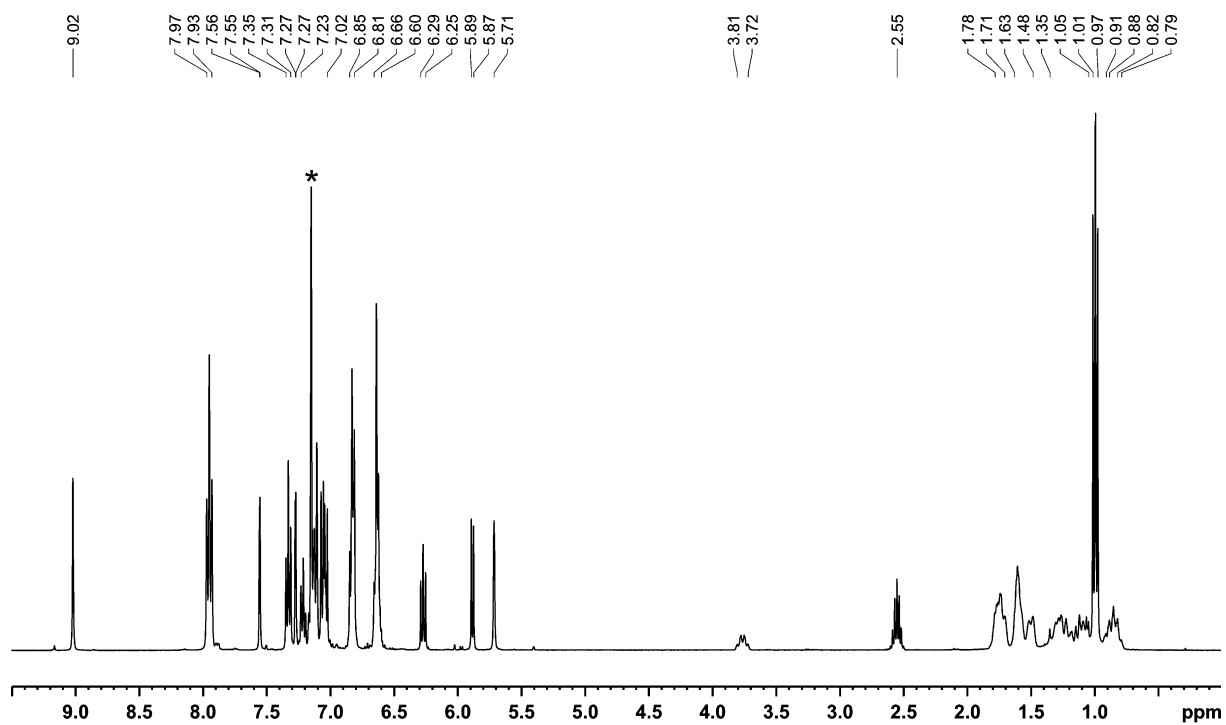


Figure S9. ^1H NMR spectrum (400.13 MHz, 300 K, C_6D_6) of $[(\text{Ar}^*\text{BIAN})\text{Co}(\text{CN})(\eta^3\text{-P}_4\text{Cy}_2)]$ (**1b-Cy**); * C_6D_6 .

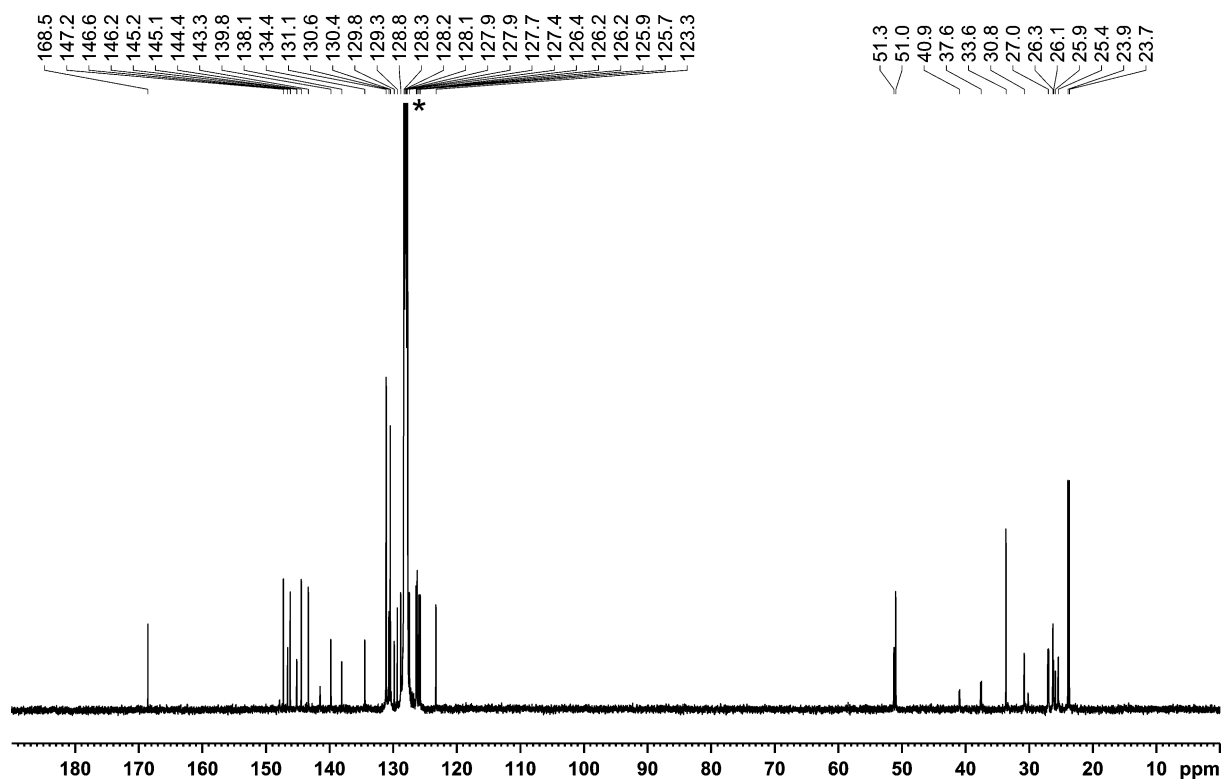


Figure S10. $^{13}\text{C}\{^1\text{H}\}$ NMR spectrum (100.61 MHz, 300 K, C_6D_6) of $[(\text{Ar}^*\text{BIAN})\text{Co}(\text{CN})(\eta^3\text{-P}_4\text{Cy}_2)]$ (**1b-Cy**); * C_6D_6 .

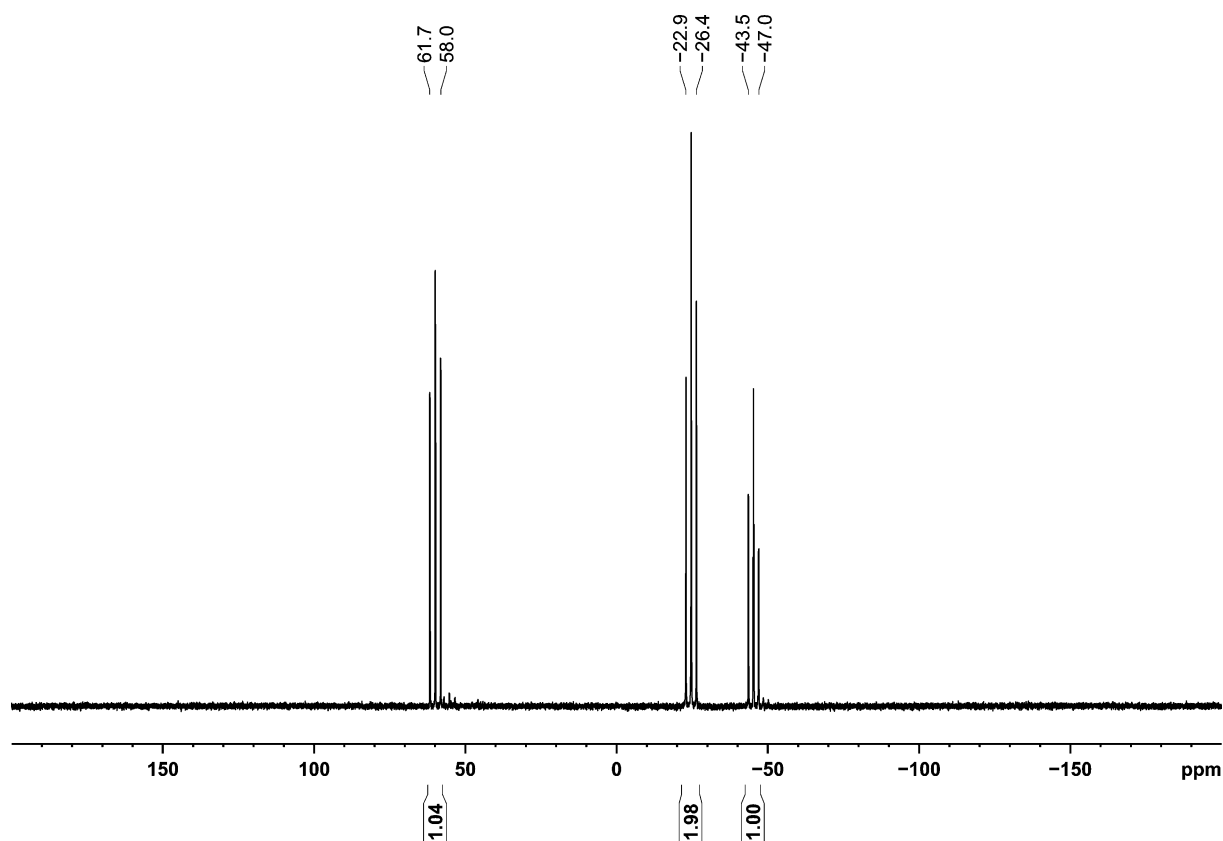


Figure S11. $^{31}\text{P}\{^1\text{H}\}$ NMR spectrum (162.04 MHz, 300 K, C_6D_6) of $[(\text{Ar}^*\text{BIAN})\text{Co}(\text{CN})(\eta^3\text{-P}_4\text{Cy}_2)]$ (**1b-Cy**).

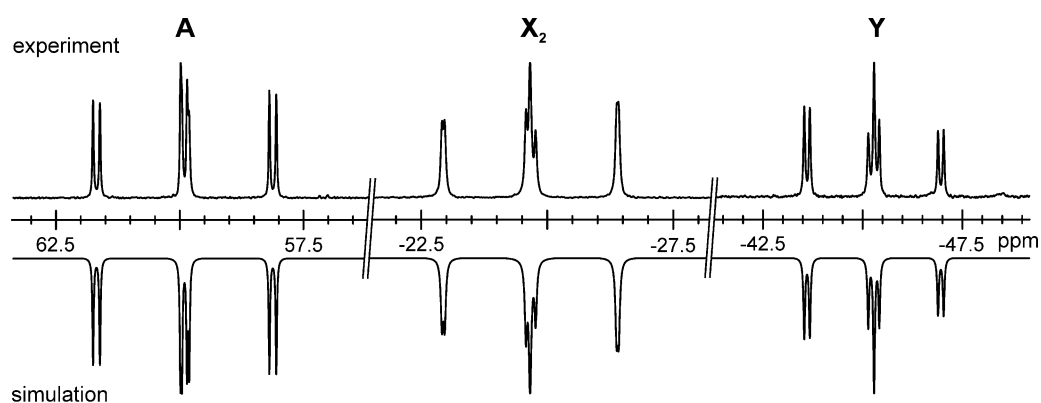
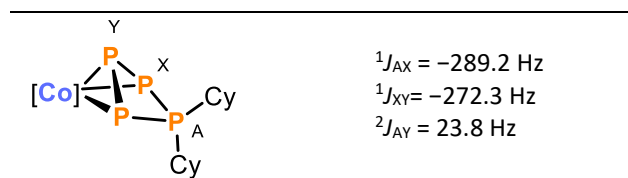
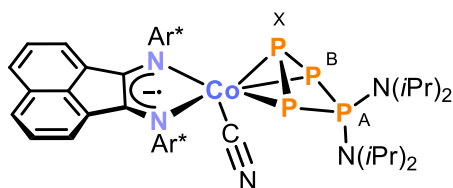


Figure S12. Section of the $^{31}\text{P}\{^1\text{H}\}$ NMR spectrum (162.04 MHz, 300 K, C_6D_6) of $[(\text{Ar}^*\text{BIAN})\text{Co}(\text{CN})(\eta^3\text{-P}_4\text{Cy}_2)]$ (**1b-Cy**); experimental (upwards) and simulation (downwards).

Table S3. Coupling constants from the iterative fit of the AX_2Y spin system and schematic representation of the CoP_4Cy_2 core of $[(\text{Ar}^*\text{BIAN})\text{Co}(\text{CN})(\eta^3\text{-P}_4\text{Cy}_2)]$ (**1b-Cy**); $\delta(\text{P}_\text{A}) = 59.9$ ppm, $\delta(\text{P}_\text{X}) = -24.7$ ppm, $\delta(\text{P}_\text{Y}) = -45.2$ ppm.



Preparation of [(Ar*BIAN)Co(CN)(η^3 -P₄(N(*i*Pr)₂)₂)] (1b-N(*i*Pr)₂)



Neat (*i*Pr₂N)₂PCl (8.2 mg, 0.031 mmol, 1.0 equiv.) was added to a deep purple solution of [K(18c-6)][(Ar*BIAN)Co(CN)(η^3 -P₃)] (50 mg, 0.031 mmol, 1.0 equiv.) in toluene (2.0 mL). The reaction mixture was stirred for one week at 40 °C. The color slowly changed to cyan during that time. The solid was removed by filtration

over a pad of silica (1.5 × 0.5 cm) and the residue washed with toluene (2 × 0.5 mL). Volatiles of the combined filtrates were removed *in vacuo* and the remaining residue taken up in *n*-hexane. Storage of the solution at -35 °C for four days gave shimmering cyan crystals, which were isolated by decantation of the mother liquor, washing with *n*-hexane (1 × 0.5 mL) and drying *in vacuo*. Yield: 5 mg (11% based on the maximum theoretical yield of 0.031 mmol).

¹H NMR (400.30 MHz, 300 K, C₆D₆): δ / ppm = 0.95-0.99 (m, 12H, -N(CH(CH₃)₂)₂), 1.15-1.19 (m, 24H, -CH(CH₃)₂ of *i*Pr overlapping with -N(CH(CH₃)₂)₂), 2.54 (sept, ³J_{HH} = 6.9 Hz, 2H, -CH(CH₃)₂ of *i*Pr), 3.87 (br sept, 2H, -N(CH(CH₃)₂)₂), 4.24 (br sept, 2H, -N(CH(CH₃)₂)₂), 5.76-5.78 (m, 4H, -CH of BIAN overlapping with -CH(Ph)₂), 6.26-6.30 (m, 2H, -CH of BIAN), 6.57-7.34 (m, 36H, -CH_{Ar} of Ph overlapping with C₆D₆ solvent signal), 7.56 (s, 2H, -CH_{Ar}), 7.84-7.86 (m, 4H, -CH_{Ar} of Ph), 8.00-8.01 (m, 4H, -CH_{Ar} of Ph), 8.88 (s, 2H, -CH(Ph)₂).

³¹P{¹H} NMR (162.04 MHz, 300 K, C₆D₆, AB₂X spin system) δ / ppm = -118.9 - -115.6 (m, 1P, P_X), -63.3 - -65.6 (m, 3P, P_{AB}).

No further characterization has been carried out due to the low amount of sample and small scale of the reaction.

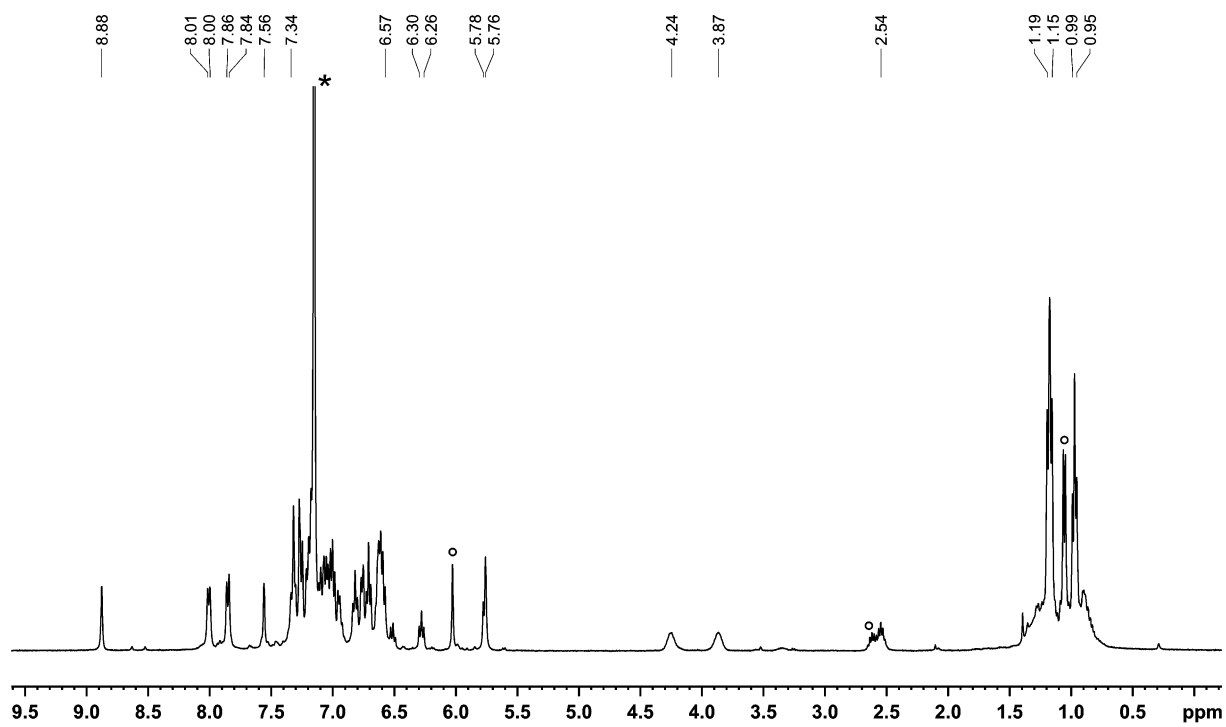


Figure S13. ^1H NMR spectrum (400.30 MHz, 300 K, C_6D_6), of $[(\text{Ar}^*\text{BIAN})\text{Co}(\text{CN})(\eta^3\text{-P}_4(\text{N}(\text{iPr})_2)_2)]$ (**1b-N(iPr)₂**); \circ free Ar^*BIAN ligand; * C_6D_6 .

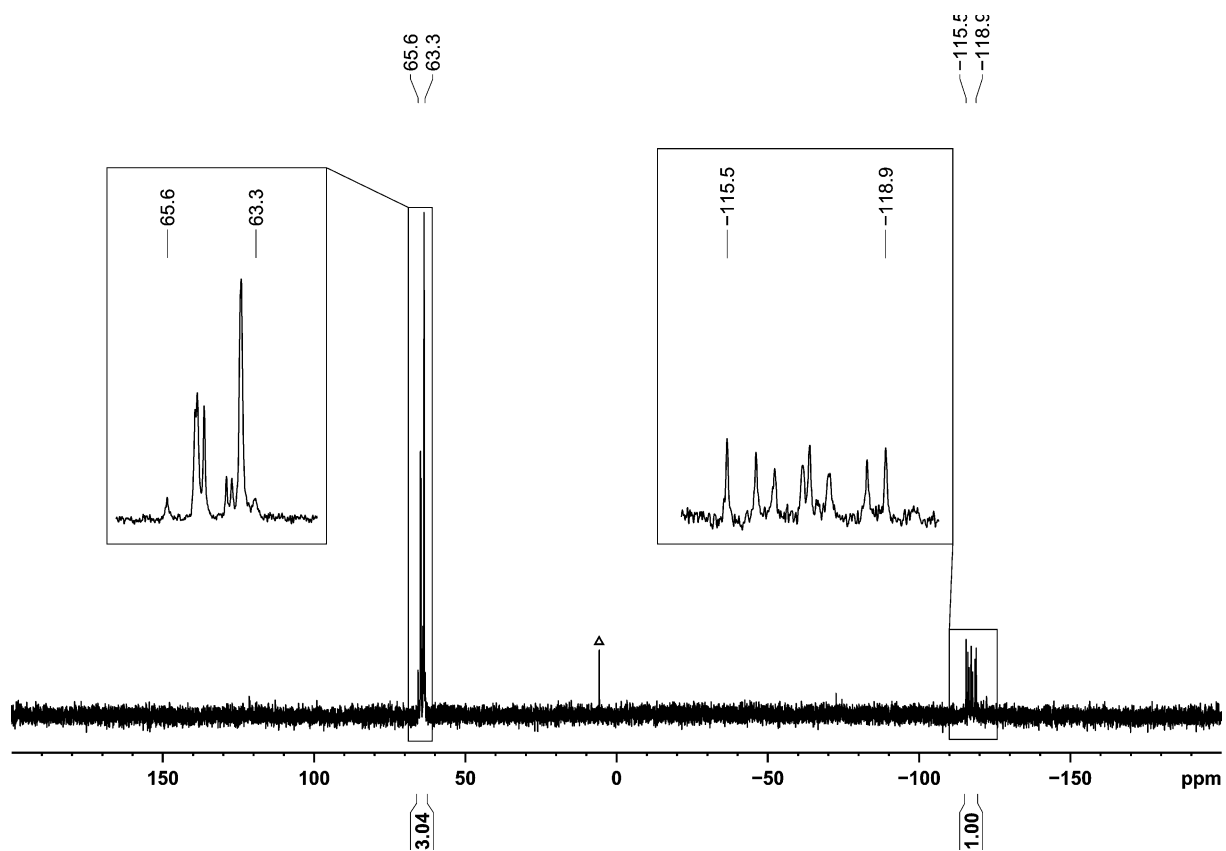
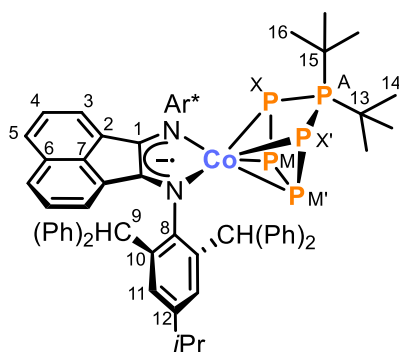


Figure S14. $^{31}\text{P}\{^1\text{H}\}$ NMR spectrum (162.04 MHz, 300 K, C_6D_6) of $[(\text{Ar}^*\text{BIAN})\text{Co}(\text{CN})(\eta^3\text{-P}_4(\text{N}(\text{iPr})_2)_2)]$ (**1b-N(iPr)₂**); Δ minor unknown impurity.

Preparation of $[(Ar^*BIAN)Co(\eta^4-P_5tBu_2)]$ (**2b-tBu**)



A stock solution of tBu_2P_5Cl (0.078 M, 1.23 mL, 0.096 mmol, 1.0 equiv.) in toluene was added dropwise to a deep purple solution of $[K(18c-6)][(Ar^*BIAN)Co(\eta^4-P_4)]$ (150 mg, 0.096 mmol, 1.0 equiv.) in toluene (25 mL). The reaction mixture was stirred for four weeks at 32 °C. The color slowly changed to dark turquoise during that time. The mixture was filtered over a pad of silica (1.5 × 1 cm) and washed with toluene (10 mL). The volume of the dark turquoise filtrate was reduced to one third and layered with *n*-pentane (12 mL). After twelve days shimmering dark turquoise crystals had formed, which were isolated by decantation of the

mother liquor, washed with *n*-pentane (1 mL) and dried *in vacuo*. A second crop of crystal was obtained by further concentrating the mother liquor and storing the solution in the freezer at -30 °C. The second fraction was isolated and combined with the first fraction. Yield: 107.0 mg (79%, combined yield of the first and second crop of crystals, based on the maximum theoretical yield of 0.096 mmol).

1H NMR (400.13 MHz, 300 K, C_6D_6): δ / ppm = 0.23 (d, $^3J_{PH} = 13.9$ Hz, 9H, $-C(C^{14}H_3)_3$), 0.92 (d, $^3J_{PH} = 12.9$ Hz, 9H, $-C(C^{16}H_3)_3$), 1.17 (d, $^3J_{HH} = 6.9$ Hz, 12H, $-CH(CH_3)_2$ of *iPr*), 2.74 (sept, $^3J_{HH} = 6.9$ Hz, 2H, $-CH(CH_3)_2$ of *iPr*), 5.24 (d, $^3J_{HH} = 7.1$ Hz, 2H, $-C^3H$ of BIAN), 6.12-6.16 (m, 2H, $-C^4H$ of BIAN), 6.51-6.58 (m, 4H, $-C^9H(Ph)_2$), 6.64-6.72 (m, 12H, $-CH_{Ar}$ of Ph), 7.10-7.21 (m, 22H, $-C^5H$ of BIAN overlapping with $-CH_{Ar}$ of Ph overlapping with C_6D_6 solvent signal), 7.70 (s, 4H, $-C^{11}H$), 7.79-7.81 (m, 8H, $-CH_{Ar}$ of Ph).

$^{13}C\{^1H\}$ NMR (100.61 MHz, 300 K, C_6D_6): δ / ppm = 24.6 (s, $-CH(CH_3)_2$ of *iPr*), 29.4 (s, $-C(C^{14}H_3)_3$), 32.2 (s, $-C(C^{16}H_3)_3$), 34.6 (s, $-CH(CH_3)_2$ of *iPr*), 41.7 (m, $-C^{15}(CH_3)_3$), 43.6 (d, $^1J_{CP} = 5.5$ Hz, $-C^{13}(CH_3)_3$), 53.1 (s, $-C^9H(Ph)_2$), 121.8 (s, $-C^3H$ of BIAN), 124.1 (s, $-C^5H$ of BIAN), 126.6 (s, $-C_{Ar}H$ of Ph), 126.8 (s, $-C_{Ar}H$ of Ph), 128.1 (s, $-C^4H$ of BIAN), 128.5 (s, $-C_{Ar}H$ of Ph overlapping with C_6D_6 solvent signal), 128.6 (s, $-C^{11}H$ overlapping with C_6D_6 solvent signal), 130.4 (s, $-C^6$ of BIAN), 131.3 (s, $-C_{Ar}H$ of Ph), 132.3 (s, $-C_{Ar}H$ of Ph), 133.6 (s, $-C^2$ of BIAN), 137.6 (s, $-C^7$ of BIAN), 138.4 (s, $-C^{10}$), 145.2 (s, $-C_{Ar}H$ of Ph), 146.0 (s, $-C^{12}$), 146.6 (s, $-C_{Ar}H$ of Ph), 150.7 (s, $-C^8N$), 156.7 (s, $-C^1=N$ of BIAN).

$^{31}P\{^1H\}$ NMR (162.04 MHz, 300 K, C_6D_6 , AMM'XX' spin system) δ / ppm = -182.7 - -174.0 (m, 2P, $P_{XX'}$), 67.1-73.3 (m, 2P, $P_{MM'}$), 176.0 (t, 1P, P_A), for parameters obtained by simulation, see Table S4.

UV/Vis (toluene, λ_{max} / nm, ϵ_{max} / $L \cdot mol^{-1} \cdot cm^{-1}$): 400sh (4500), 580 (6000), 670 (6000).

Elemental Analysis calcd. for $C_{90}H_{86}CoN_2P_5$ (Mw = 1409.49 $g \cdot mol^{-1}$): C 76.69, H 6.15, N 1.99; found C 76.91, H 6.19, N 1.90.

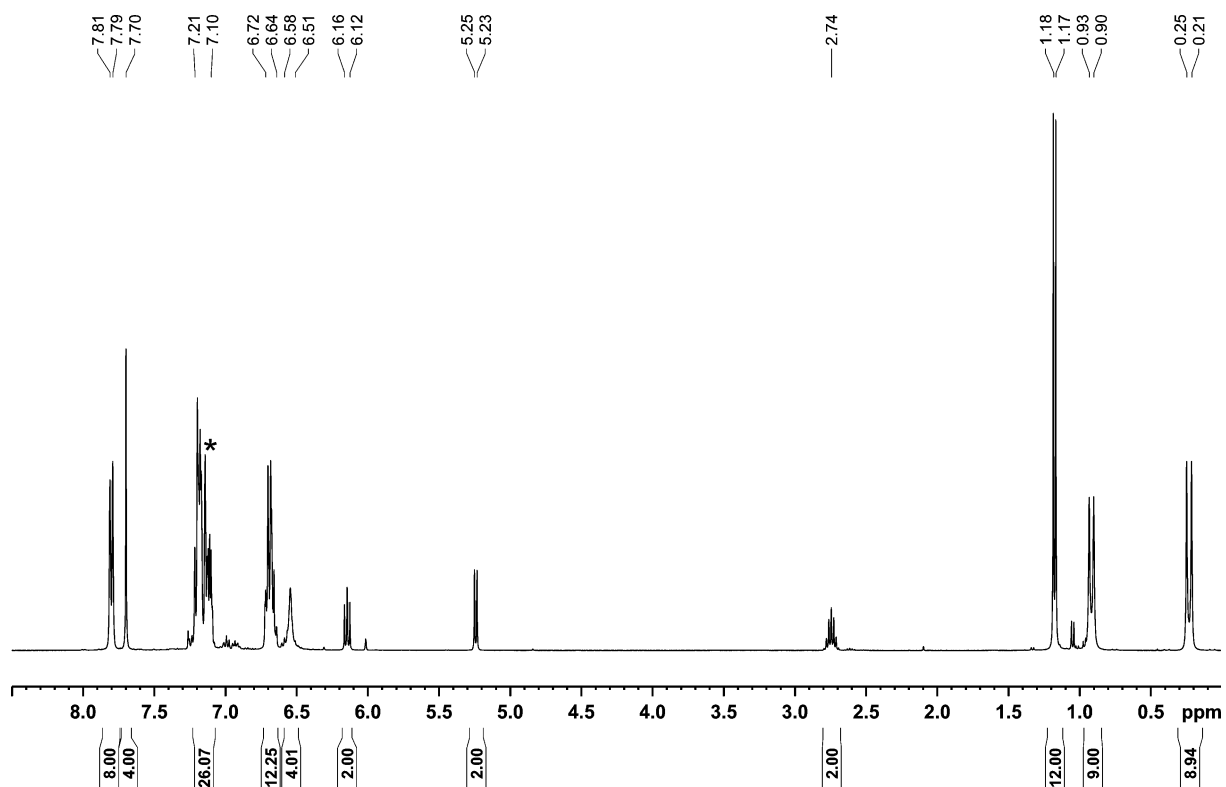


Figure S15. ^1H NMR spectrum (400.13 MHz, 300 K, C_6D_6) of $[(\text{Ar}^*\text{BIAN})\text{Co}(\eta^4\text{-P}_5\text{tBu}_2)]$ (**2b-tBu**); * C_6D_6 .

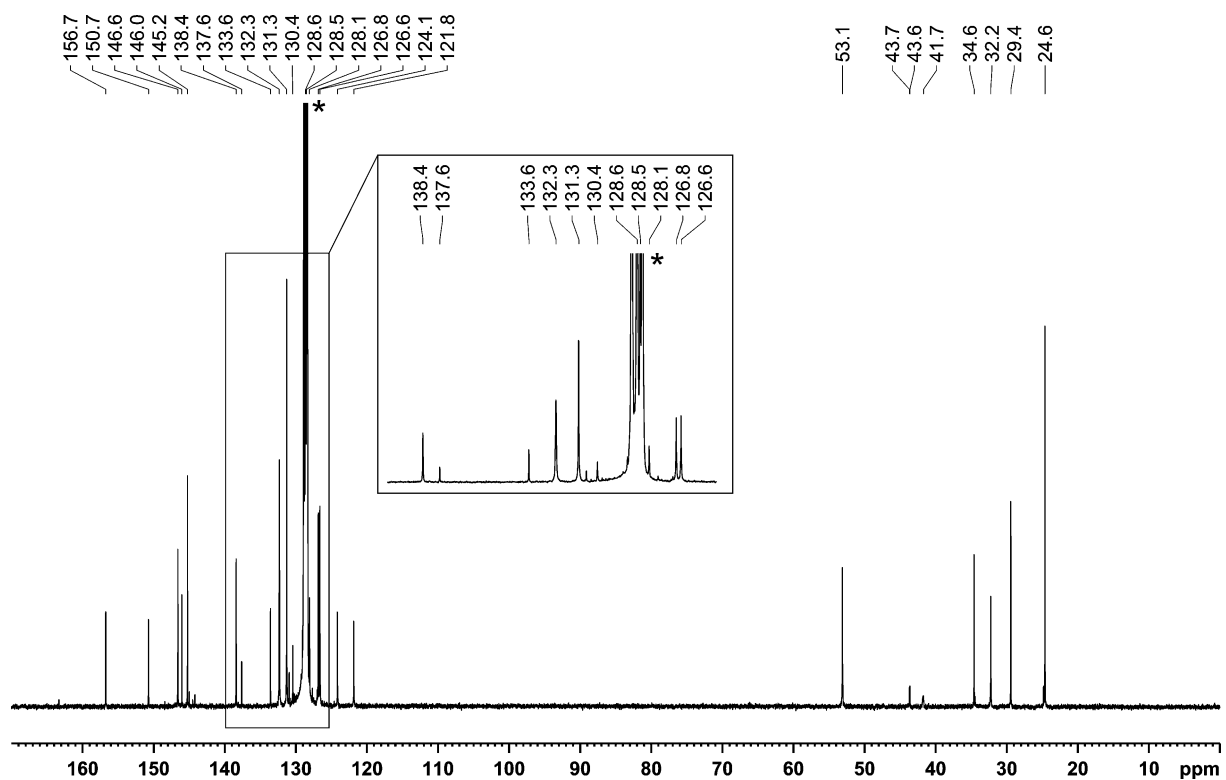


Figure S16. $^{13}\text{C}\{^1\text{H}\}$ NMR spectrum (100.61 MHz, 300 K, C_6D_6) of $[(\text{Ar}^*\text{BIAN})\text{Co}(\eta^4\text{-P}_5\text{tBu}_2)]$ (**2b-tBu**); * C_6D_6 .

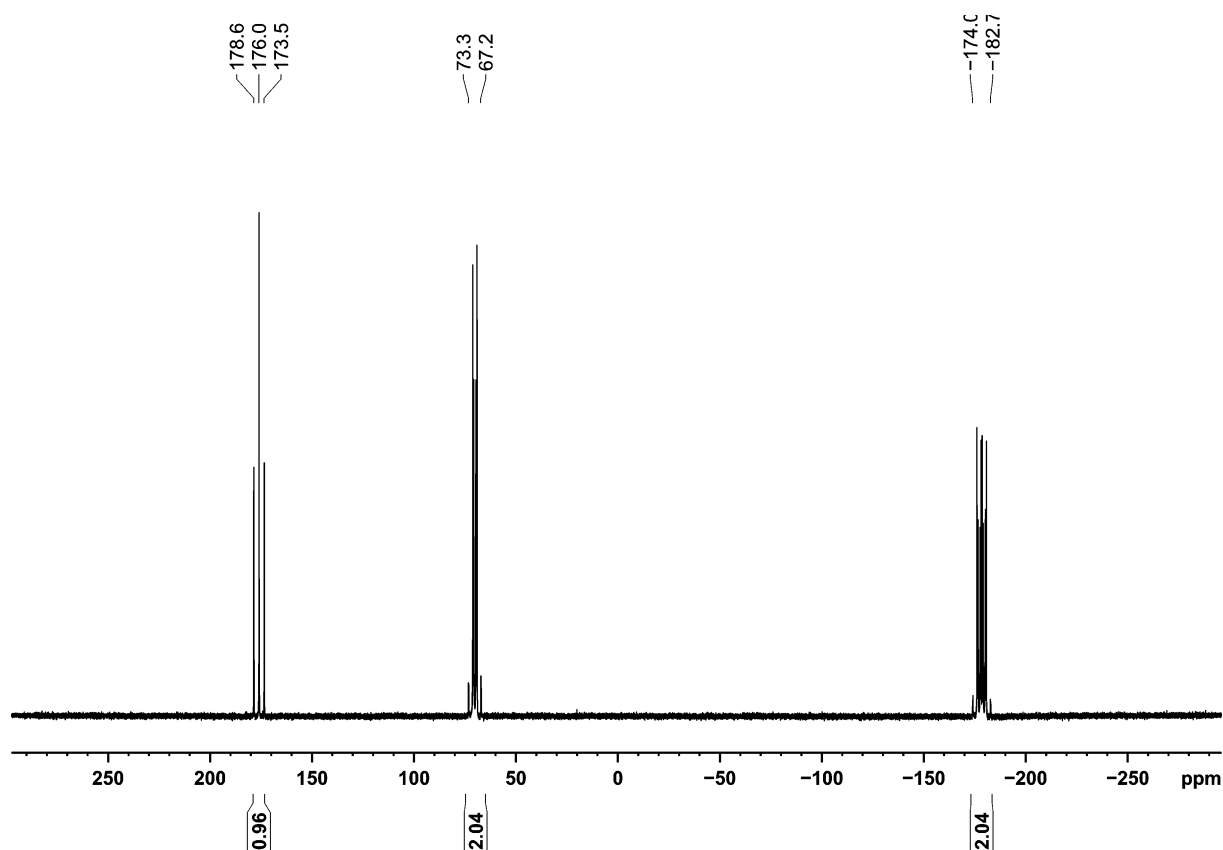


Figure S17. $^{31}\text{P}\{^1\text{H}\}$ NMR spectrum (162.04 MHz, 300 K, C_6D_6) of $[(\text{Ar}^*\text{tBu})\text{Co}(\eta^4\text{-P}_5\text{tBu}_2)]$ (**2b-tBu**).

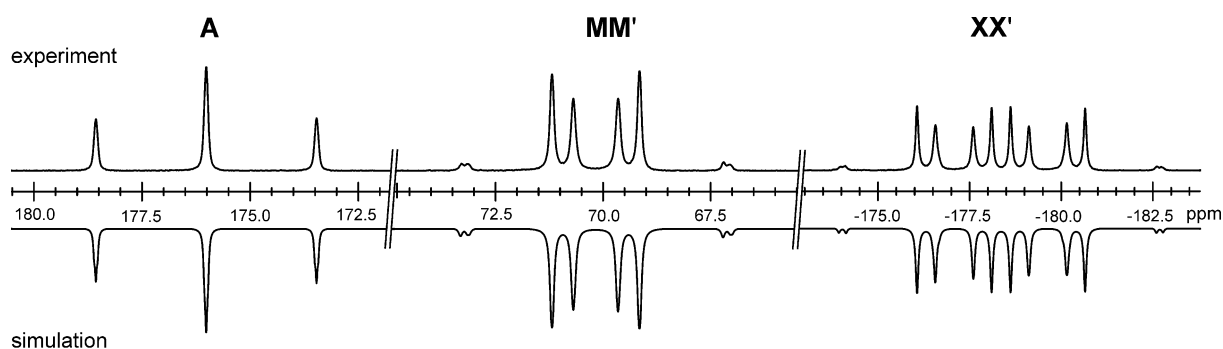
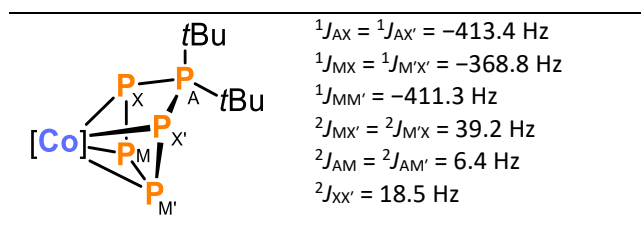
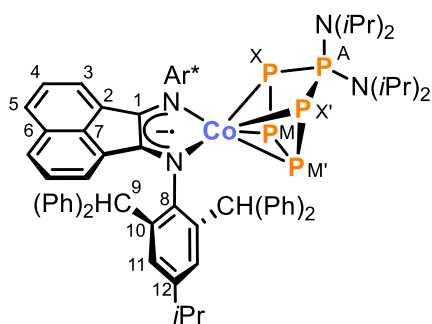


Figure S18. Section of the $^{31}\text{P}\{^1\text{H}\}$ NMR spectrum (162.04 MHz, 300 K, C_6D_6) of $[(\text{Ar}^*\text{tBu})\text{Co}(\eta^4\text{-P}_5\text{tBu}_2)]$ (**2b-tBu**); experimental (upwards) and simulation (downwards).

Table S4. Coupling constants from the iterative fit of the AMM'XX' spin system and schematic representation of the $\text{CoP}_5(\text{tBu})_2$ core of $[(\text{Ar}^*\text{tBu})\text{Co}(\eta^4\text{-P}_5\text{tBu}_2)]$ (**2b-tBu**); $\delta(\text{P}_A) = 176.0$ ppm, $\delta(\text{P}_M) = 70.2$ ppm, $\delta(\text{P}_X) = -178.4$ ppm.



Preparation of [(Ar*BIAN)Co(η^4 -P₅(N(*i*Pr)₂))₂] (2b-N(*i*Pr)₂)



Toluene (11 ml) was added to neat (*i*Pr₂N)₂PCl (34 mg, 0.128 mmol, 1.0 equiv.) and [K(18c-6)][(Ar*BIAN)Co(η^4 -P₄)] (200 mg, 0.128 mmol, 1.0 equiv.). The purple reaction mixture was stirred for one day. The color turned to dark turquoise during that time. The mixture was filtered over a pad of silica (2 × 1.5 cm) and washed with toluene (3 × 10 mL). The volume of the dark turquoise filtrate was reduced to approximately 8 mL and layered with *n*-pentane (32 mL). Storage of the solution at room temperature gave shimmering dark turquoise crystals, which were isolated by decantation of the mother

liquor, washed with *n*-pentane (1 × 3 mL) and dried *in vacuo*. The crystalline solid contains 0.5 molecules of toluene per molecule of compound after drying as indicated by the ¹H/¹³C{¹H} NMR spectra and elemental analysis. Yield: 139.0 mg (73% based on the maximum theoretical yield of 0.128 mmol).

¹H NMR (400.13 MHz, 300 K, C₆D₆): δ / ppm = 0.64 (d, ³J_{HH} = 6.8 Hz, 12H, -N(CH(CH₃)₂)₂), 0.79 (d, ³J_{HH} = 6.9 Hz, 12H, -N(CH(CH₃)₂)₂), 1.12 (d, ³J_{HH} = 6.9 Hz, 12H, -CH(CH₃)₂ of *i*Pr), 2.70 (sept, ³J_{HH} = 6.9 Hz, 2H, -CH(CH₃)₂ of *i*Pr), 3.13 (sept, ³J_{HH} = 6.7 Hz, 2H, -N(CH(CH₃)₂)₂), 3.58 (br sept, 2H, -N(CH(CH₃)₂)₂), 5.23 (d, ³J_{HH} = 7.1 Hz, -C³H of BIAN), 6.13-6.17 (m, 2H, -C⁴H of BIAN), 6.57-6.70 (m, 16H, -CH_{Ar} of Ph overlapping with -C⁹H(Ph)₂), 7.09-7.26 (m, 22H, -CH_{Ar} of Ph overlapping with d (³J_{HH} = 8.2 Hz, 2H, -C⁵H of BIAN) overlapping with C₆D₆ solvent signal), 7.65 (s, 4H, -C¹¹H), 7.86-7.88 (m, 8H, -CH_{Ar} of Ph).

¹³C{¹H} NMR (100.61 MHz, 300 K, C₆D₆): δ / ppm = 24.2 (s, -N(CH(CH₃)₂)₂), 24.6 (s, -CH(CH₃)₂ of *i*Pr), 24.8 (s, -N(CH(CH₃)₂)₂), 34.5 (s, -CH(CH₃)₂ of *i*Pr), 48.1 (s, -N(CH(CH₃)₂)₂), 52.4 (s, -N(CH(CH₃)₂)₂), 53.1 (s, -C⁹H(Ph)₂), 121.6 (s, -C³H of BIAN), 123.9 (s, -C⁵H of BIAN), 126.6 (s, -C_{Ar}H of Ph), 126.9 (s, -C_{Ar}H of Ph), 128.1 (s, -C⁴H of BIAN), 128.5 (s, -C_{Ar}H of Ph overlapping with C₆D₆ solvent signal), 128.5 (s, -C_{Ar}H of Ph overlapping with C₆D₆ solvent signal), 129.3 (s, -C¹¹H), 130.4 (s, -C⁶ of BIAN), 131.3 (s, -C_{Ar}H of Ph), 132.4 (s, -C_{Ar}H of Ph), 133.6 (s, -C² of BIAN), 137.4 (s, -C⁷ of BIAN), 138.6 (s, -C¹⁰), 145.0 (s, -C_{Ar} of Ph), 145.9 (s, -C¹²), 147.0 (s, -C_{Ar} of Ph), 151.2 (s, -C⁸N), 156.9 (s, -C¹=N of BIAN).

³¹P{¹H} NMR (162.04 MHz, 300 K, C₆D₆, AMM'XX' spin system): δ / ppm = -144.3 - -135.8 (m, 2P, P_{XX'}), 39.4 - 45.4 (m, 2P, P_{MM'}), 135.4 (t, 1P, P_A), for parameters obtained by simulation, see Table S5.

UV/Vis (toluene, λ_{\max} / nm, ϵ_{\max} / L·mol⁻¹·cm⁻¹): 425 (14500), 580 (23500), 675 (21000).

Elemental analysis calcd. for (C₉₄H₉₆CoN₄P₅)·(toluene)_{0.5} (Mw = 1495.63 g·mol⁻¹): C 75.96, H 6.54, N 3.63; found C 76.31, H 6.47, N 3.52.

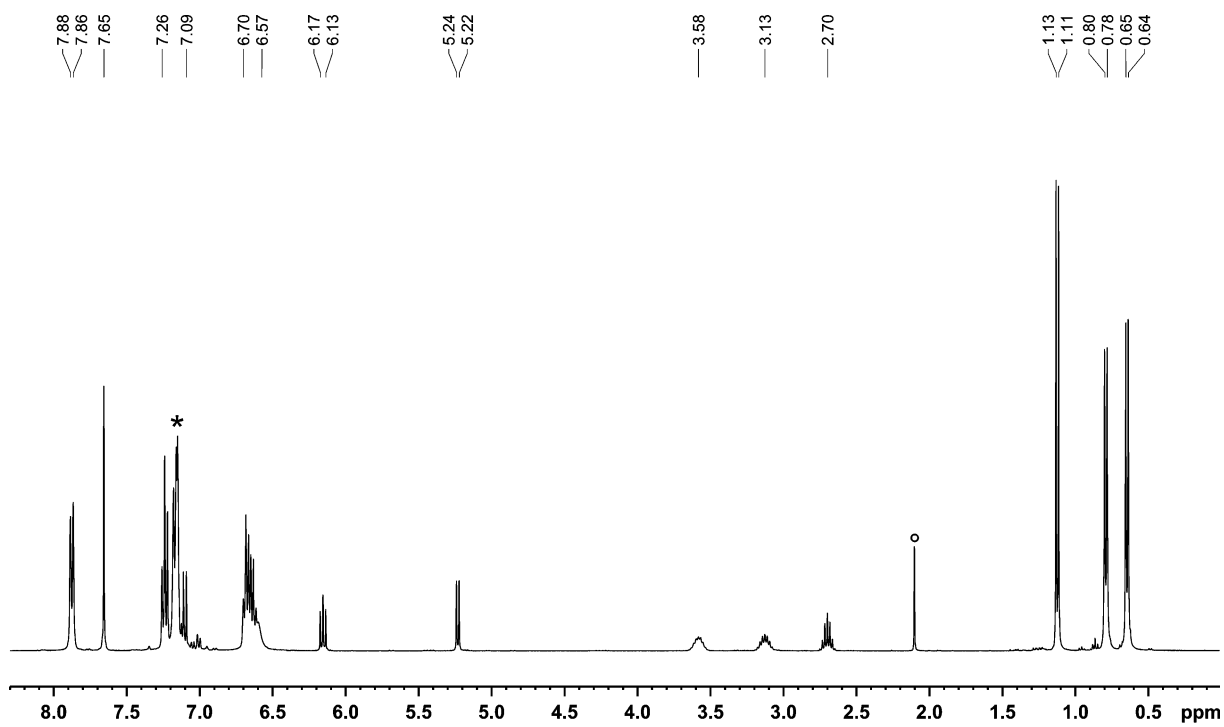


Figure S19. ^1H NMR spectrum (400.13 MHz, 300 K, C_6D_6) of $[(\text{Ar}^*\text{BIAN})\text{Co}(\eta^4\text{-P}_5(\text{N}(\text{iPr})_2)_2)]$ (**2b-N(iPr)₂**·(toluene)_{0.5}); ○ toluene, * C_6D_6 .

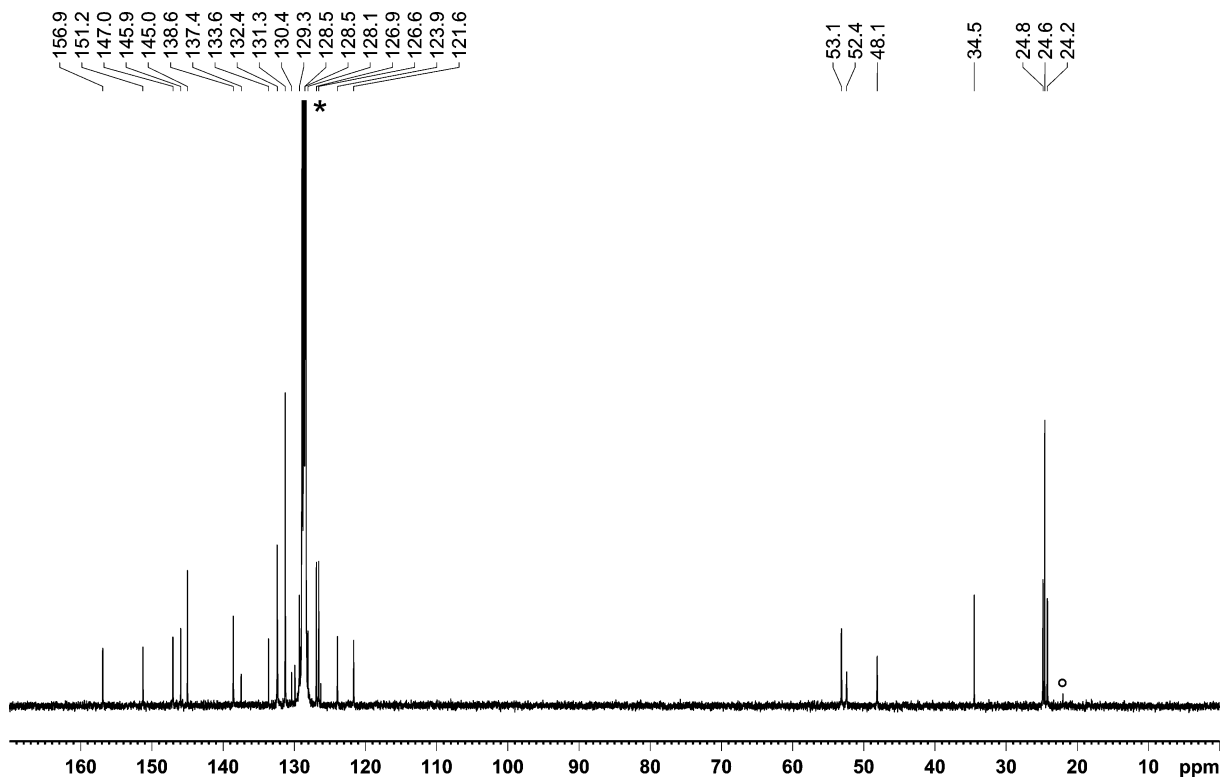


Figure S20. $^{13}\text{C}\{^1\text{H}\}$ NMR spectrum (100.61 MHz, 300 K, C_6D_6) of $[(\text{Ar}^*\text{BIAN})\text{Co}(\eta^4\text{-P}_5(\text{N}(\text{iPr})_2)_2)]$ (**2b-N(iPr)₂**·(toluene)_{0.5}); ○ toluene, * C_6D_6 .

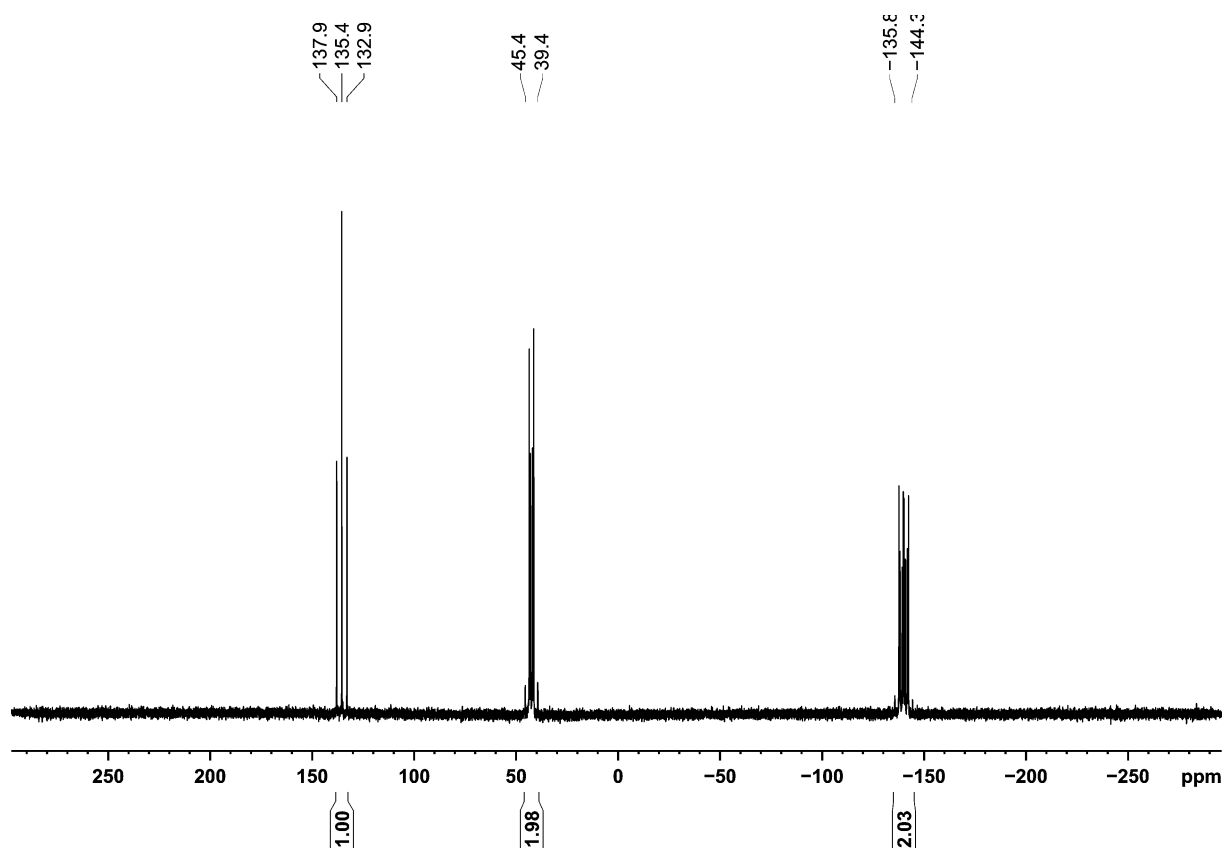


Figure S21. $^{31}\text{P}\{^1\text{H}\}$ NMR spectrum (162.04 MHz, 300 K, C_6D_6) of $[(\text{Ar}^*\text{BIAN})\text{Co}(\eta^4\text{-P}_5(\text{N}(\text{iPr})_2)_2)]$ (**2b-N(iPr)₂**)·(toluene)_{0.5}.

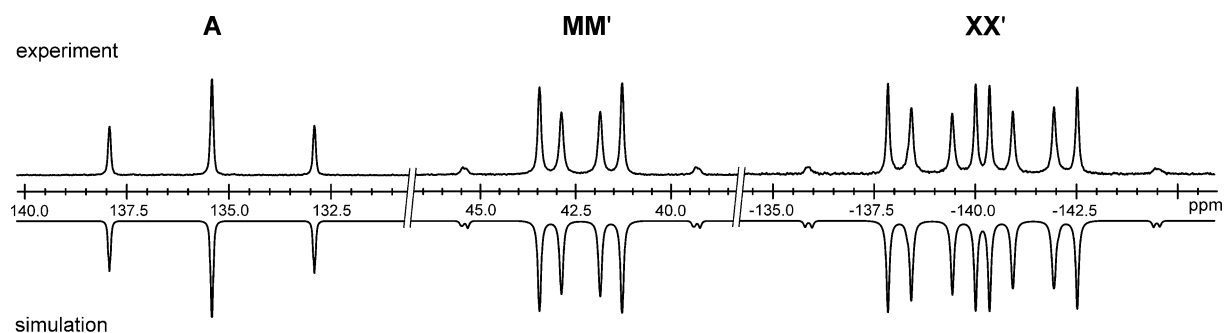
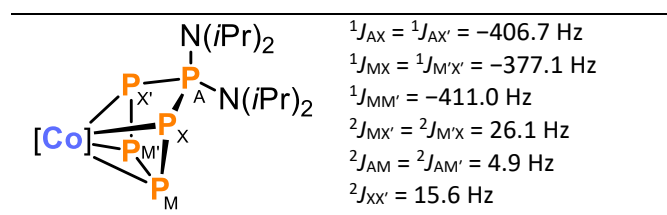
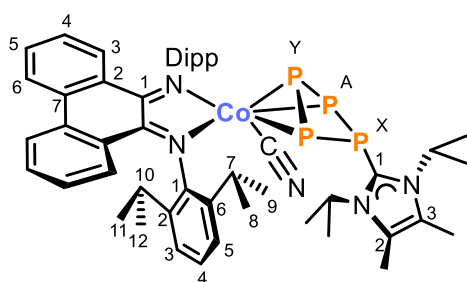


Figure S22. Section of the $^{31}\text{P}\{^1\text{H}\}$ NMR spectrum (162.04 MHz, 300 K, C_6D_6) of $[(\text{Ar}^*\text{BIAN})\text{Co}(\eta^4\text{-P}_5(\text{N}(\text{iPr})_2)_2)]$ (**2b-N(iPr)₂**); experimental (upwards) and simulation (downwards).

Table S5. Coupling constants from the iterative fit of the AMM'XX' spin system and schematic representation of the $\text{CoP}_5(\text{N}(\text{iPr})_2)_2$ core of $[(\text{Ar}^*\text{BIAN})\text{Co}(\eta^4\text{-P}_5(\text{N}(\text{iPr})_2)_2)]$ (**2b-N(iPr)₂**); $\delta(\text{P}_A) = 135.4$ ppm, $\delta(\text{P}_M) = 42.4$ ppm, $\delta(\text{P}_X) = -140.2$ ppm.



Preparation of [(PHDI)Co(CN)(η^3 -P₄Lc)] (3a)



A beige suspension of [(Lc)₄P₄][OTf]₄ (37.9 mg, 0.026 mmol, 0.25 equiv.) in toluene (2.5 mL) was added dropwise to a dark purple suspension of [nBu₄N][(PHDI)Co(CN)(η^3 -P₃)]·(toluene)_{0.1} (100.4 mg, 0.105 mmol, 1.0 equiv.) in toluene (4 mL). The reaction mixture was stirred at room temperature for 5 d. The color slowly turned to dark blue during that time. The pure product precipitated from the reaction mixture as dark purple solid. To collect the product, the reaction suspension

was filtered over a Whatman filter and the solid was redissolved in THF (1.5 mL). The solvent was removed *in vacuo* and the dark purple residue was washed with *n*-hexane (2 × 1 mL) and dried *in vacuo*. Yield: 35.3 mg (36% based on the maximum theoretical yield of 0.105 mmol).

UV/vis (THF, λ_{max} / nm, ϵ_{max} / L·mol⁻¹·cm⁻¹): 310sh (28000), 330sh (27000), 355sh (26000), 370 (27000), 390sh (24000), 400sh (20000), 600 (30000).

¹H NMR (400.30 MHz, 300 K, thf-*d*₈): δ / ppm = 0.36 (d, ³J_{HH} = 6.8 Hz, 6H, -CH(C¹¹H₃)₂ of Dipp), 0.87 (d, ³J_{HH} = 6.8 Hz, 6H, -CH(C⁸H₃)₂ of Dipp), 1.27 (d, ³J_{HH} = 6.7 Hz, 6H, -CH(C¹²H₃)₂ of Dipp), 1.36 (d, ³J_{HH} = 6.9 Hz, 12H, -CH(CH₃)₂ of Lc), 1.51 (d, ³J_{HH} = 6.5 Hz, 6H, -CH(C⁹H₃)₂ of Dipp), 2.14 (s, 6H, -CH₃ of Lc), 2.33-2.14 (m, 2H, -C¹⁰H(CH₃)₂ of Dipp), 4.38-4.48 (sept., ³J_{HH} = 6.7 Hz, 2H, -C⁷H(CH₃)₂ of Dipp), 4.60-4.69 (m, 2H, -CH(CH₃)₂ of Lc), 6.82-6.86 (m, 2H, -C⁴H of PHDI), 7.08-7.10 (m, 2H, -C⁵H of Dipp), 7.20 (t, ³J_{HH} = 7.7 Hz, 2H, -C⁴H of Dipp), 7.31-7.33 (m, 2H, -C³H of Dipp), 7.38-7.44 (m, 4H, -C⁵H of PHDI overlapping with -C³H of PHDI), 8.31-8.33 (m, 2H, -C⁶H of PHDI).

¹³C{¹H} NMR (100.66 MHz, 300 K, thf-*d*₈): δ / ppm = 10.6 (s, -CH₃ of Lc), 21.8 (s, -CH(CH₃)₂ of Lc), 24.9 (s, -CH(C¹¹H₃)₂ of Dipp overlapping with thf-*d*₈ solvent signal), 25.4 (s, -CH(C⁸H₃)₂ of Dipp overlapping with thf-*d*₈ solvent signal), 26.2 (s, -CH(C¹²H₃)₂ of Dipp), 26.3, 27.2 (s, -CH(C⁹H₃)₂ of Dipp), 28.7 (s, -C¹⁰H(CH₃)₂ of Dipp), -C¹⁰H(CH₃)₂ of Dipp), 28.9 (s, -C⁷H(CH₃)₂ of Dipp), 52.4 (m, -CH(CH₃)₂ of Lc), 124.3 (s, -C³H of Dipp), 124.7 (s, -C⁶H of PHDI), 125.2 (s, -C⁵H of Dipp), 126.2 (s, -C⁴H of Dipp), 127.2 (s, -C³H or -C⁵H of PHDI), 127.3 (s, -C⁴H of PHDI), 128.1 (s, -C² or -C³ of Lc), 128.1 (s, -C² or -C³ of Lc), 129.4 (s, -C³H or -C⁵H of PHDI), 130.1 (s, -C² of PHDI), 130.6 (s, -C¹ or -C⁷ of PHDI), 138.4 (s, -C² of Dipp), 141.4 (s, -C⁶ of Dipp), 150.6 (s, -C≡N), 151.3 (s, -C¹ of Dipp), 152.2 (s, -C¹ of Lc), 153.6 (s, -C¹ or -C⁷ of PHDI).

³¹P{¹H} NMR (162.04 MHz, 300 K, thf-*d*₈, A₂XY spin system): δ / ppm = -43.3 - -40.6 (m, 1H, P_Y), -30.5 - -26.5 (m, 1H, P_X), 78.5 - 81.6 (m, 2H, P_A), for parameters obtained by simulation, see Table S6.

IR (solid state): ν / cm⁻¹ = 2958m (C-H), 2924m (C-H), 2864 (C-H), 2083 (C≡N), 1489m, 1458m, 1439m, 1412w, 1381m, 1358m, 1315m, 1252m, 1242m, 1221m, 1159w, 1113w, 1053m, 931w, 791m, 754s, 723s, 694w, 604w, 507w, 436w, 401w.

Elemental analysis calcd. for C₅₀H₆₂CoN₅P₄·(C₄H₈O)_{0.4} (Mw = 944.75 g·mol⁻¹) C 65.60, H 6.96, N 7.41; found C 65.67, H 6.85, N 7.11.

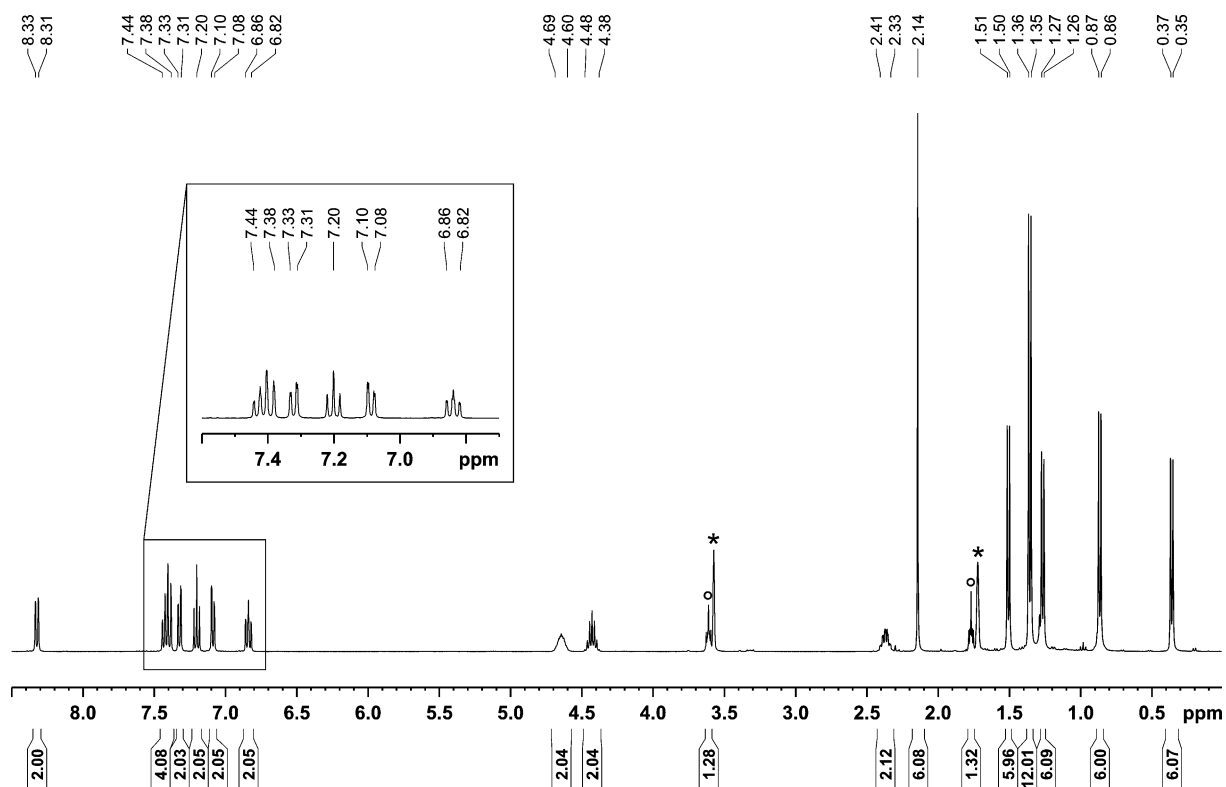


Figure S23. ^1H NMR spectrum (400.30 MHz, 300 K, $\text{thf-}d_8$) of $[(\text{PHDI})\text{Co}(\text{CN})(\eta^3\text{-P}_4\text{Lc})]$ (**3a**)· $(\text{THF})_{0.4}$; * $\text{thf-}d_8$, o THF.

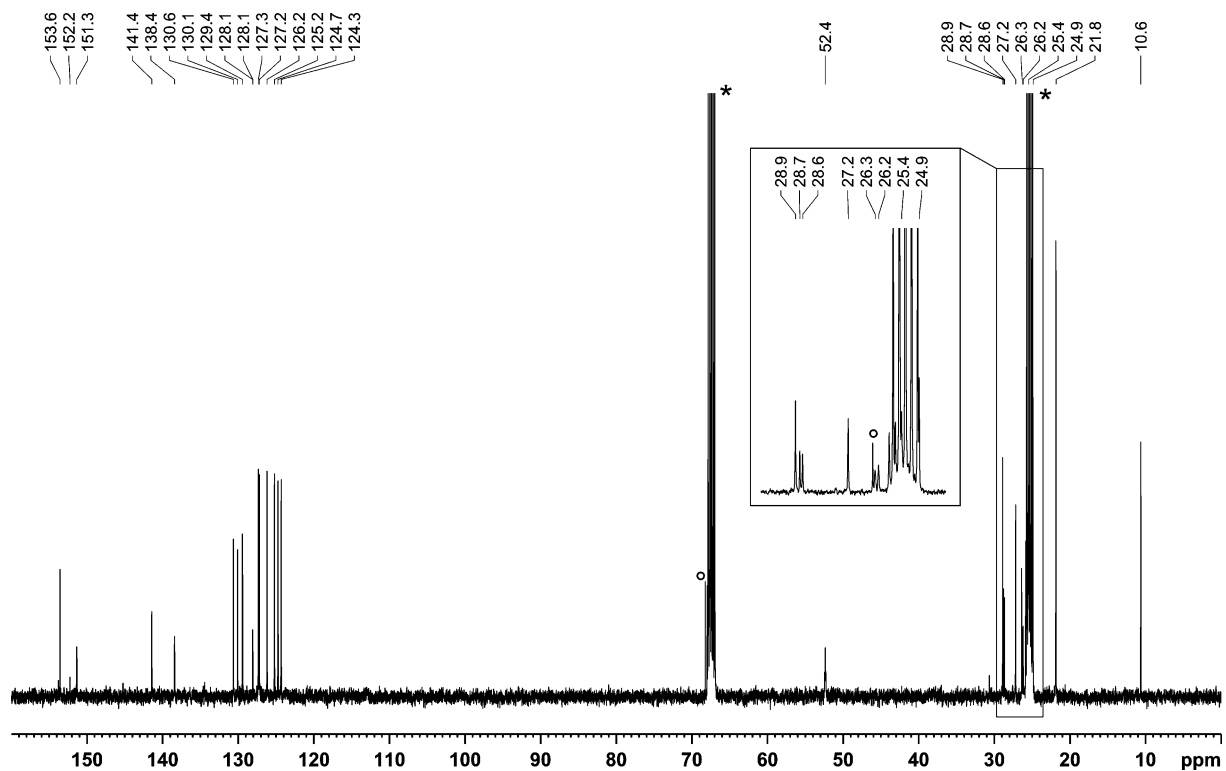


Figure S24. $^{13}\text{C}\{^1\text{H}\}$ NMR spectrum (100.66 MHz, 300 K, $\text{thf-}d_8$) of $[(\text{PHDI})\text{Co}(\text{CN})(\eta^3\text{-P}_4\text{Lc})]$ (**3a**)· $(\text{THF})_{0.4}$; * $\text{thf-}d_8$, o THF.

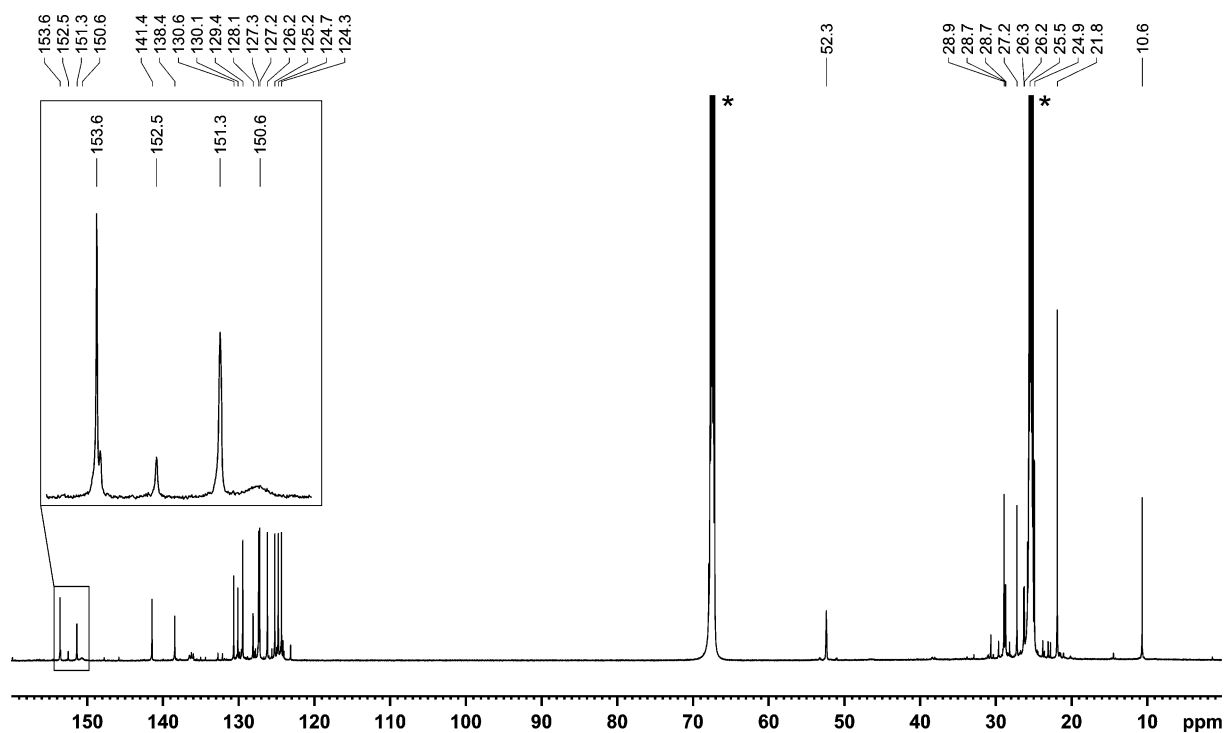


Figure S25. $^{13}\text{C}\{^1\text{H}\}$ NMR spectrum (150.93 MHz, 300 K, $\text{thf-}d_8$) of $[(\text{PHDI})\text{Co}(\text{CN})(\eta^3\text{-P}_4\text{Lc})]$ (**3a**)· $(\text{THF})_{0.4}$; * $\text{thf-}d_8$.

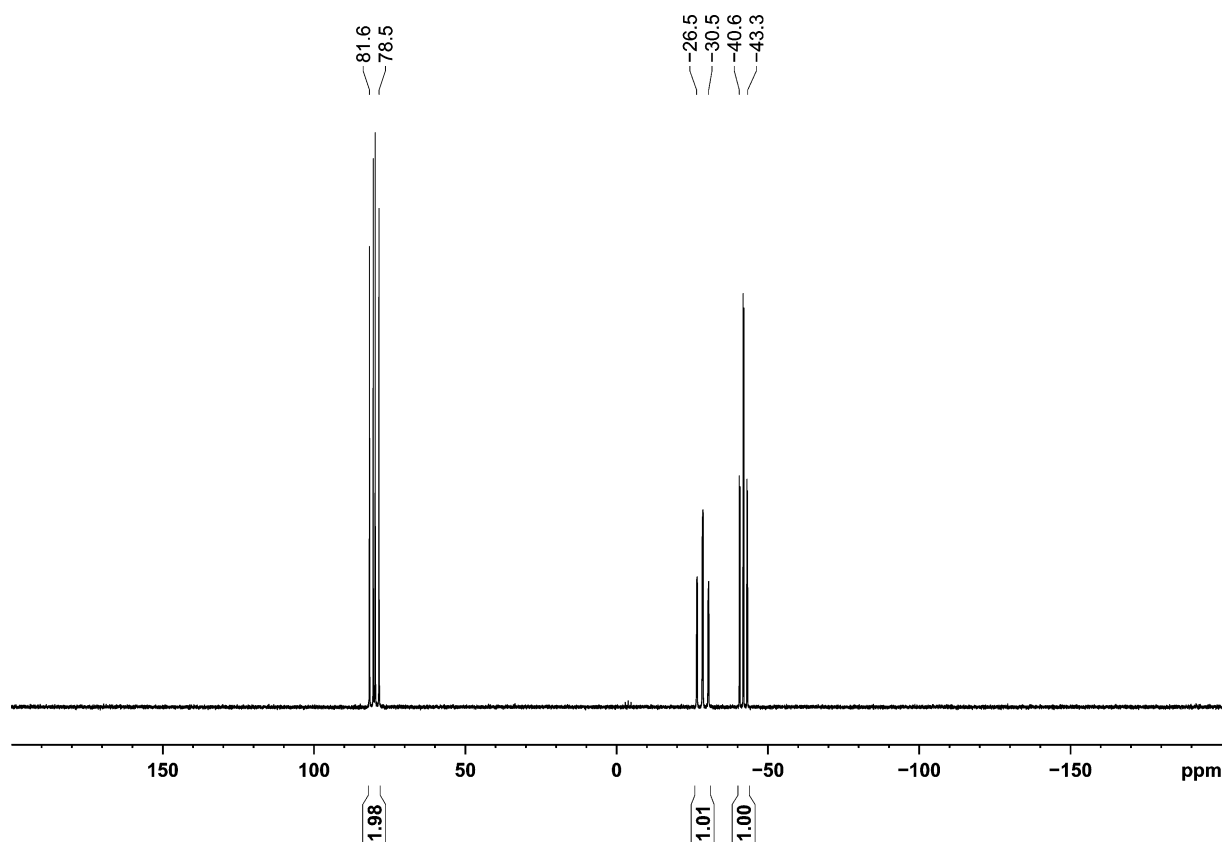


Figure S26. $^{31}\text{P}\{^1\text{H}\}$ NMR spectrum (162.04 MHz, 300 K, $\text{thf-}d_8$) of $[(\text{PHDI})\text{Co}(\text{CN})(\eta^3\text{-P}_4\text{Lc})]$ (**3a**)· $(\text{THF})_{0.4}$.

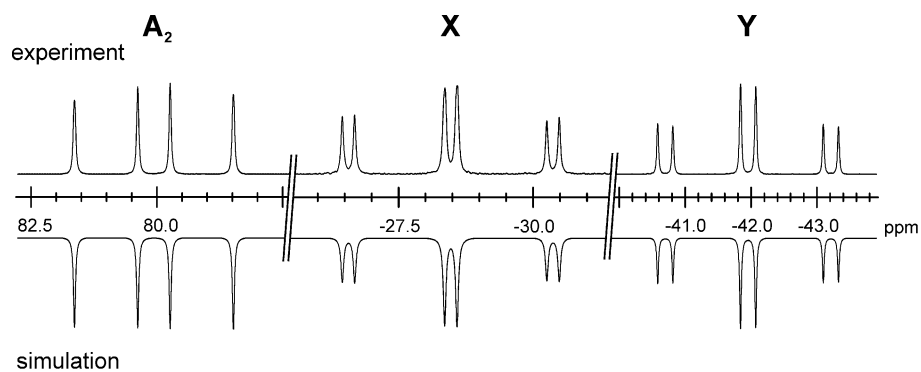
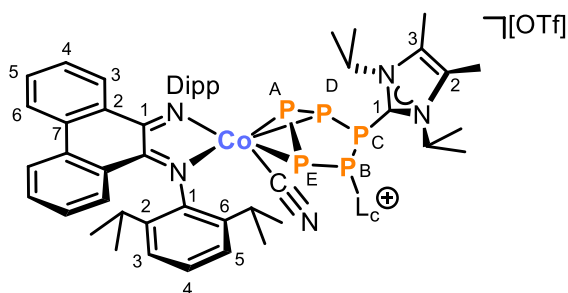


Figure S27. Section of the $^{31}\text{P}\{^1\text{H}\}$ NMR spectrum (161.98 MHz, 300 K, $\text{thf-}d_8$) of $[(\text{PHDI})\text{Co}(\text{CN})(\eta^3\text{-P}_4\text{Lc})]$ (**3a**); experimental (upwards) and simulation (downwards).

Table S6. Coupling constant from the iterative fit of the A_2XY spin system and schematic representation of the $\text{CoP}_4(\text{Lc})$ core of $[(\text{PHDI})\text{Co}(\text{CN})(\eta^3\text{-P}_4\text{Lc})]$ (**3a**); $\delta(\text{P}_\text{A}) = 80.1$ ppm, $\delta(\text{P}_\text{X}) = -28.5$ ppm, $\delta(\text{P}_\text{Y}) = -42.0$ ppm.



Preparation of $[(\text{PHDI})\text{Co}(\text{CN})(\eta^3\text{-P}_5(\text{Lc})_2)][\text{OTf}]$ (**4a**[OTf])



To a dark purple suspension of $[\text{nBu}_4\text{N}][(\text{PHDI})\text{Co}(\text{CN})(\eta^3\text{-P}_3)] \cdot (\text{toluene})_{0.1}$ (97.1 mg, 0.102 mmol, 1.0 equiv.) in thf (2.5 mL) was added dropwise a beige suspension of $[(\text{Lc})_4\text{P}_4][\text{OTf}]_4$ (73.4 mg, 0.051 mmol, 0.50 equiv.) in thf (3.5 mL) upon which the color immediately changed to blue. The reaction mixture was stirred at 40 °C for 3 d. The solvent was removed and methylcyclohexane (2 × 30 mL) was added at room temperature to the

dark blue residue. The solution was heated to and stirred at 45 °C for 20 minutes. The blue solution was filtered over a Whatman filter at 45 °C and slowly cooled to room temperature. Dark blue powder of pure **4a**[OTf] was isolated by filtering the suspension over a Whatman filter, dissolving the residue in THF (3 mL), removing the solvent *in vacuo*, washing with *n*-hexane (4 × 0.5 mL) and drying the pure product *in vacuo*. Yield fraction 1: 19.2 mg (14% based on the maximum theoretical yield of 0.102 mmol). This crop was used for the characterization of **4a**[OTf]. The residue was recrystallized from Et₂O (1 × 25 mL, 1 × 20 mL) and the solvent was reduced to 5 mL. After storing at 4 °C for 8 days, dark blue crystals were isolated by decanting off the mother liquor, washing with *n*-hexane (4 × 1 mL) and drying *in vacuo*. Yield crop 2: 22.1 mg (13% based on the maximum theoretical yield of 0.102 mmol). As indicated by the ¹H/¹³C{¹H} NMR spectra and elemental analysis, the crystals contained one molecule of $[\text{nBu}_4\text{N}]\text{OTf}$ per molecule of **4a**[OTf] due to their similar solubility.

UV/vis (THF, λ_{max} / nm, ϵ_{max} / L·mol⁻¹·cm⁻¹): 290 (31000), 300sh (27000), 350 (22000), 370sh (17000), 630 (20000).

¹H NMR (400.13 MHz, 300 K, C₆D₆): δ / ppm = 0.47 (d, ³J_{HH} = 6.7 Hz, 3H, -CH(CH₃)₂ of Dipp), 0.52 (d, ³J_{HH} = 6.8 Hz, 3H, -CH(CH₃)₂ of Dipp), 1.27 (d, ³J_{HH} = 6.8 Hz, 3H, -CH(CH₃)₂ of Dipp), 1.35-1.44 (m, 30H, -CH(CH₃)₂ of Dipp overlapping with -CH(CH₃)₂ of Lc), 1.52 (d, ³J_{HH} = 6.7 Hz, 6H, -CH(CH₃)₂ of Lc), 1.67 (s, 6H, -CH₃ of Lc), 1.73 (s, 6H, -CH₃ of Lc), 2.02 (d, ³J_{HH} = 6.4 Hz, 3H, -CH(CH₃)₂ of Dipp), 2.34 (sept. ³J_{HH} = 6.7 Hz, 1H, -CH(CH₃)₂ of Dipp), 2.44 (sept. ³J_{HH} = 6.8 Hz, 1H, -CH(CH₃)₂ of Dipp), 4.94 (sept. ³J_{HH} = 6.6 Hz, 1H, -CH(CH₃)₂ of Dipp), 5.14 (sept. ³J_{HH} = 6.6 Hz, 1H, -CH(CH₃)₂ of Dipp), 5.47-5.73 (br m, 1H, -CH(CH₃)₂ of Lc), 5.78-5.89 (br m, 1H, -CH(CH₃)₂ of Lc), 6.80-6.85 (m, 2H, -C⁴H of PHDI), 7.08-7.12 (m, 2H, -C⁵H of PHDI), 7.13-7.15 (m, 1H, -C⁵H of Dipp overlapping with C₆D₆ solvent signal), 7.21-7.22 (m, 1H, -C⁵H of Dipp), 7.25-7.28 (m, 1H, -C⁴H of Dipp), 7.32-7.38 (m, 2H, -C³H of Dipp overlapping with -C⁴H of Dipp), 7.50-7.52 (m, 1H, -C³H of Dipp), 7.76-7.81 (m, 2H, -C³H of PHDI), 7.88-7.90 (m, 2H, -C⁶H of PHDI).

¹³C{¹H} NMR (100.61 MHz, 300 K, C₆D₆): δ / ppm = 10.3 (s, -CH₃ of Lc), 10.6 (s, -CH₃ of Lc), 21.7 (s, -CH(CH₃)₂ of Lc), 21.8 (s, -CH(CH₃)₂ of Lc), 22.1 (s, -CH(CH₃)₂ of Lc), 24.2 (s, -CH(CH₃)₂ of Dipp), 24.4 (s, -CH(CH₃)₂ of Dipp), 24.8 (s, -CH(CH₃)₂ of Dipp), 25.0 (s, -CH(CH₃)₂ of Dipp), 25.9 (s, -CH(CH₃)₂ of Dipp), 26.0 (s, -CH(CH₃)₂ of Dipp), 26.1 (s, -CH(CH₃)₂ of Dipp), 26.3 (s, -CH(CH₃)₂ of Dipp), 26.6 (s, -CH(CH₃)₂ of Dipp), 26.7 (s, -CH(CH₃)₂ of Dipp), 28.6 (s, -CH(CH₃)₂ of Dipp), 28.6 (s, -CH(CH₃)₂ of Dipp), 28.7 (s, -CH(CH₃)₂ of Dipp), 28.9 (s, -CH(CH₃)₂ of Dipp), 29.2 (s, -CH(CH₃)₂ of Dipp), 29.3 (s, -CH(CH₃)₂ of Dipp), 52.1-52.4 (m, -CH(CH₃)₂ of Lc), 53.5-53.7 (m, -CH(CH₃)₂ of Lc), 124.2 (s, -C⁶H of PHDI), 124.3 (s, -C⁵H of Dipp), 124.4 (s, -C⁵H of Dipp), 124.6 (s, -C³H of Dipp), 124.6 (s, -C³H of Dipp), 124.9 (s, -C³H of Dipp), 126.5 (s, -C⁴H of Dipp), 127.2 (s, -C⁴H of PHDI), 127.4 (s, -C⁴H of PHDI), 127.9 (s, -C⁵H of PHDI), 129.0 (s, -C³H of PHDI), 129.3 (s, -C² of PHDI), 129.4 (s, -C² of PHDI), 129.6 (s, -C² of Lc or -C³ of Lc), 129.8 (s, -C³H of PHDI), 130.1 (s, -C² of Lc or -C³ of Lc), 130.9 (s, -C⁷ of PHDI), 131.3 (s, -C⁷ of PHDI), 137.3 (d, J_{CP} = 5.4 Hz, -C² of Dipp or -C⁶ of Dipp), 138.2 (d, J_{CP} = 3.3 Hz, -C² of Dipp or -C⁶ of Dipp), 142.9 (d, J_{CP} = 5.1 Hz, -C² of Dipp or -C⁶ of Dipp), 143.0 (d, J_{CP} = 6.5 Hz, -C² of Dipp or -C⁶ of Dipp), 153.4 (d, J_{CP} = 7.2 Hz, -C¹ of Dipp), 155.0 (d, J_{CP} = 7.8 Hz, -C¹ of Dipp), 157.4 (s, -C¹ of PHDI), 157.9 (s, -C¹ of PHDI). C≡N, -C¹ of Lc: not detected. Note: Carbon atoms

$-C^1$, $-C^2$ and $-C^6$ of the Dipp-substituents appear as doublets in the $^{13}C\{^1H\}$ NMR spectrum due to the through space coupling with the phosphorus atoms P_B and P_D of the *cyclo*- P_5 ring.

$^{31}P\{^1H\}$ NMR (161.98 MHz, 300 K, C_6D_6 , ABCDE spin system): δ / ppm = -133.4 - -129.0 (m, 1H, P_E), -91.9 - -87.3 (m, 1H, P_D), 9.1-13.5 (m, 1H, P_C), 89.9-94.5 (m, 1H, P_B), 119.3-124.1 (m, 1H, P_A), for parameters obtained by simulation, see Table S7.

$^{19}F\{^1H\}$ NMR (376.66 MHz, 300 K, C_6D_6): δ / ppm = -78.2 (s, 3F, OTf).

IR (solid state): ν / cm^{-1} = 2956m (CH), 2923m (CH), 2862m (CH), 2098m (CN), 1621m, 1493m, 1464m, 1441m, 1381m, 1358m, 1317m, 1259s, 1223m, 1147m, 1030s, 754s, 723m, 636vs, 405m.

Elemental analysis of fraction 1 calcd. for $C_{62}H_{82}CoF_3N_7O_3P_5S \cdot (C_6H_{14})_{0.8}$ (Mw = 1345.18 $g \cdot mol^{-1}$) C 59.65, H 6.98, N 7.29, S 2.38; found C 59.99, H 6.53, N 7.06, S 2.04.

Elemental analysis of fraction 2 calcd. for $C_{62}H_{82}CoF_3N_7O_3P_5S \cdot (C_{17}H_{36}F_3NO_3S)_{1.0}$ (Mw = 1667.78 $g \cdot mol^{-1}$) C 56.89, H 7.13, N 6.72, S 3.84; found C 56.71, H 6.92, N 6.65, S 4.04.

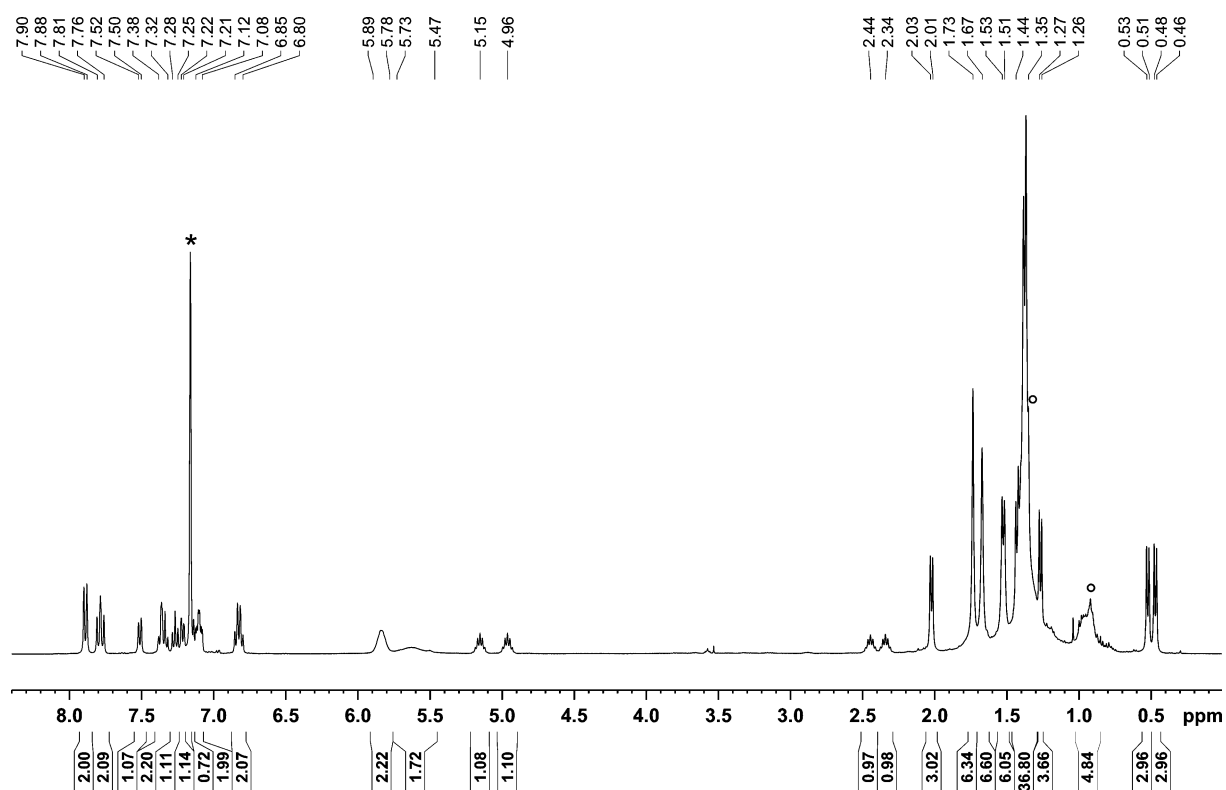


Figure S28. 1H NMR spectrum (400.13 MHz, 300 K, C_6D_6) of $[(PHDI)Co(CN)(\eta^3-P_5(Lc)_2)](OTf)$ (**4a**[OTf])·(*n*-hexane) $_{0.8}$; * C_6D_6 , o *n*-hexane.

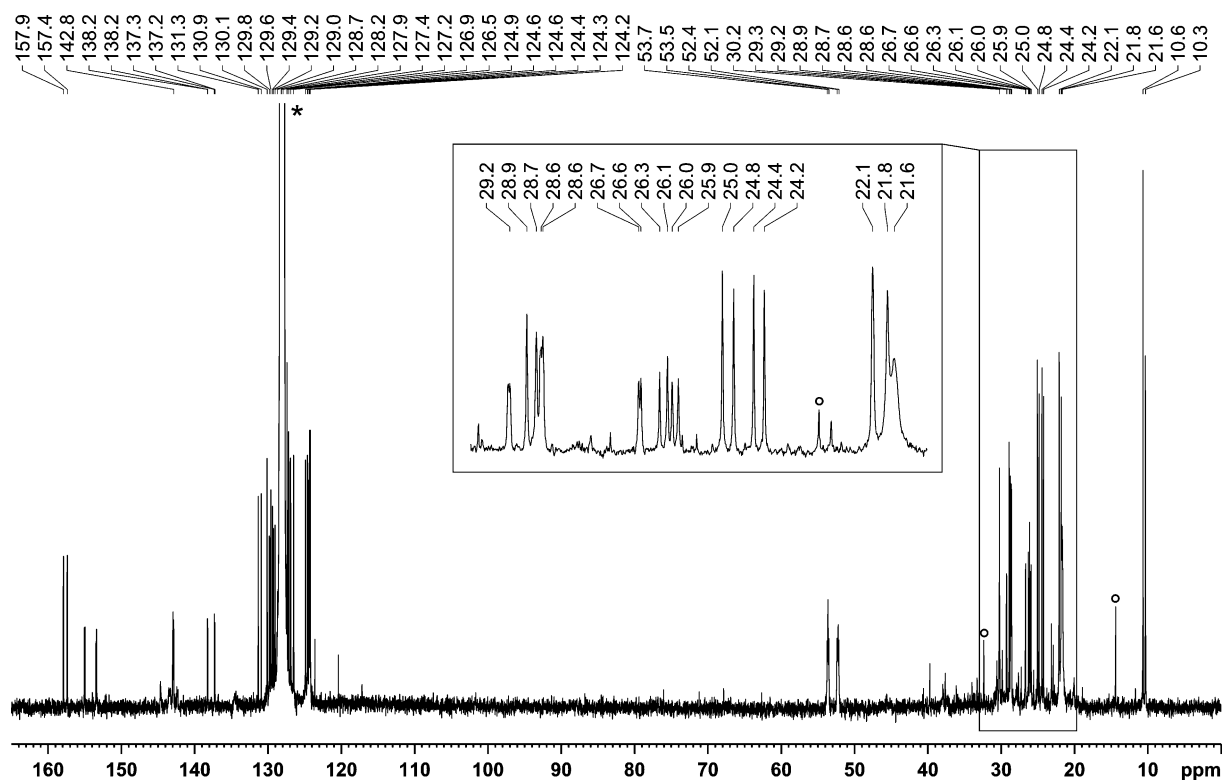


Figure S29. $^{13}\text{C}\{^1\text{H}\}$ NMR spectrum (100.61 MHz, 300 K, C_6D_6) of $[(\text{PHDI})\text{Co}(\text{CN})(\eta^3\text{-P}_5(\text{Lc})_2)][\text{OTf}] \cdot (n\text{-hexane})_{0.8}$; * C_6D_6 , o $n\text{-hexane}$.

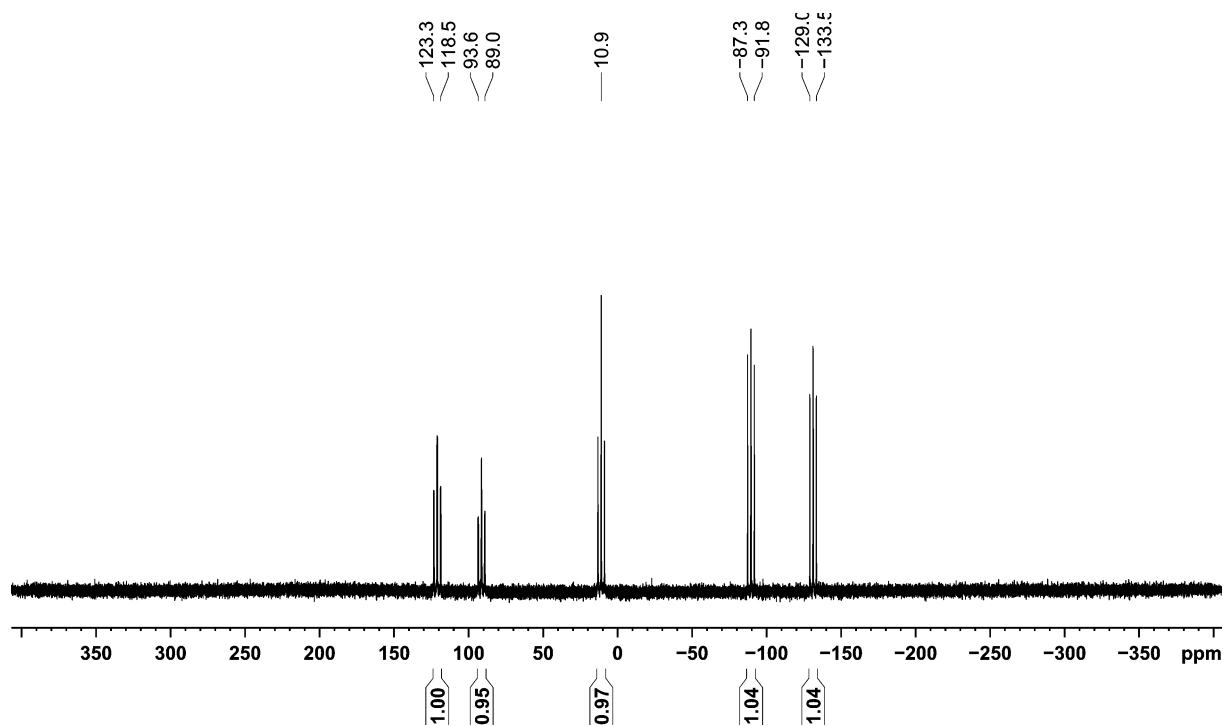


Figure S30. $^{31}\text{P}\{^1\text{H}\}$ NMR spectrum (161.98 MHz, 300 K, C_6D_6) of $[(\text{PHDI})\text{Co}(\text{CN})(\eta^3\text{-P}_5(\text{Lc})_2)][\text{OTf}] \cdot (n\text{-hexane})_{0.8}$.

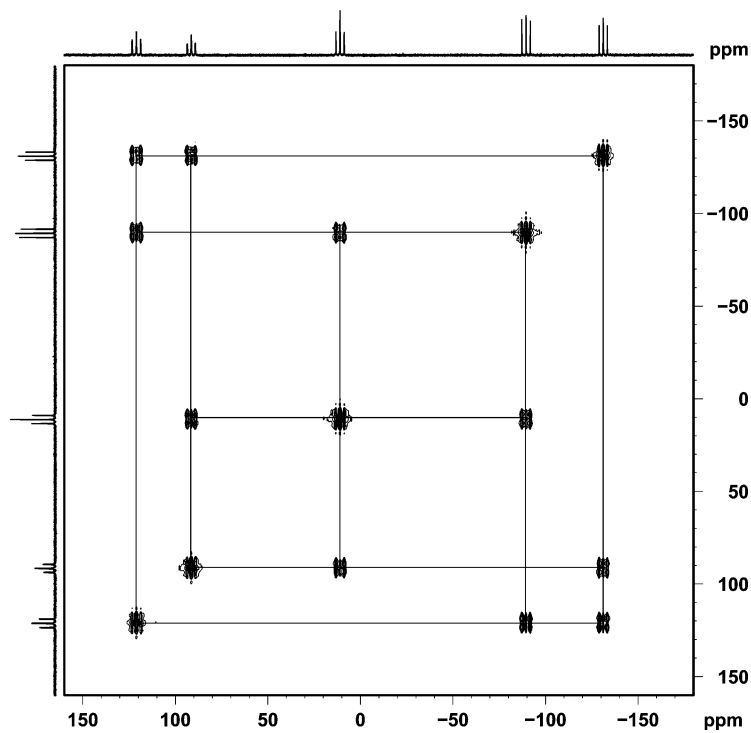


Figure S31. ^{31}P - ^{31}P -COSY NMR spectrum (161.98 MHz, 300 K, C_6D_6) of $[(\text{PHDI})\text{Co}(\text{CN})(\eta^3\text{-P}_5(\text{Lc})_2)][\text{OTf}]$ (**4a**[OTf]) $\cdot(n\text{-hexane})_{0.8}$; $^1J_{\text{PP}}$ coupling is highlighted by squares.

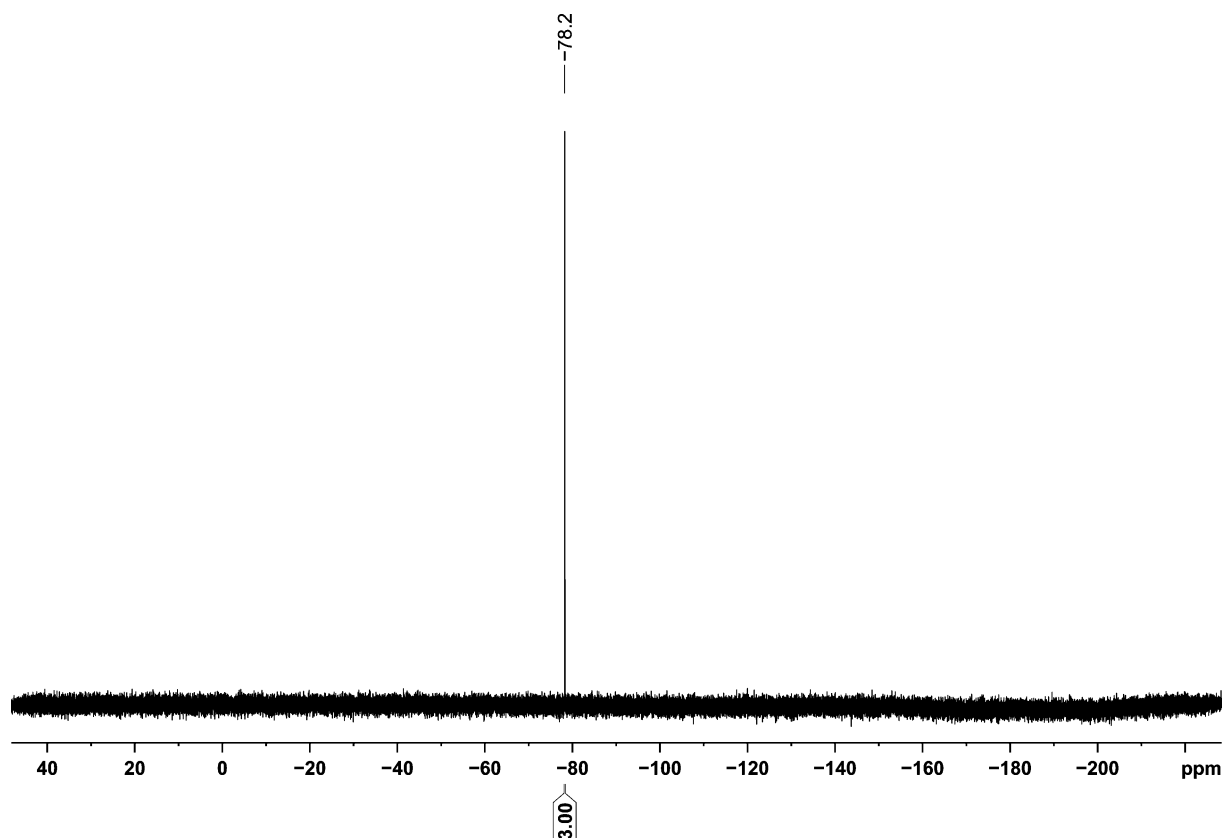


Figure S32. $^{19}\text{F}\{^1\text{H}\}$ NMR (376.66 MHz, 300 K, C_6D_6) of $[(\text{PHDI})\text{Co}(\text{CN})(\eta^3\text{-P}_5(\text{Lc})_2)][\text{OTf}]$ (**4a**[OTf]) $\cdot(n\text{-hexane})_{0.8}$.

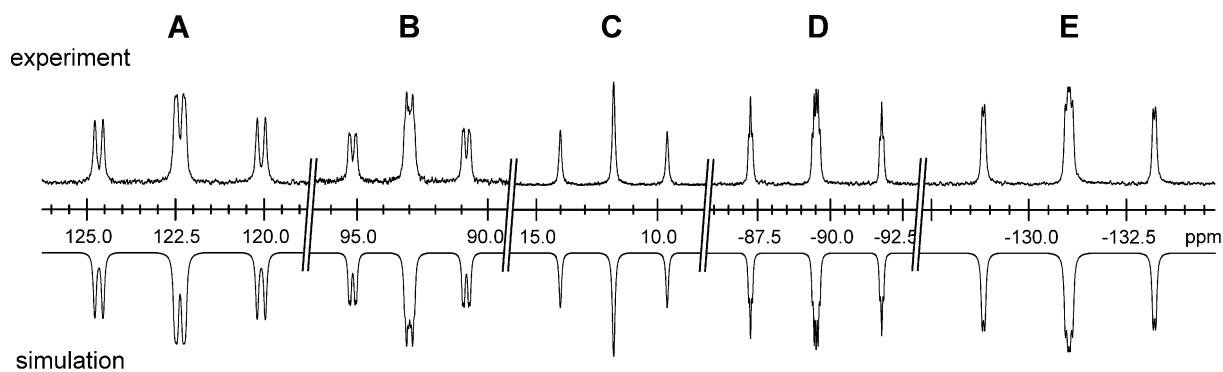
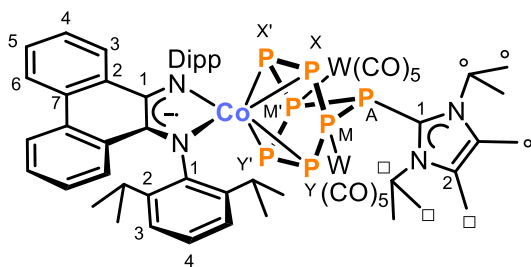


Figure S33. Section of the $^{31}\text{P}\{^1\text{H}\}$ NMR spectrum (161.98 MHz, 300 K, C_6D_6) of $[(\text{PHDI})\text{Co}(\text{CN})(\eta^3\text{-P}_5(\text{Lc})_2)][\text{OTf}]$ (**4a**[OTf]); experimental (upwards) and simulation (downwards).

Table S7. Coupling constants from the iterative fit of the ABCDE spin system and schematic representation of the $\text{CoP}_5(\text{Lc})_2$ core of $[(\text{PHDI})\text{Co}(\text{CN})(\eta^3\text{-P}_5(\text{Lc})_2)][\text{OTf}]$ (**4a**[OTf]); $\delta(\text{P}_\text{A}) = 122.4$ ppm, $\delta(\text{P}_\text{B}) = 93.0$ ppm, $\delta(\text{P}_\text{C}) = 11.8$ ppm, $\delta(\text{P}_\text{D}) = -89.5$ ppm, $\delta(\text{P}_\text{E}) = -131.0$ ppm.

	$^1J_{\text{AE}} = -365.0$ Hz	$^2J_{\text{AB}} = 37.3$ Hz
	$^1J_{\text{AD}} = -377.0$ Hz	$^2J_{\text{AC}} = 5.5$ Hz
	$^1J_{\text{BE}} = -345.1$ Hz	$^2J_{\text{CE}} = 2.2$ Hz
	$^1J_{\text{BC}} = -360.1$ Hz	$^2J_{\text{BD}} = 11.0$ Hz
	$^1J_{\text{CD}} = -354.9$ Hz	$^2J_{\text{ED}} = 10.9$ Hz

Preparation of [(PHDI)Co(μ : η^4 , κ^1 -P₅Lc){W(CO)₅}] (5a-W(CO)₅) and [(PHDI)Co(μ_3 : η^4 , η^1 , η^1 -P₇Lc){W(CO)₅}]₂ (6a-{W(CO)₅})₂



A suspension of [(Lc)₄P₄][OTf]₄ (211.1 mg, 0.146 mmol, 1.0 equiv.) in THF (7 mL) was added dropwise to a dark green solution of [K(18c-6)][(PHDI)Co(η^4 -P₄)] (319.7 mg, 0.293 mmol, 2.0 equiv.) in THF (3 mL) at ambient temperature and the blue green reaction mixture was stirred for 1.5 h. During that time, a stirred and colourless solution of [W(CO)₆] (185.5 mg, 0.527 mmol, 3.6 equiv.) in THF (1.5 mL) was irradiated

with UV-light (365 nm) for 1 h. The resulting deep yellow solution was added dropwise to the reaction mixture and stirred for an additional 2 h. The volatiles were removed and the residue was dried *in vacuo* at 35 °C for 1 h. The residue was extracted into toluene (3 × 5 mL) and filtered through a pad of silica gel (1.5 × 2 cm) and washed with toluene (7 mL). The dark blue filtrate was concentrated to 10 mL and layered with *n*-hexane (12 mL). Purple crystals were formed upon storage at room temperature for six days, which were isolated by decantation of the mother liquor, washing with *n*-hexane (2 × 5 mL) and Et₂O (1 × 5 mL) and subsequent drying *in vacuo*. As indicated by the ¹H/¹³C{¹H} NMR spectra and elemental analysis, the crystals contained 0.5 molecules of *n*-hexane per molecule of **6a**-{W(CO)₅}₂. Yield: 53.5 mg (22% based on the maximum theoretical yield of 0.146 mmol).

UV/vis (THF, λ_{\max} / nm, ϵ_{\max} / L·mol⁻¹·cm⁻¹): 320sh (55000), 360sh (40000), 540 (14000), 700 (47000).

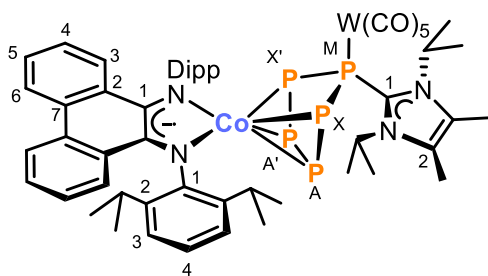
¹H NMR (400.30 MHz, 300 K, thf-*d*₈): δ / ppm = 0.51 (d, ³J_{HH} = 6.7 Hz, 12H, -CH(CH₃)₂ of Dipp), 1.46-1.54 (br m, 6H, -CH(C^oH₃)₂ of Lc), 1.60 (d, ³J_{HH} = 7.0 Hz, -CH(C^oH₃)₂ of Lc), 1.76 (d, ³J_{HH} = 6.7 Hz, 12H, -CH(CH₃)₂ of Dipp), 2.20 (s, 3H, -C^oH₃ of Lc), 2.3 (s, 3H, -C^oH₃ of Lc), 3.13-3.24 (br m, 1H, -C^oH(CH₃)₂ of Lc), 3.71 (sept., 4H, -CH(CH₃)₂ of Dipp), 4.42-4.69 (br m, 1H, -C^oH(CH₃)₂ of Lc), 6.67-6.71 (m, 2H, -C⁴H of PHDI), 6.75-6.78 (m, 2H, -C³H of PHDI), 7.40-7.44 (m, 2H, -C⁵H of PHDI), 7.48-7.50 (m, 4H, -C³H of Dipp), 7.56-7.59 (m, 2H, -C⁴H of Dipp), 8.19-8.21 (m, 2H, -C⁶H of PHDI).

¹³C{¹H} NMR (125.76 MHz, 300 K, thf-*d*₈): δ / ppm = 10.1 (s, -C^oH₃ of Lc), 10.4 (s, -C^oH₃ of Lc), 21.5 (s, -CH(C^oH₃)₂ of Lc), 22.9 (s, -CH(C^oH₃)₂ of Lc), 25.8 (s, -CH(CH₃)₂ of Dipp), 26.1 (s, -CH(CH₃)₂ of Dipp), 31.0 (s, -CH(CH₃)₂ of Dipp), 54.7 (s, -C^oH(CH₃)₂ of Lc), 124.5 (s, -C⁶H of PHDI), 125.6 (s, -C³H of Dipp), 126.2 (s, -C⁵H of PHDI), 126.9 (s, -C⁴H of PHDI), 128.1 (s, -C⁴H of Dipp), 129.3 (s, -C³H of PHDI), 129.6 (s, -C² of Lc), 130.7 (s, -C² of PHDI), 131.5 (s, -C⁷ of PHDI), 133.9 (s, -C¹ of Lc), 141.9 (s, -C² of Dipp), 147.2 (s, -C¹ of PHDI), 151.7 (s, -C¹ of Dipp), 197.0 (s, -W(CO)₅). -C^oH(CH₃)₂ of Lc, C≡N: not detected.

³¹P{¹H} NMR (162.04 MHz, 240 K, thf-*d*₈, AMM'XX'YY' spin system): δ / ppm = -181.4 - -177.1 (m, 2H, P_{YY'}), -88.3 - -81.6 (m, 2P, P_{XX'}), -47.1 - -41.9 (m, 2P, P_{MM'}), 68.6-74.0 (m, 1P, P_A), for parameters obtained by simulation, see Table S9. The convergence was only achieved if coupling constants close to zero (< 0.5 Hz) were fixed. These values are omitted in the NMR report.

IR (solid state): ν / cm⁻¹ = 2950m (CH), 2865m (CH), 2063s (CO), 1982m (CO), 1909s (CO), 1438m, 1361m, 1245w, 1053w, 933w, 791w, 752m, 721m, 590m, 570m, 494w, 420w.

Elemental analysis calcd. for C₅₉H₆₂CoN₄O₁₀P₇W₂·(C₆H₁₄)_{0.5} (Mw = 1673.68 g·mol⁻¹) C 44.49, H 4.16, N 3.35; found C 44.26, H 3.98, N 3.44.



The solvent of the mother liquor of the isolation of compound **6a-W(CO)₅**₂ was removed and the residue was extracted into Et₂O (30 mL). The solvent was reduced to 10 mL upon which a deep blue solid formed. After storage at room temperature for 1 d the suspension was filtered over a Whatman filter and the deep blue solid was dried *in vacuo*. As indicated by the ¹H/¹³C{¹H} NMR spectra and elemental analysis, the crystals contained 0.1 molecules of

toluene per molecule of **5a-W(CO)₅**. Yield: 64.3 mg (34% based on the maximum theoretical yield of 0.146 mmol).

UV/vis (THF, λ_{max} / nm, ε_{max} / L·mol⁻¹·cm⁻¹): 330 (53000), 430sh (16000), 590 (36000), 600sh (34000), 660 (53000).

¹H NMR (400.30 MHz, 300 K, C₆D₆): δ / ppm = 0.81-0.83 (m, 12H, -CH(CH₃)₂ of Dipp), 0.86-0.88 (m, 12H, -CH(CH₃)₂ of L_C overlapping with -CH₃ of L_C), 1.06 (d, ³J_{HH} = 6.8 Hz, 12H, -CH(CH₃)₂ of L_C), 1.92-1.93 (m, 12H, -CH(CH₃)₂ of Dipp), 3.92 (br m, 4H, -CH(CH₃)₂ of Dipp), 5.45-5.47 (m, 2H, -CH(CH₃)₂ of L_C), 6.80-6.85 (m, 2H, -C⁴H of PHDI), 7.08-7.11 (m, 2H, -C³H of PHDI), 7.22-7.26 (m, 2H, -C⁵H of PHDI), 7.53-7.60 (m, 6H, -C³H of Dipp overlapping with -C⁴H of Dipp), 7.95-7.97 (m, 2H, -C⁶H of PHDI).

¹³C{¹H} NMR (100.65 MHz, 300 K, C₆D₆): δ / ppm = 9.4 (s, -CH₃ of L_C), 20.6 (s, -CH(CH₃)₂ of L_C), 21.2 (s, -CH(CH₃)₂ of L_C), 25.2 (s, -CH(CH₃)₂ of Dipp), 26.0 (s, -CH(CH₃)₂ of Dipp), 30.1 (s, -CH(CH₃)₂ of Dipp), 50.6 (s, -CH(CH₃)₂ of L_C), 124.3 (s, -C⁶ of PHDI), 125.0 (s, -C³ or -C⁴ of Dipp), 125.5 (s, -C⁵ of PHDI), 126.5 (s, -C² of L_C), 126.7 (s, -C⁴ of PHDI), 127.3 (s, -C³ or -C⁴ of Dipp), 128.9 (s, -C³ of PHDI), 130.4 (s, -C² of PHDI), 130.9 (s, -C⁷ of PHDI), 141.3 (s, -C² of Dipp), 148.1 (s, -C¹ of PHDI), 154.1 (s, -C¹ of Dipp), 197.5 (s, -W(CO)₅). C≡N, -C¹ of L_C: not detected.

³¹P{¹H} NMR (162.04 MHz, 300 K, C₆D₆, AA'MXX' spin system): δ / ppm = -90.3 - -82.3 (m, 2H, P_{XX'}), 50.8-55.5 3 (m, 1H, P_M), 79.2-85.5 (m, 2H, P_{AA'}), for parameters obtained by simulation, see Table S8.

IR (solid state): ν / cm⁻¹ = 2950m (CH), 2870m (CH), 2060s (CO), 1980m (CO), 1910vs (CO), 1630w, 1140m, 1360m, 1250w, 1050w, 933w, 791w, 752m, 725m, 594s, 571s, 478m, 436m.

Elemental analysis calcd. for C₅₄H₆₂CoN₄O₅P₅W·(C₇H₈)_{0.1} (Mw = 1253.97 g·mol⁻¹) C 52.39, H 5.05, N 4.47; found C 52.40, H 4.99, N 4.23.

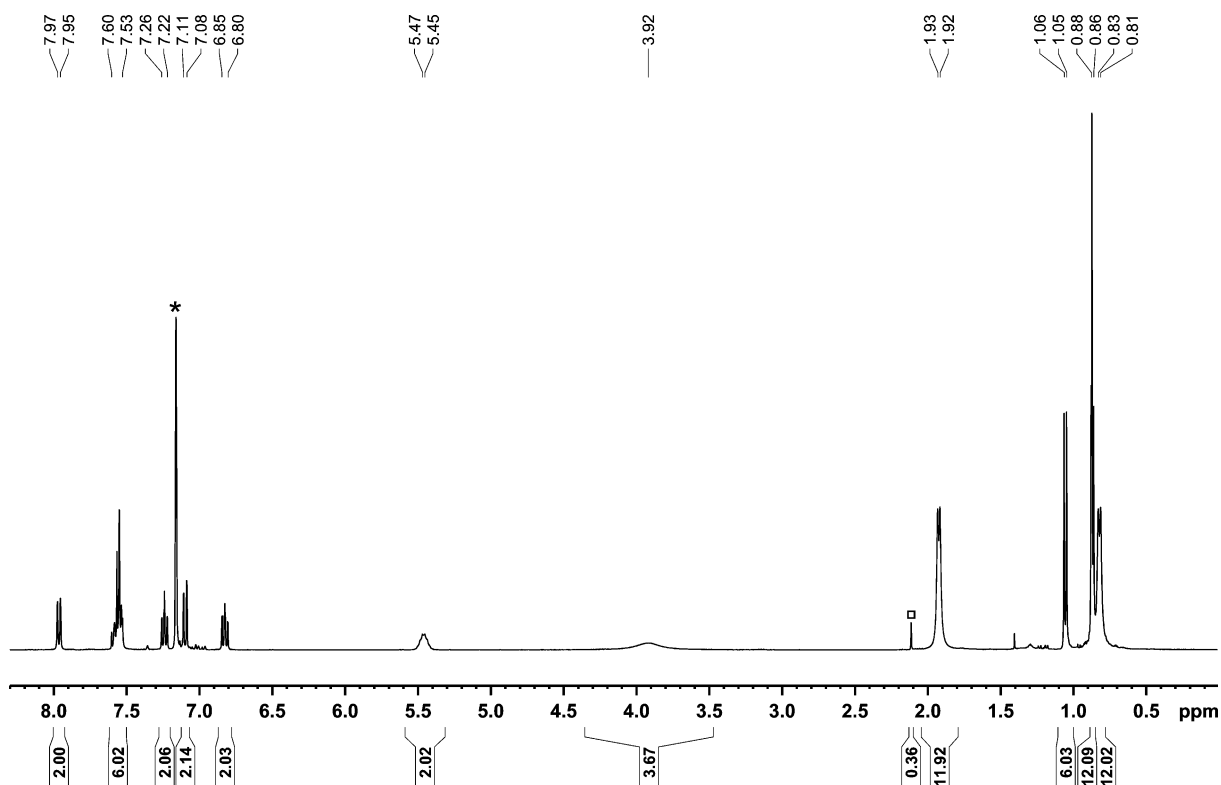


Figure S34. ^1H NMR spectrum (400.30 MHz, 300 K, C_6D_6) of $[(\text{PHDI})\text{Co}(\mu:\eta^4, \kappa^1\text{-P}_5\text{Lc})\{\text{W}(\text{CO})_5\}] (\mathbf{5a}\text{-W}(\text{CO})_5)\cdot(\text{toluene})_{0.1}$; * C_6D_6 , \square toluene.

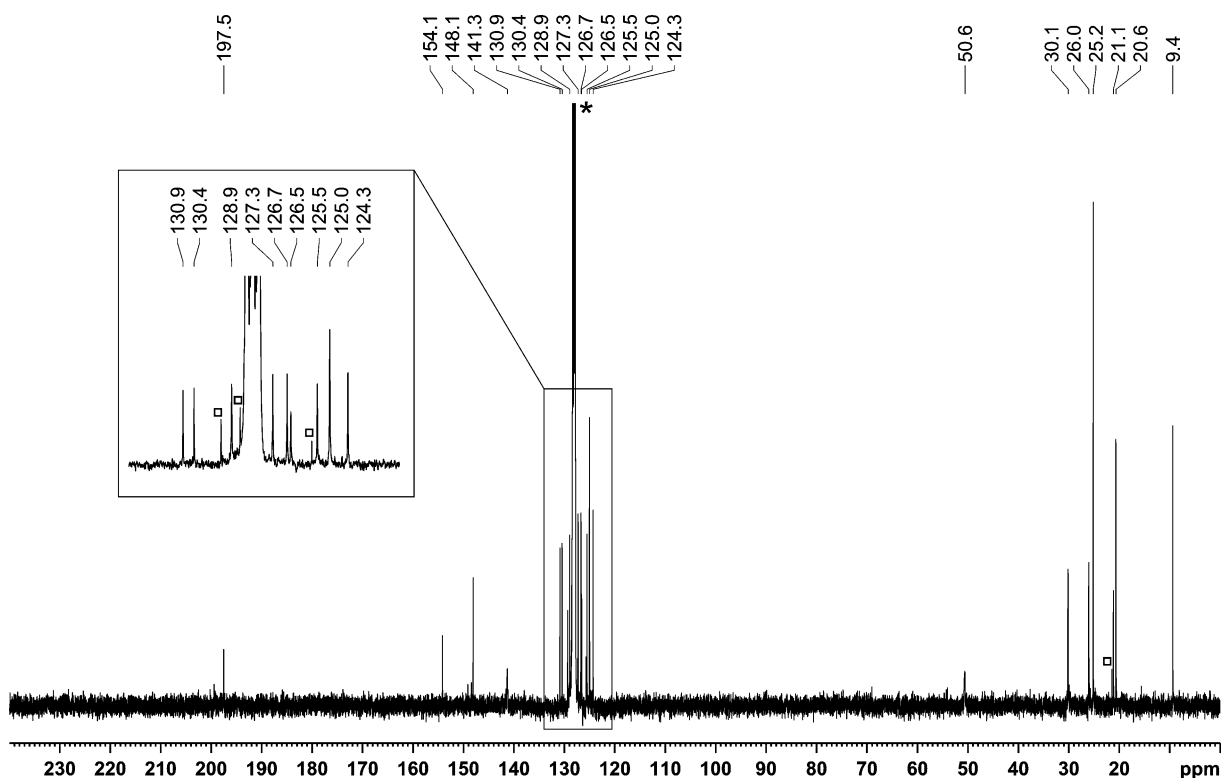


Figure S35. $^{13}\text{C}\{^1\text{H}\}$ NMR spectrum (100.65 MHz, 300 K, C_6D_6) of $[(\text{PHDI})\text{Co}(\mu:\eta^4, \kappa^1\text{-P}_5\text{Lc})\{\text{W}(\text{CO})_5\}] (\mathbf{5a}\text{-W}(\text{CO})_5)\cdot(\text{toluene})_{0.1}$; * C_6D_6 , \square toluene.

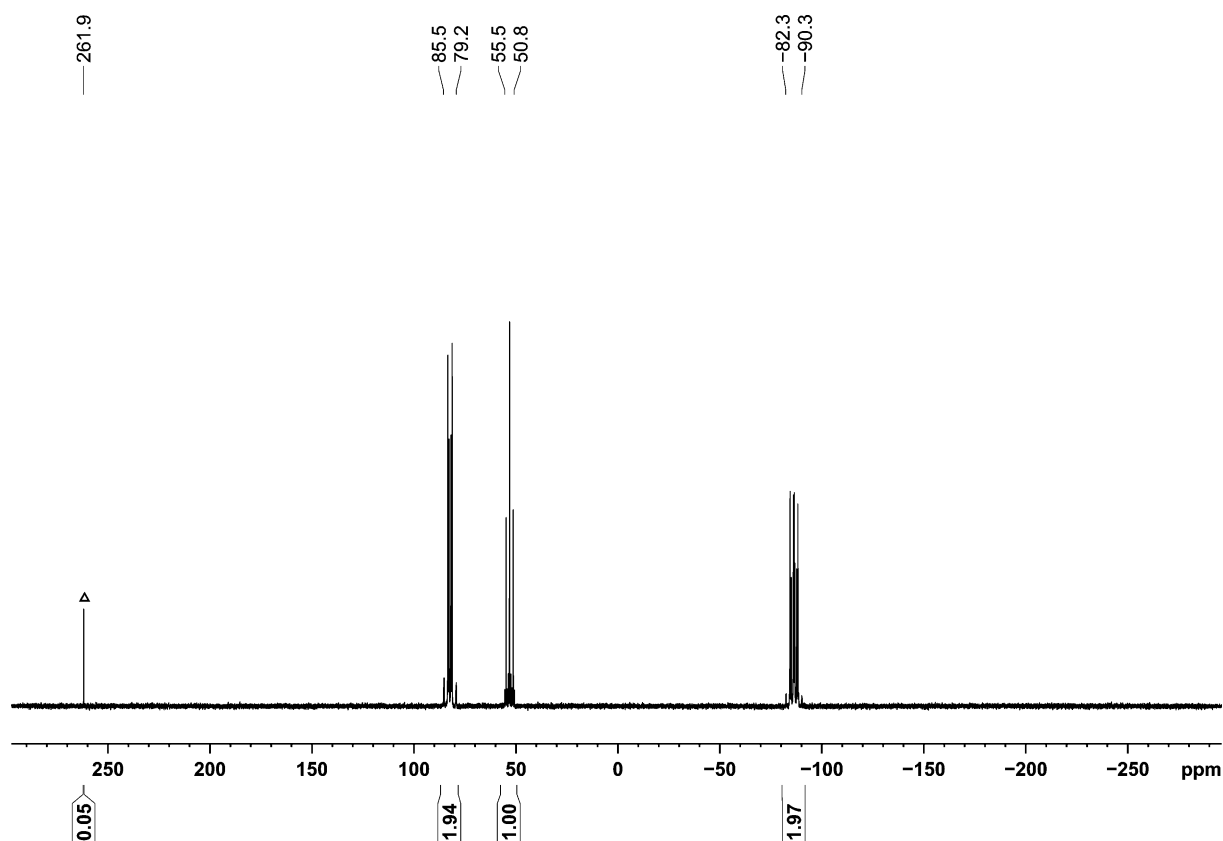


Figure S36. $^{31}\text{P}\{^1\text{H}\}$ NMR spectrum (162.04 MHz, 300 K, C_6D_6) of $[(\text{PHDI})\text{Co}(\mu:\eta^4, \kappa^1\text{-P}_5\text{Lc})\{\text{W}(\text{CO})_5\}]$ (**5a-W(CO)₅**)·(toluene)_{0.1}; Δ $[(\text{PHDI})\text{Co}]_2(\mu, \eta^4:\eta^4\text{-P}_4)$.^[15]

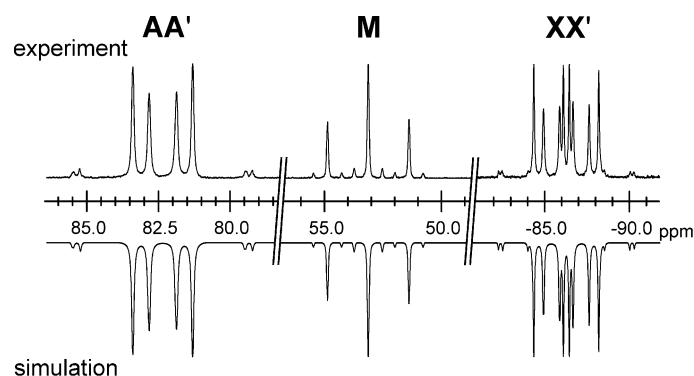
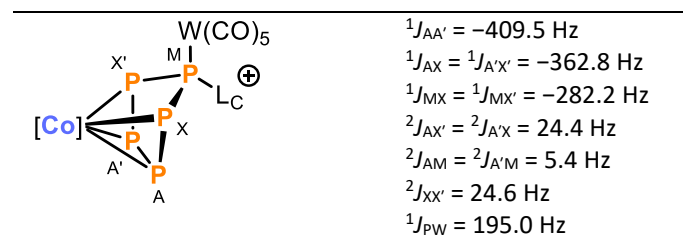


Figure S37. Section of the $^{31}\text{P}\{^1\text{H}\}$ NMR spectrum (162.04 MHz, 300 K, C_6D_6) of $[(\text{PHDI})\text{Co}(\mu:\eta^4, \kappa^1\text{-P}_5\text{Lc})\{\text{W}(\text{CO})_5\}]$ (**5a-W(CO)₅**); experimental (upwards) and simulation (downwards).

Table S8. Coupling constant from the iterative fit of the AA'MXX' spin system and schematic representation of the CoP_5Lc core of $[(\text{PHDI})\text{Co}(\mu:\eta^4, \kappa^1\text{-P}_5\text{Lc})\{\text{W}(\text{CO})_5\}]$ (**5a-W(CO)₅**); $\delta(\text{P}_{\text{AA}'}) = 82.3$ ppm, $\delta(\text{P}_{\text{M}}) = 53.1$ ppm, $\delta(\text{P}_{\text{XX}'}) = -86.3$ ppm.



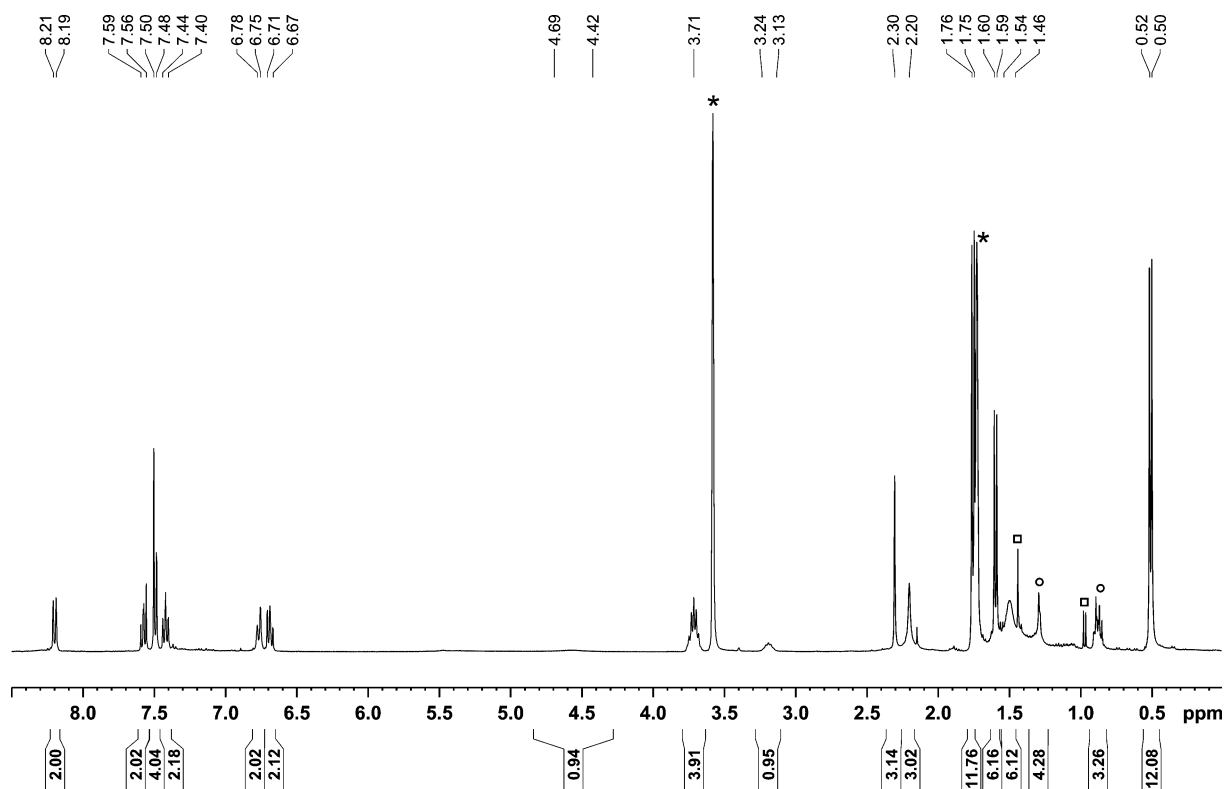


Figure S38. ^1H NMR spectrum (400.30 MHz, 300 K, $\text{thf-}d_8$) of $[(\text{PHDI})\text{Co}(\mu^3\text{-}\eta^4, \eta^1, \eta^1\text{-P}_7\text{Lc})\{\text{W}(\text{CO})_5\}_2]$ (**6a**- $\{\text{W}(\text{CO})_5\}_2$) $\cdot(n\text{-hexane})_{0.5}$; * $\text{thf-}d_8$, \circ $n\text{-hexane}$, \square minor unknown impurities.

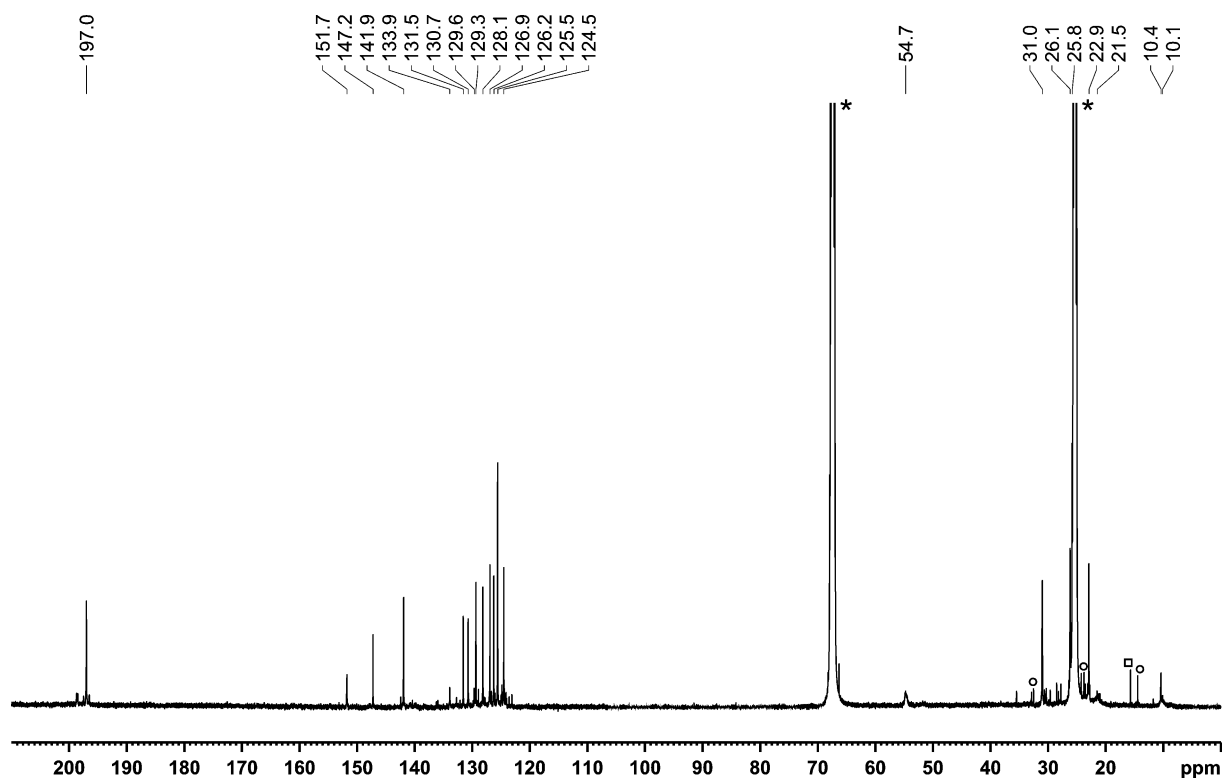


Figure S39. $^{13}\text{C}\{^1\text{H}\}$ NMR spectrum (125.76 MHz, 300 K, $\text{thf-}d_8$) of $[(\text{PHDI})\text{Co}(\mu^3:\eta^4,\eta^1,\eta^1\text{-P}_7\text{Lc})\{\text{W}(\text{CO})_5\}_2]$ (**6a-W(CO)₅**)₂·(*n*-hexane)_{0.5}; * $\text{thf-}d_8$, \circ *n*-hexane, \square minor unknown impurity.

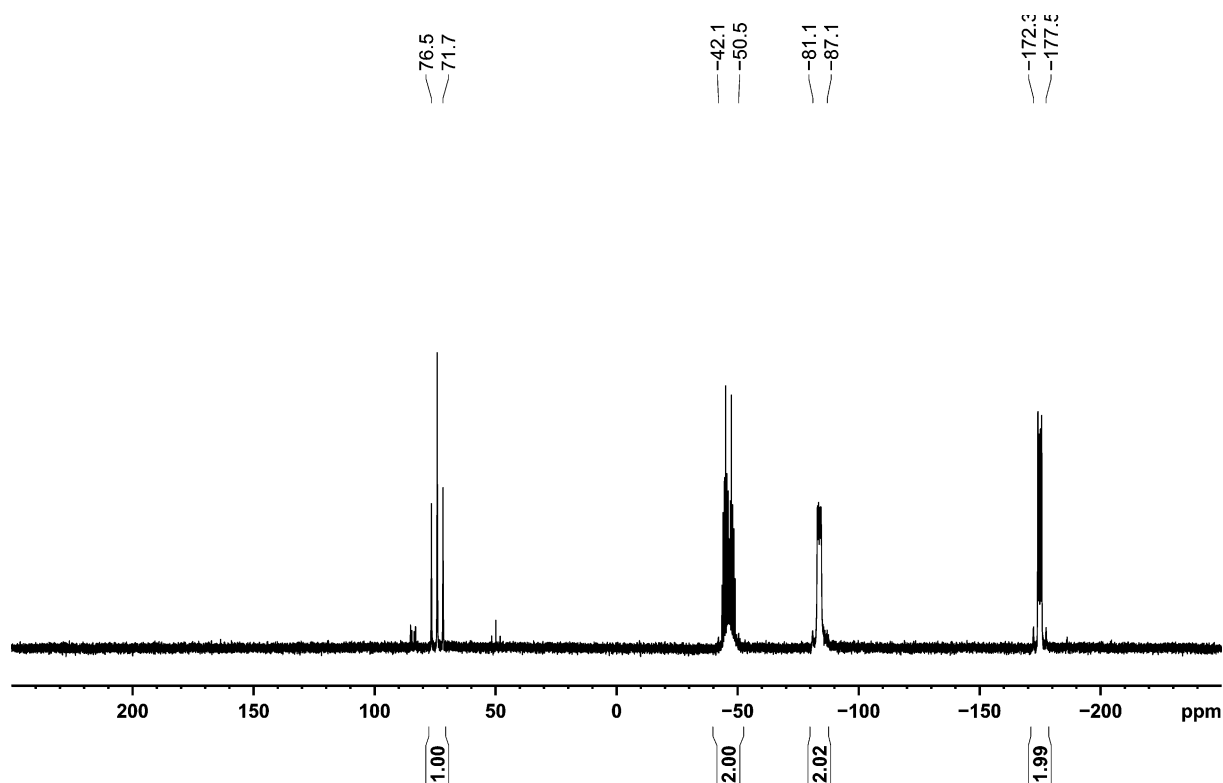


Figure S40. $^{31}\text{P}\{^1\text{H}\}$ NMR spectrum (161.98 MHz, 320 K, $\text{thf-}d_8$) of $[(\text{PHDI})\text{Co}(\mu^3:\eta^4,\eta^1,\eta^1\text{-P}_7\text{Lc})\{\text{W}(\text{CO})_5\}_2]$ (**6a-W(CO)₅**)₂·(*n*-hexane)_{0.5}.

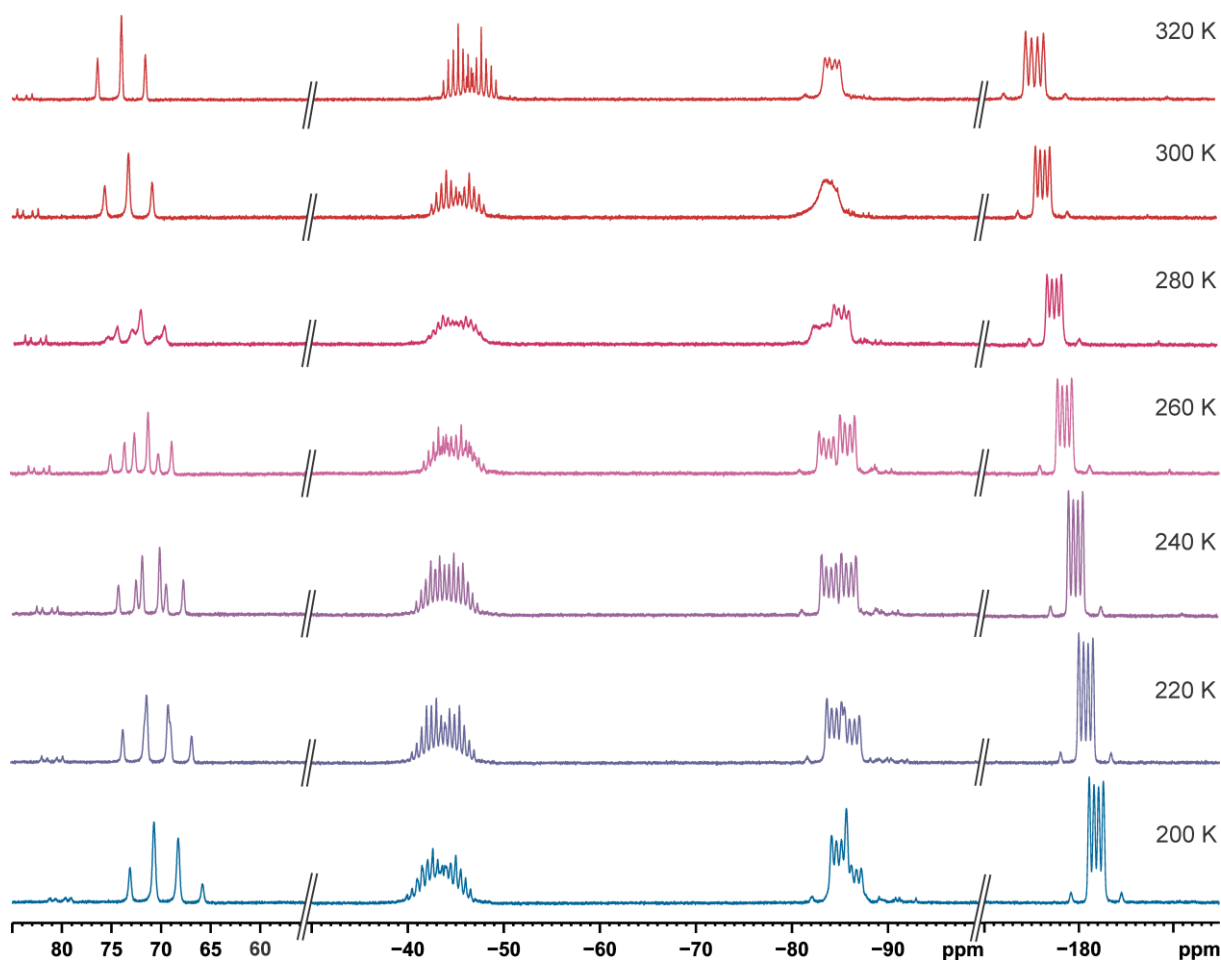


Figure S41. Variable temperature $^{31}\text{P}\{^1\text{H}\}$ NMR spectra (161.98 MHz, $\text{thf-}d_8$) of $[(\text{PHDI})\text{Co}(\mu^3\text{:}\eta^4, \eta^1, \eta^1\text{-P}_7\text{Lc})\{\text{W}(\text{CO})_5\}_2]$ (**6a**- $\{\text{W}(\text{CO})_5\}_2$).

Variable temperature (VT) $^{31}\text{P}\{^1\text{H}\}$ NMR spectroscopy revealed the presence of a second isomer in solution at low temperatures, as deduced from the splitting of the resonances at $\delta = 74.0$ ppm (P_A), $\delta = -46.3$ ppm ($\text{P}_{MM'}$) and $\delta = -83.8$ ppm ($\text{P}_{XX'}$). At room temperature, the two isomers are in fast equilibrium on the NMR time scale, which is slowed down at low temperature. The second isomer might arise from the hindered rotation of an *iPr* group of the L_C -substituents. The ^1H NMR spectrum of **6a**- $\{\text{W}(\text{CO})_5\}_2$ recorded at room temperature supports this proposal due to the broadened signals of only one of the *iPr* groups, suggesting dynamic behavior (Figure S38). Additionally, distinct positional disorder of one *iPr* group is observed in the solid-state structure of **6a**- $\{\text{W}(\text{CO})_5\}_2$ (Figure S87).

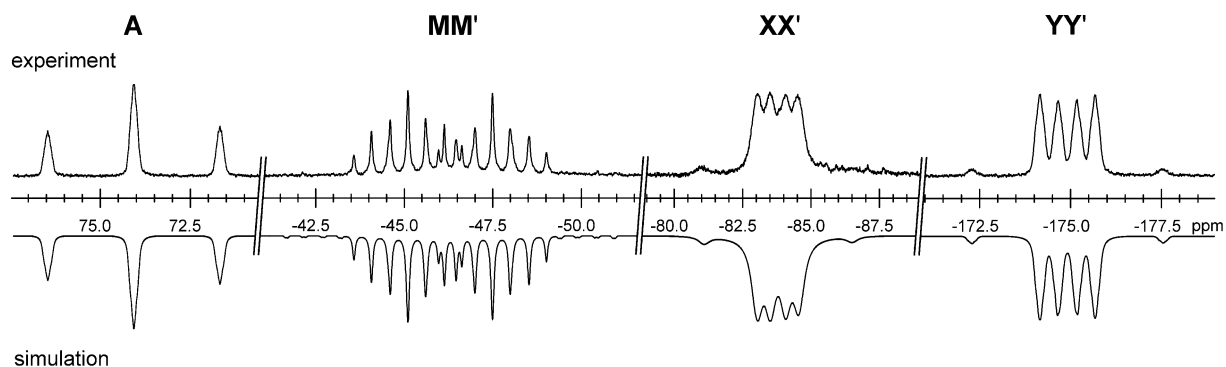
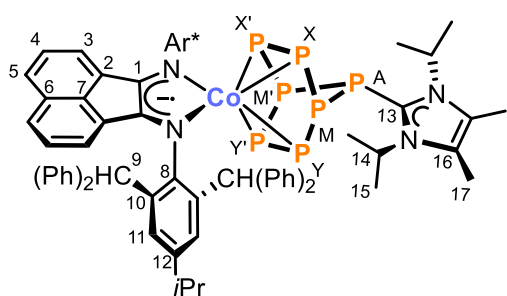


Figure S42. Section of the $^{31}\text{P}\{^1\text{H}\}$ NMR spectrum (161.98 MHz, 320 K, C_6D_6) of $[(\text{PHDI})\text{Co}(\mu^3:\eta^4,\eta^1,\eta^1\text{-P}_7\text{Lc})\{\text{W}(\text{CO})_5\}_2]$ (**6a**- $\{\text{W}(\text{CO})_5\}_2$); experimental (upwards) and simulation (downwards).

Table S9. Coupling constant from the iterative fit of the $\text{AMM}'\text{XX}'\text{YY}'$ spin system and schematic representation of the CoP_7Lc core $[(\text{PHDI})\text{Co}(\mu^3:\eta^4,\eta^1,\eta^1\text{-P}_7\text{Lc})\{\text{W}(\text{CO})_5\}_2]$ (**6a**- $\{\text{W}(\text{CO})_5\}_2$); $\delta(\text{P}_A) = 74.0$ ppm, $\delta(\text{P}_{\text{MM}'}) = -46.3$ ppm, $\delta(\text{P}_{\text{XX}'}) = -83.8$ ppm, $\delta(\text{P}_{\text{YY}'}) = -174.9$ ppm.

	$^1J_{\text{XX}'} = -393.6$ Hz
	$^1J_{\text{YY}'} = -383.6$ Hz
	$^1J_{\text{AM}} = ^1J_{\text{AM}'} = -387.4$ Hz
	$^1J_{\text{MX}} = ^1J_{\text{M}'\text{X}'} = -264.0$ Hz
	$^1J_{\text{MY}} = ^1J_{\text{M}'\text{Y}'} = -257.1$ Hz
	$^2J_{\text{AY}} = ^2J_{\text{A}'\text{Y}'} = 15.8$ Hz
	$^2J_{\text{AX}} = ^2J_{\text{A}'\text{X}'} = 6.7$ Hz
	$^2J_{\text{MY}'} = ^2J_{\text{M}'\text{Y}} = 10.8$ Hz
	$^2J_{\text{MX}'} = ^2J_{\text{M}'\text{X}} = 16.8$ Hz
	$^2J_{\text{XY}} = ^2J_{\text{X}'\text{Y}'} = 23.0$ Hz
$^3J_{\text{XY}'} = ^3J_{\text{X}'\text{Y}} = -0.6$ Hz	

Preparation of [(Ar*BIAN)Co(η^2 : η^2 -P₇Lc)] (6b)



[(Lc)₄P₄][OTf]₄ (69 mg, 0.048 mmol, 0.5 eq.) was added to a deep purple solution of [K(18c-6)][(Ar*BIAN)Co(η^4 -P₄)] (150 mg, 0.096 mmol, 1.0 eq.) in THF (4 mL). After stirring at ambient temperature overnight, the color had changed to a deep blue and volatiles were removed *in vacuo*. The dark solid was extracted with 1,4-dioxane (5 × 1 mL) and the extracts were filtered over a pad of silica (2 × 0.5 cm) and washed with 1,4-dioxane (2 × 1 mL). The volume of the dark blue filtrate was

reduced to approximately 5 mL and layered with *n*-hexane (20 mL). After five days shimmering dark blue crystals have formed, which were isolated by decantation of the mother liquor, washed with *n*-hexane (4 × 1 mL) and dried *in vacuo*. To remove residual [K(18c-6)]OTf the solids were dissolved in toluene (4 mL) and filtered over a pad of silica (2 × 0.5 cm) and washed with 1,4-dioxane (2 × 1 mL). All volatiles were removed under vacuum and the residue was washed with *n*-hexane (3 × 1 mL) and dried *in vacuo*. Yield: 57 mg (78% based on the maximum theoretical yield of 0.048 mmol).

¹H NMR (400.13 MHz, 300 K, C₆D₆): δ / ppm = 0.60 (d, ³J_{HH} = 6.6 Hz, 12H, -C¹⁵H), 1.01 (s, 6H, -C¹⁷H), 1.18 (d, ³J_{HH} = 6.9 Hz, 12H, -CH(CH₃)₂ of *i*Pr), 2.77 (sept, ³J_{HH} = 6.9 Hz, 2H, -CH(CH₃)₂ of *i*Pr), 3.67 (br s, 2H, -C¹⁴H), 5.58 (d, ³J_{HH} = 7.1 Hz, 2H, -C³H of BIAN), 6.36 – 6.40 (m, 2H, -C⁴H of BIAN), 6.65 – 6.68 (m, 4H, -CH_{Ar} of Ph), 6.73 – 6.79 (m, 12H, -CH_{Ar} of Ph overlapping with -C⁹H(Ph)₂), 7.13 – 7.17 (m, 6H, -CH_{Ar} of Ph overlapping with C₆D₆ solvent signal), 7.23 – 7.27 (m, 10H, -CH_{Ar} overlapping with -C⁵H of BIAN), 7.54 (s, 4H, -C¹¹H), 7.92 – 7.94 (m, 8H, -CH_{Ar} of Ph).

¹³C{¹H} NMR (100.61 MHz, 300 K, C₆D₆): δ / ppm = 9.4 (s, -C¹⁷H), 20.9 (s, -C¹⁵H), 24.2 (s, -CH(CH₃)₂ of *i*Pr), 34.0 (s, -CH(CH₃)₂ of *i*Pr), 52.2 (s, -C⁹H(Ph)₂), 52.4 (br s, -C¹⁴H), 120.4 (s, -C³H of BIAN), 122.7 (s, -C⁵H of BIAN), 125.7 (s, -C_{Ar}H of Ph), 126.0 (s, -C_{Ar}H of Ph), 127.7 (s, -C⁴H of BIAN overlapping with C₆D₆ solvent signal), 127.8 (s, -C¹⁶ overlapping with C₆D₆ solvent signal), 127.9 (s, -C_{Ar}H of Ph overlapping with C₆D₆ solvent signal), 128.0 (s, -C¹¹H overlapping with C₆D₆ solvent signal), 128.1 (s, -C_{Ar}H of Ph overlapping with C₆D₆ solvent signal), 130.3 (s, -C² of BIAN), 130.8 (s, -C_{Ar}H of Ph), 131.6 (s, -C_{Ar}H of Ph), 134.1 (s, -C⁶ of BIAN), 136.1 (s, -C¹⁰), 136.9 (s, -C⁷ of BIAN), 144.7 (s, -C¹²), 145.0 (s, -C_{Ar} of Ph), 146.5 (s, -C_{Ar} of Ph), 152.6 (s, -C¹=N of BIAN), 154.9 (s, -C⁸N).

³¹P{¹H} NMR (202.46 MHz, 300 K, thf-*d*₈, AMM'XX'YY' spin system) δ / ppm = -139.9 - -136.2 (m, 2P, P_{YY'}), -78.7 – 74.9 (m, 2P, P_{XX'}), -27.2 – 21.2 (m, 2P, P_{MM'}), 48.3 – 51.8 (m, 1P, P_A).

UV/Vis (toluene, λ_{\max} / nm, ϵ_{\max} / L·mol⁻¹·cm⁻¹): 320sh (13000), 440 (6000), 560 (9000), 660 (14000).

Elemental analysis calcd. for C₉₃H₈₈CoN₄P₇ (Mw = 1537.5 g·mol⁻¹): C 72.65, H 5.77, N 3.64; found C 73.06, H 6.24, N 3.48.

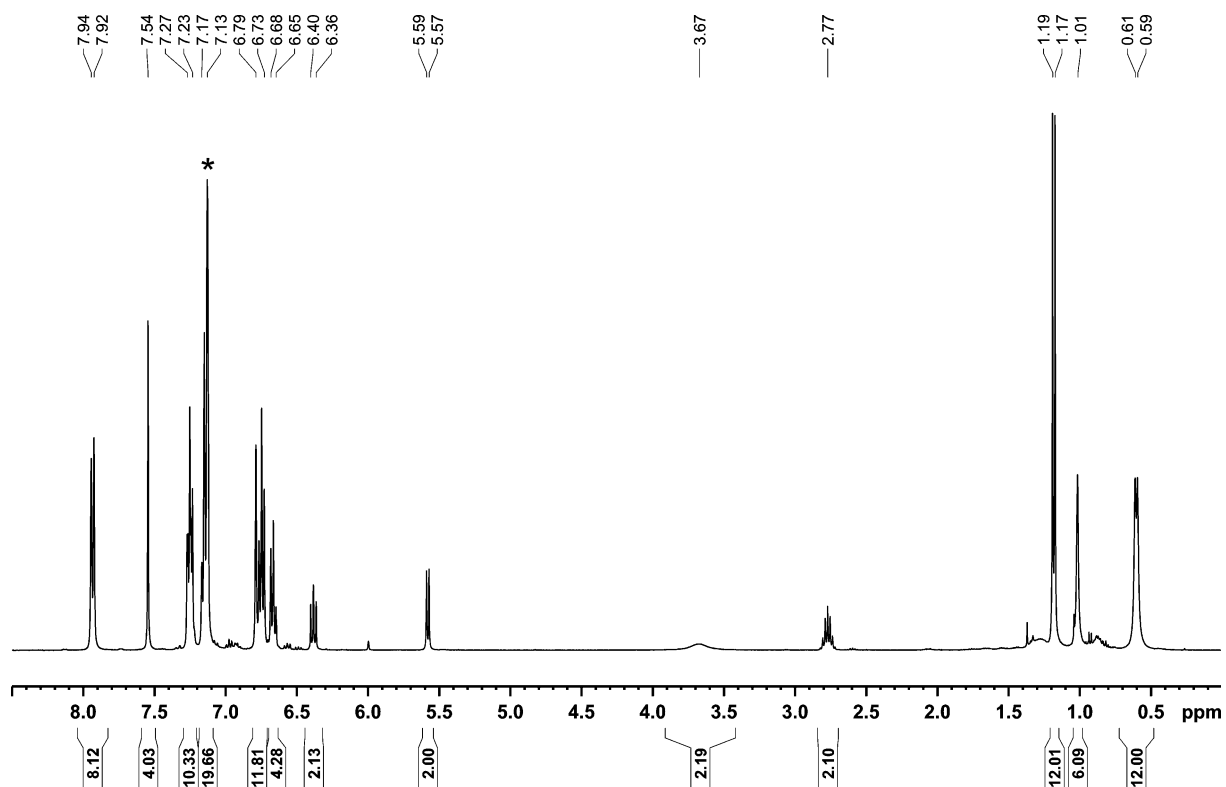


Figure S43. ^1H NMR spectrum (400.13 MHz, 300 K, C_6D_6) of $[(\text{Ar}^*\text{BIAN})\text{Co}(\eta^2:\eta^2\text{-P}_7\text{Lc})]$ (**6b**); * C_6D_6 .

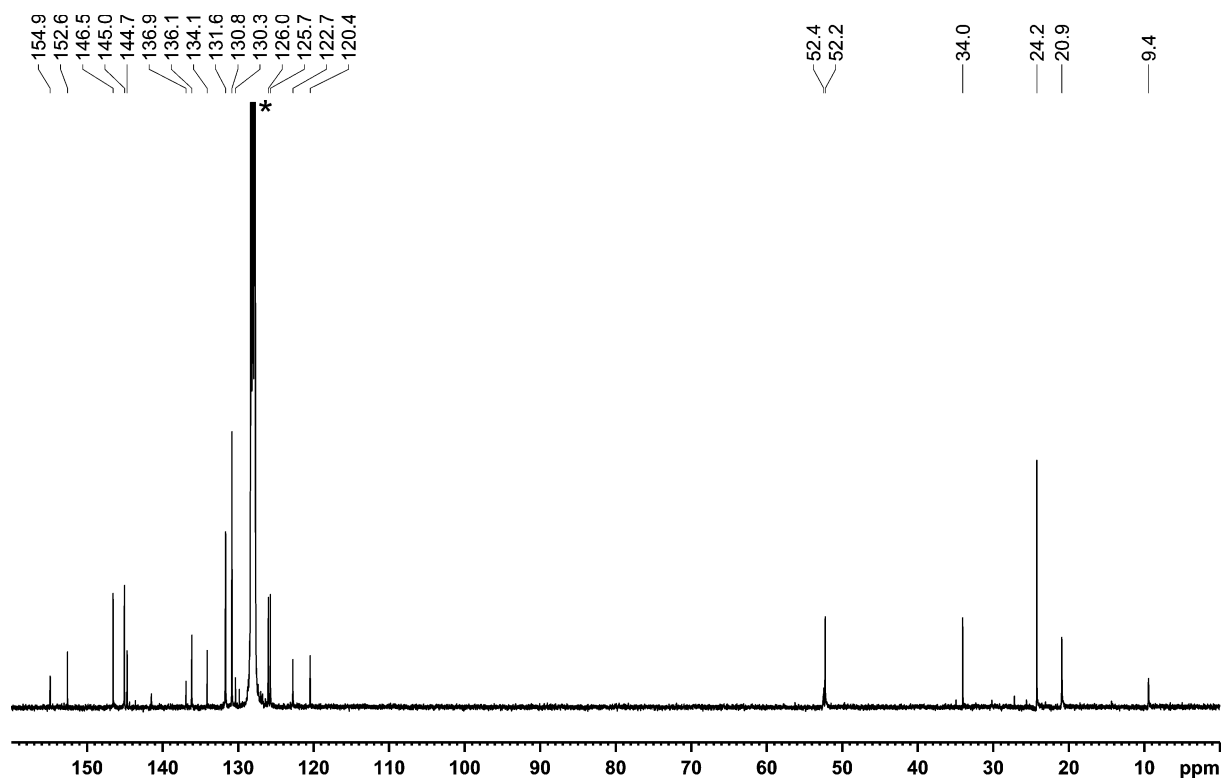


Figure S44. $^{13}\text{C}\{^1\text{H}\}$ NMR spectrum (100.61 MHz, 300 K, C_6D_6) of $[(\text{Ar}^*\text{BIAN})\text{Co}(\eta^2:\eta^2\text{-P}_7\text{Lc})]$ (**6b**); * C_6D_6 .

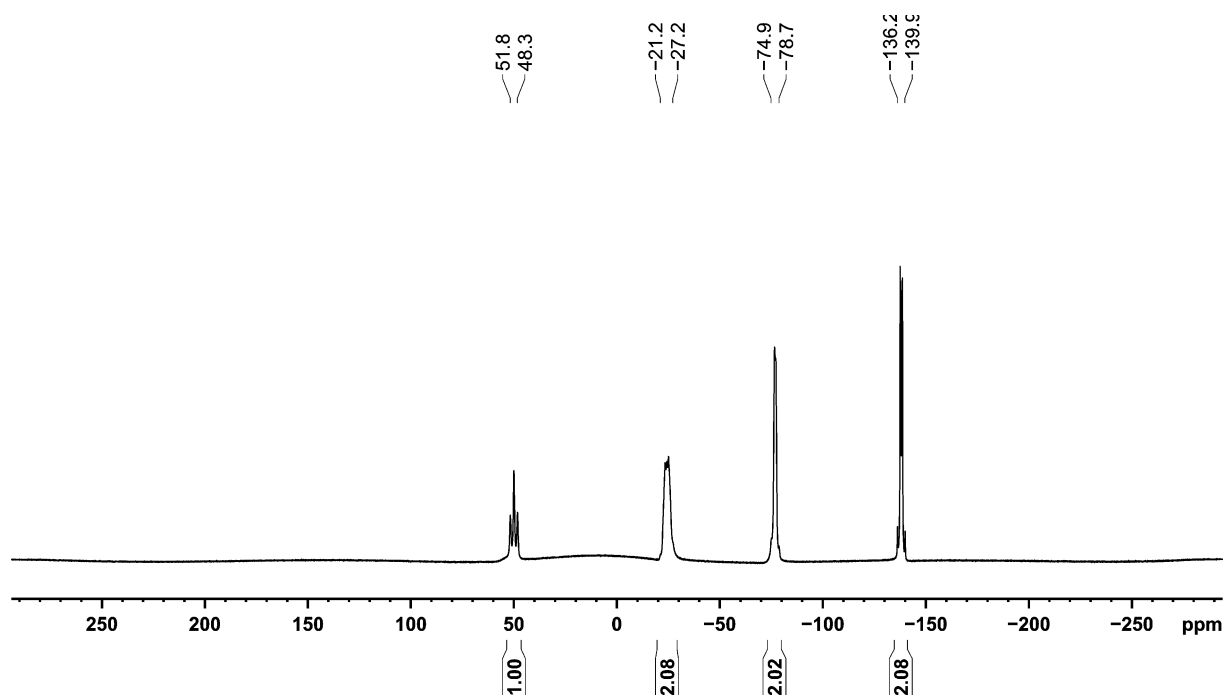


Figure S45. $^{31}\text{P}\{^1\text{H}\}$ NMR spectrum (202.46 MHz, 300 K, thf-d_8) of $[(\text{Ar}^*\text{BIAN})\text{Co}(\eta^2:\eta^2\text{-P7Lc})]$ (**6b**).

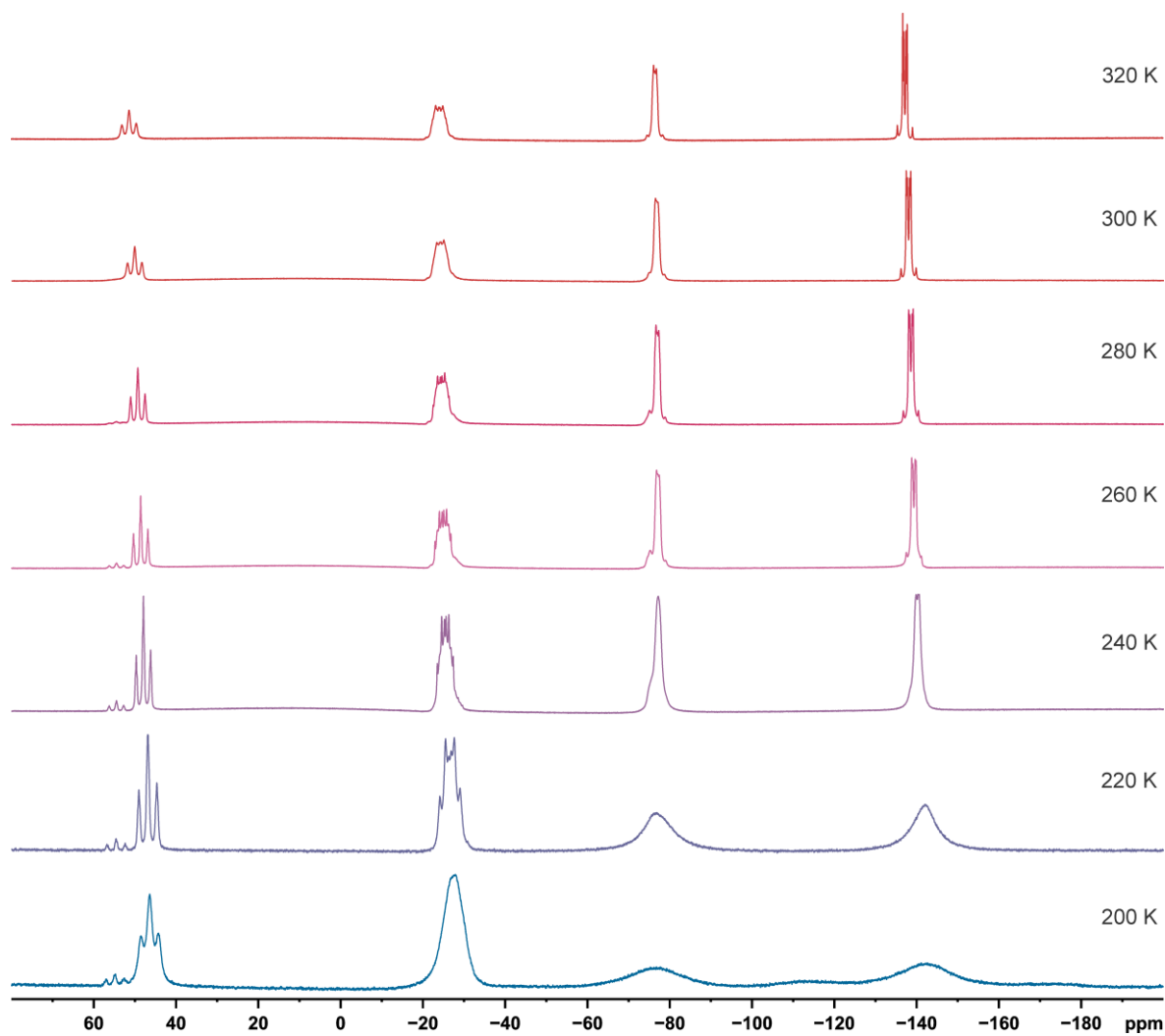


Figure S46. Variable temperature $^{31}\text{P}\{^1\text{H}\}$ NMR spectra (202.46 MHz, thf-d_8) of $[(\text{Ar}^*\text{BIAN})\text{Co}(\eta^2:\eta^2\text{-P7Lc})]$ (**6b**).

2. VT $^{31}\text{P}\{^1\text{H}\}$ NMR reaction monitoring

$[\text{K}(\mathbf{18c-6})][(\text{PHDI})\text{Co}(\eta^4\text{-P}_4)]$ (**J**) + 0.5 $[(\text{Lc})_4\text{P}_4][\text{OTf}]_4$ (**G** $[\text{OTf}]_4$)

G $[\text{OTf}]_4$ (17.4 mg, 0.01 mmol, 0.5 equiv.) was submitted to a J. Young valve NMR tube and cooled to -80°C . A solution of **J** (25 mg, 0.02 mmol, 1.0 equiv.) in $\text{thf-}d_8$ (0.6 mL) at -80°C was added to the J. Young valve NMR tube. The measurements were performed in a temperature range from 200 K to 300 K in 20 K steps. Note: Compounds **5a**- $\text{W}(\text{CO})_5$ and **6a**- $\text{W}(\text{CO})_5)_2$ were isolated and characterized as their respective $[\text{W}(\text{CO})_5]$ adducts, however no $[\text{W}(\text{CO})_5](\text{THF})$ was added to this reaction to prevent the formation of isomers of compound **5a** (*vide infra*, Figure S61). Thus, the $^{31}\text{P}\{^1\text{H}\}$ NMR chemical shifts of the products differ from those of the isolated compounds (see Figure S36, Figure S40).

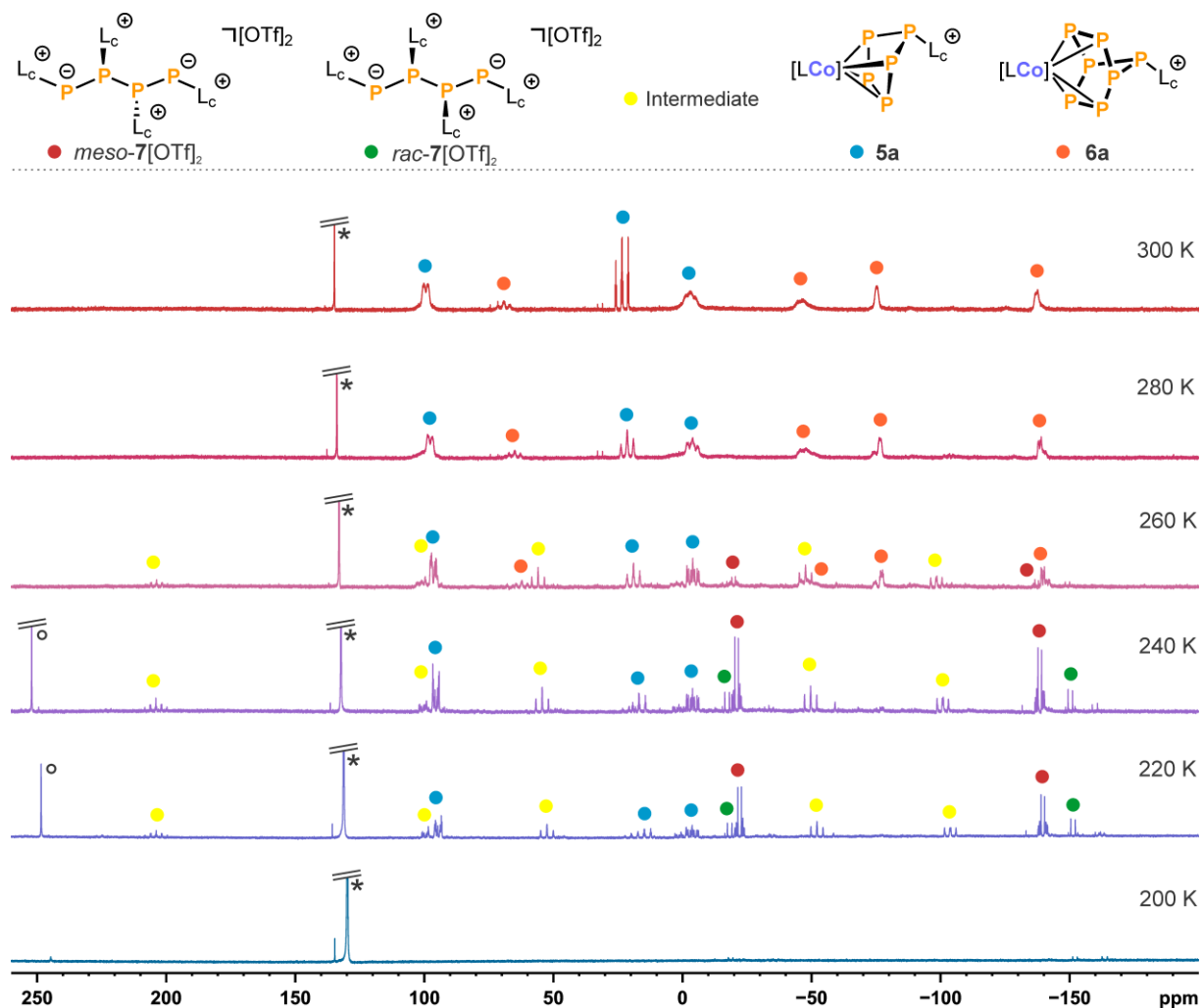


Figure S47. $^{31}\text{P}\{^1\text{H}\}$ VT NMR monitoring (161.98 MHz, $\text{thf-}d_8$) of the reaction between $[\text{K}(\mathbf{18c-6})][(\text{PHDI})\text{Co}(\eta^4\text{-P}_4)]$ (**J**, marked with *) + 0.5 $[(\text{Lc})_4\text{P}_4][\text{OTf}]_4$ (**G** $[\text{OTf}]_4$).^[1,7] Products are marked in *yellow* (AEMXY spin system, intermediate), *blue* (AA'MXX' spin system, compound **5a**), *red* (AA'XX' spin system, *meso-7* $[\text{OTf}]_2$), *green* (AA'XX' spin system, *rac-7* $[\text{OTf}]_2$), and *orange* (AMM'XX'YY' spin system, compound **6a**); $[\text{LCo}] = (\text{PHDI})\text{Co}; \circ [(\text{PHDI})\text{Co}]_2(\mu, \eta^4:\eta^4\text{-P}_4)$.^[15]

At 220 K, the formation of three polyphosphido species is observed. The AA'XX' spin system (*red*) is assigned to the $2R^*,3S^*$ diastereomer of dicationic tetraphosphane $[(\text{Lc})_4\text{P}_4][\text{OTf}]_2$ (*meso-7* $[\text{OTf}]_2$), which is formed through the reduction of **G** $[\text{OTf}]_4$ with **J**. **J** is in turn oxidized to $[(\text{PHDI})\text{Co}]_2(\mu, \eta^4:\eta^4\text{-P}_4)$, however this oxidation product does not take part in the reaction, as shown by additional experiments (*vide infra*).^[15] The second AA'XX' spin system (*green*) is assigned to the $(2R,3R)/(2S,3S)$ -configured diastereomer *rac-7* $[\text{OTf}]_2$. The formation of *rac/meso-7* $[\text{OTf}]_2$ has also been observed in reactions of **G** $[\text{OTf}]_4$ with anionic arene and alkene metalates (*vide infra*) and we obtained X-ray quality

crystals of *meso*-**7**[OTf]₂ from the reaction of [K(18c-6)][Fe(anthracene)₂] with **G**[OTf]₄ (*vide infra*).^[4] However, *rac/meso*-**7**[OTf]₂ is not stable in solution and easily forms side products such as [(L_C)₂P]⁺ or [(L_C)₃P₇]³⁺, which prevents its isolation and characterization in solution.^[7] Nonetheless, the reduction to **7**[OTf]₂ presents the first step in the degradation of **G**[OTf]₄ toward a reactive [L_C-P]⁺ moiety. This transient and reactive P₁ building block forms compound **5a** (marked in *blue*) through a [4+1] P-P condensation with **J**. At this temperature, two isomers of **5a** are detectable. One more transient pentaphosphido species can be identified arising as a low intensity AEMXY spin system (*yellow*). All efforts to obtain crystals of this transient species suitable for SCXRD failed due to the high thermal sensitivity of the complex. At 260 K, the signal intensities of the AEMXY spin system and of **7**[OTf]₂ decrease relative to the AA'MXX' spin system of compound **5a**, while the AMM'XX'YY' spin system of compound **6a** arises. This suggests the formation of **6a** through an independent reaction pathway *via* the rearrangement of the intermediary pentaphosphido compound arising as an AEMXY spin system.

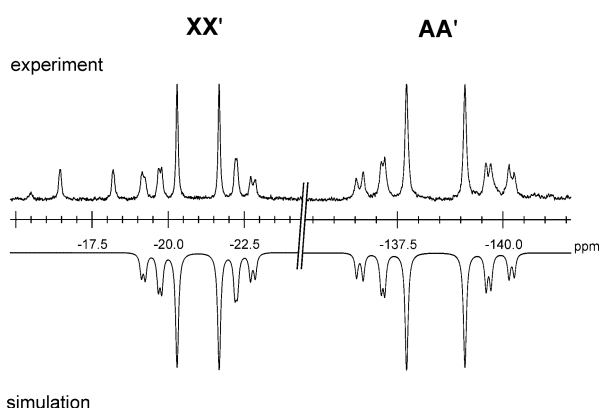
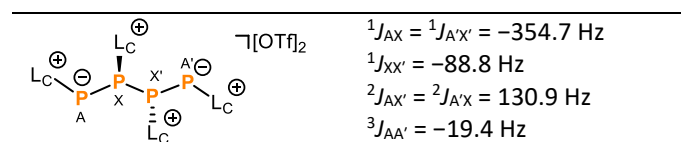


Figure S48. Section of the ³¹P{¹H} NMR spectrum (161.98 MHz, 240 K, thf-*d*₈) of the reaction between [K(18c-6)][(PHDI)Co(η⁴-P₄)] (**J**) and [(L_C)₄P₄][OTf]₄ (**G**[OTf]₄), showing the AA'XX' spin system assigned to *meso*-[(L_C)₄P₄][OTf]₂ (*meso*-**7**[OTf]₂); experimental (upwards) and simulation (downwards).

Table S10. Coupling constant from the iterative fit of the AA'XX' spin system and schematic representation of *meso*-[(L_C)₄P₄][OTf]₂ (*meso*-**7**[OTf]₂); δ(P_{AA'}) = -138.4 ppm, δ(P_{XX'}) = -21.0 ppm.



Our assignment of the major AA'XX' spin system at δ = -138.4 ppm (P_{AA'}) and δ = -21.0 ppm (P_{XX'}) to *meso*-[(L_C)₄P₄][OTf]₂ is based on the magnitude of the ¹J_{PP} and ²J_{PP} coupling constants derived from the iterative fit of the experimental ³¹P{¹H} NMR spectrum. The small magnitude of the ¹J_{XX'} coupling constant indicates an anti-periplanar disposition of the phosphorus lone pairs. The large ²J_{AX'}/²J_{A'X} coupling constant is consistent with the gauche alignment of the free electron pairs of the phosphorus atoms at 1,3 distance. Taking into account that the bulky imidazoliumyl substituents are located as far apart from each other as possible, these conformational preferences suggest that the *meso*-diastereomer is the preferred diastereomer both in solution and solid state (see Figure S92).^[16-19]}

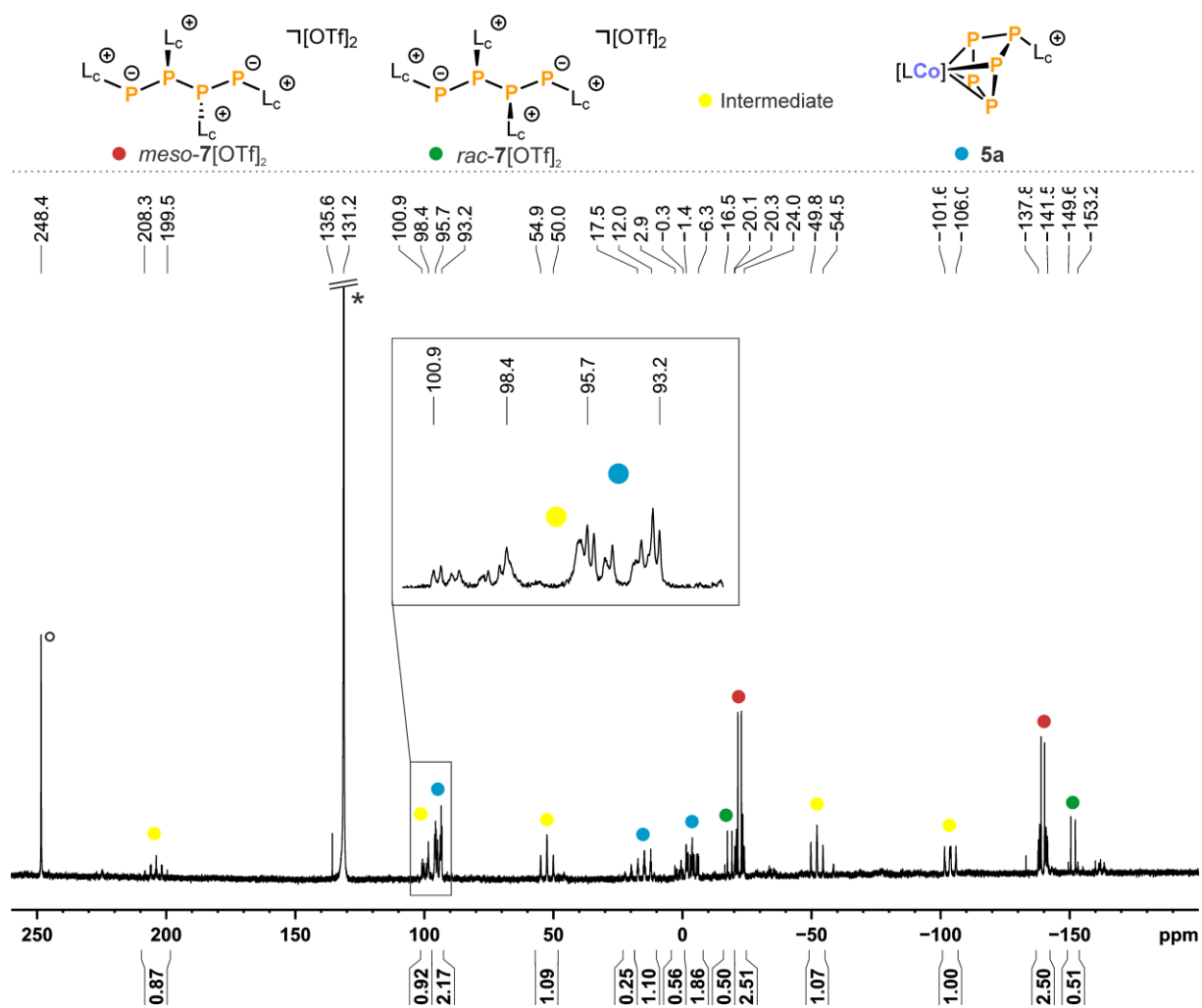


Figure S49. $^{31}\text{P}\{^1\text{H}\}$ NMR spectrum (161.98 MHz, 220 K, $\text{thf-}d_8$) of the reaction between $[\text{K}(\text{18c-6})][(\text{PHDI})\text{Co}(\eta^4\text{-P}_4)]$ (**J**, marked with *) + 0.5 $[(\text{Lc})_4\text{P}_4][\text{OTf}]_4$ (**G** $[\text{OTf}]_4$).^[1,7] Products are marked in *yellow* (AEMXY spin system, intermediate), *blue* (AA'MXX' spin system, compound **5a**), *red* (AA'XX' spin system, *meso-7* $[\text{OTf}]_2$), *green* (AA'XX' spin system, *rac-7* $[\text{OTf}]_2$), and *orange* (AMM'XX'YY' spin system, compound **6a**); $[\text{LCo}] = (\text{PHDI})\text{Co}; \circ [((\text{PHDI})\text{Co})_2(\mu, \eta^4: \eta^4\text{-P}_4)]$.^[15]

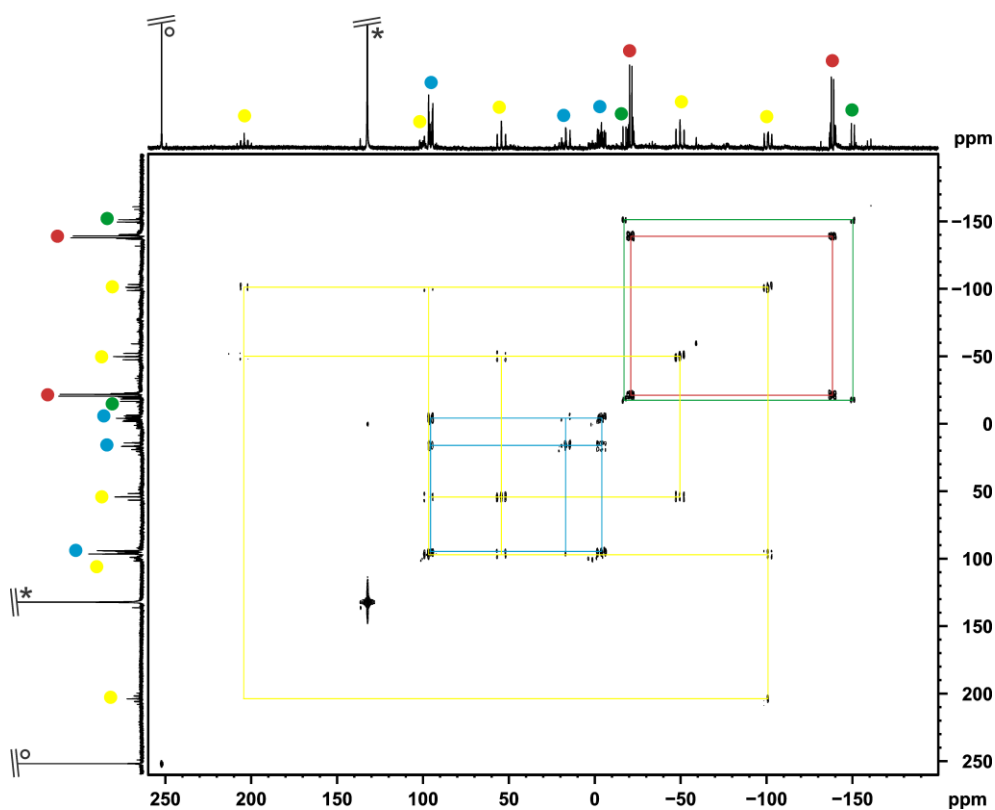


Figure S50. ^{31}P - ^{31}P -COSY NMR spectrum of the reaction between $[\text{K}(\text{18c-6})][(\text{PHDI})\text{Co}(\eta^4\text{-P}_4)]$ (**J**, marked with *) + 0.5 $[(\text{Lc})_4\text{P}_4][\text{OTf}]_4$ (**G**[OTf] $_4$) at 240 K. $^{[1,7]}\text{J}_{\text{PP}}$ coupling is highlighted in *yellow* (AEMXY spin system), *blue* (AA'MXX' spin system, compound **5a**), *red* (AA'XX' spin system, *meso*-**7**[OTf] $_2$), *green* (AA'XX' spin system, *rac*-**7**[OTf] $_2$); $^\circ [(\text{PHDI})\text{Co}]_2(\mu,\eta^4:\eta^4\text{-P}_4)$.^[15]

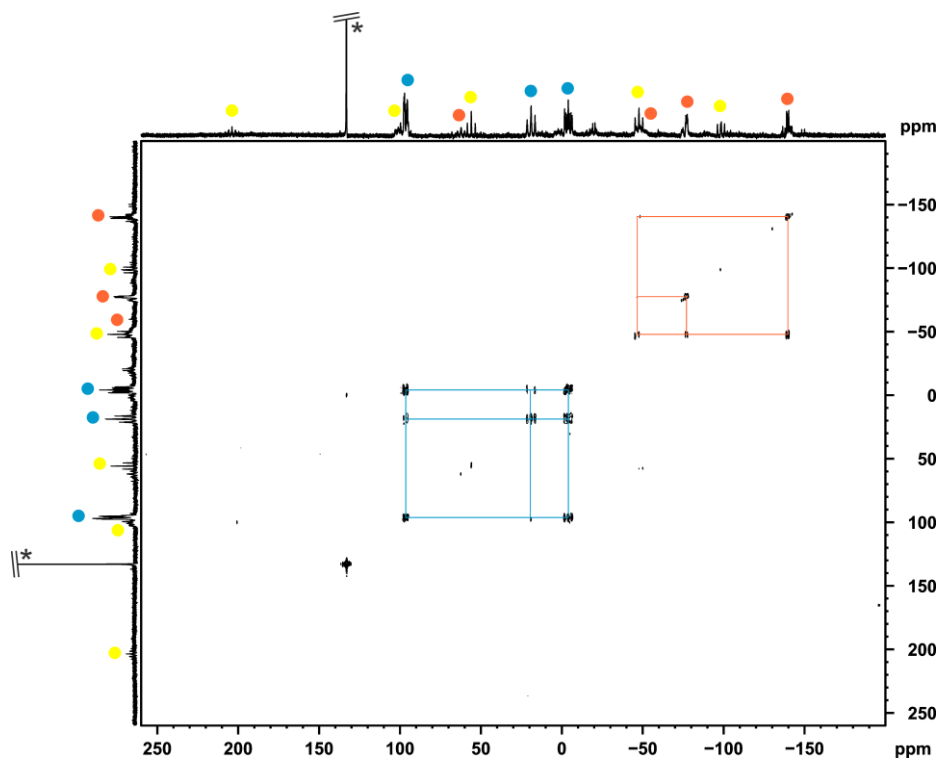


Figure S51. ^{31}P - ^{31}P -COSY NMR spectrum of the reaction between $[\text{K}(\text{18c-6})][(\text{PHDI})\text{Co}(\eta^4\text{-P}_4)]$ (**J**, marked with *) and 0.5 equiv. $[(\text{Lc})_4\text{P}_4][\text{OTf}]_4$ (**G**[OTf] $_4$) at 260 K. $^{[1,7]}\text{J}_{\text{PP}}$ coupling is highlighted in *blue* (AA'MXX' spin system, compound **5a**) and *orange* (AMM'XX'YY' spin system, compound **6a**).

[K(18c-6)][(Ar*BIAN)Co(η^4 -P₄)] (K) + 0.5 [(Lc)₄P₄][OTf]₄ (G[OTf]₄)

G[OTf]₄ (11.5 mg, 0.01 mg, 0.5 equiv.) was submitted to a J. Young valve NMR tube and cooled to -80 °C. A solution of K (25 mg, 0.02 mmol, 1.0 equiv.) in thf-*d*₈ (0.6 mL) at -80 °C was added to the J. Young valve NMR tube. The measurements were performed in a temperature range from 220 K to 300 K in 10 K or 20 K steps.

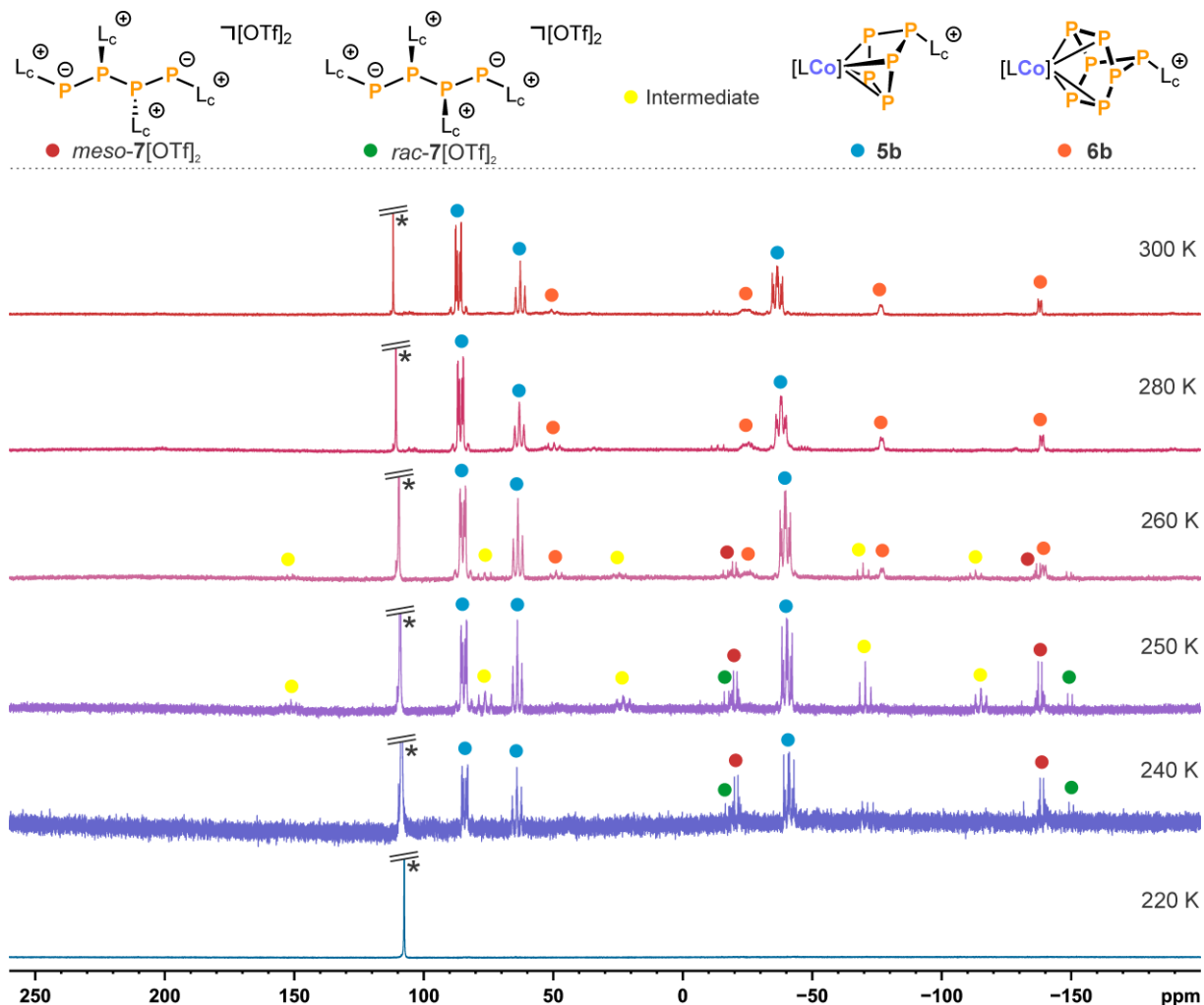


Figure S52. ³¹P{¹H} VT NMR monitoring (161.98 MHz, thf-*d*₈) of the reaction between [K(18c-6)][(Ar*BIAN)Co(η^4 -P₄)] (K, marked with *) + 0.5 [(Lc)₄P₄][OTf]₄ (G[OTf]₄).^[2,7] Products are marked in yellow (AEMXY spin system), blue (AA'MXX' spin system, compound **5b**), red (AA'XX' spin system, *meso*-**7**[OTf]₂), green (AA'XX' spin system, *rac*-**7**[OTf]₂), and orange (AMM'XX'YY' spin system, compound **6b**); [LCo] = (Ar*BIAN)Co;

At 240 K, the formation of compound **5b** (marked in blue) through a [4+1] P–P condensation reaction is observed, as well as the characteristic AA'XX' spin system of the dicationic tetraphosphane *rac/meso*-[(Lc)₄P₄][OTf]₂ (*rac/meso*-**7**[OTf]₂, both isomers marked in red and green), which is formed through the reduction of G[OTf]₄ with K. At 250 K and 260 K, an AEMXY spin system is present. This compound is converting into compound **6b** upon warming to room temperature. Crystals of this transient species suitable for SCXRD could not be obtained due to the high thermal sensitivity of the complex.

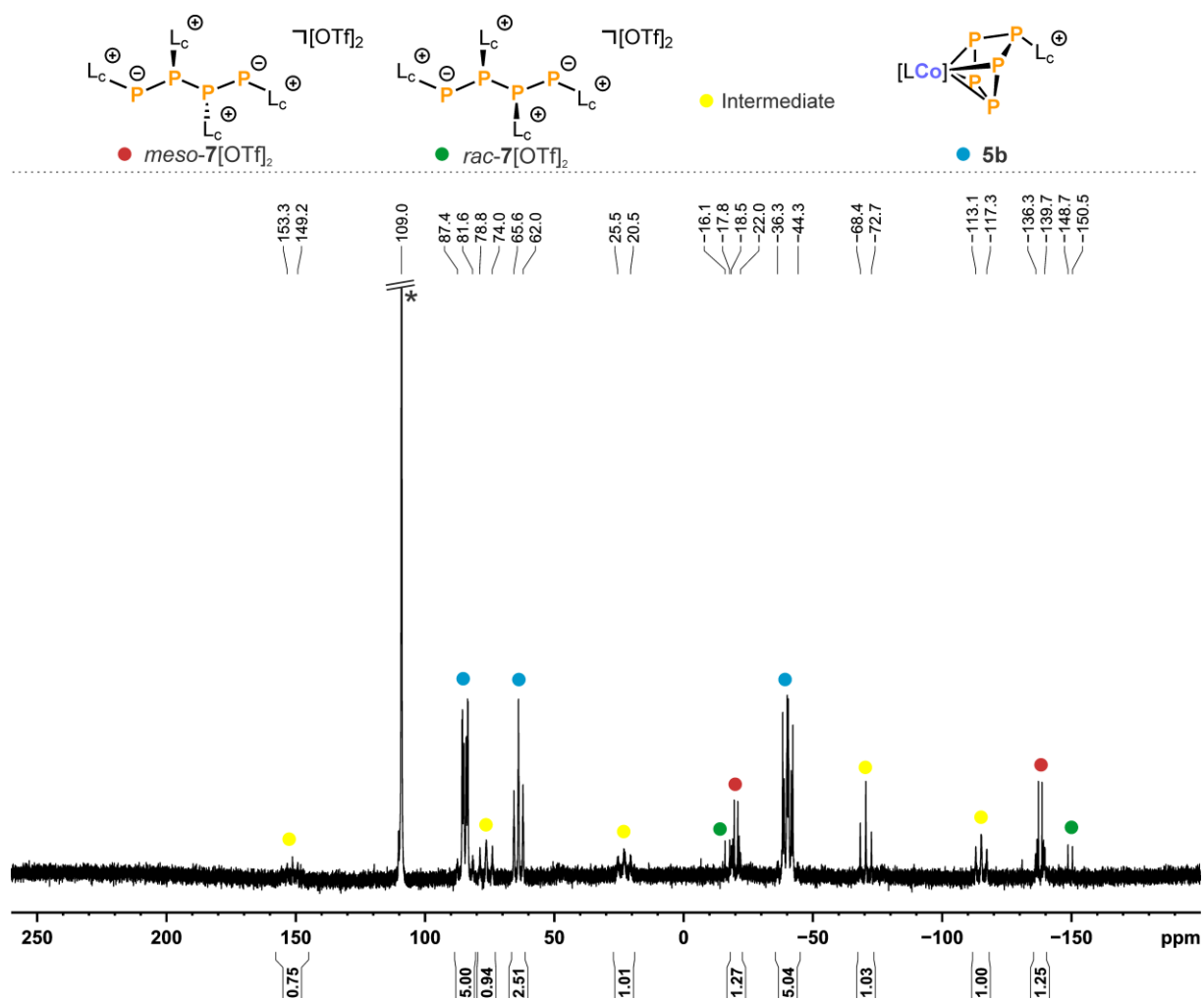


Figure S53. $^{31}\text{P}\{^1\text{H}\}$ NMR spectrum (161.98 MHz, 250 K, $\text{thf-}d_3$) of the reaction between $[\text{K}(18\text{c-}6)][(\text{Ar}^*\text{BIAN})\text{Co}(\eta^4\text{-P}_4)]$ (**K**, marked with *) + 0.5 $[(\text{Lc})_4\text{P}_4][\text{OTf}]_4$ (**G[OTf]** $_4$).^[2,7] Products are marked in *yellow* (AEMXY spin system), *blue* (AA'MXX' spin system, compound **5b**), *red* (AA'XX' spin system, meso-7[OTf]_2), *green* (AA'XX' spin system, rac-7[OTf]_2).

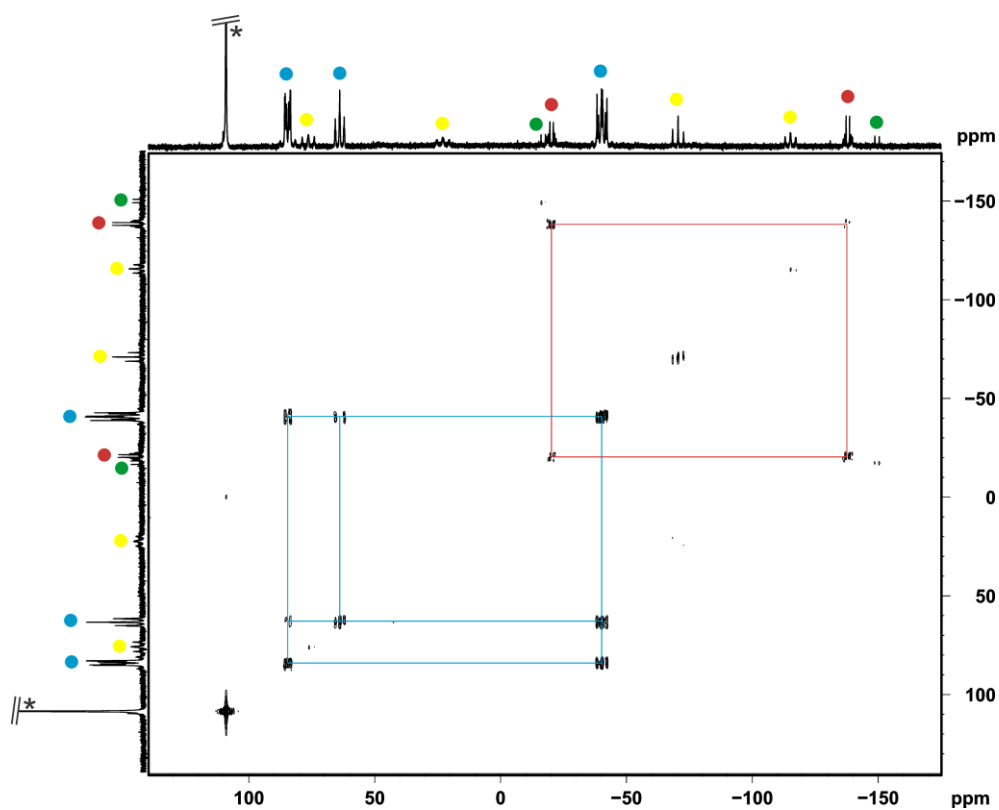


Figure S54. ^{31}P - ^{31}P -COSY NMR spectrum of the reaction between $[\text{K}(\text{18c-6})][(\text{Ar}^*\text{BIAN})\text{Co}(\eta^4\text{-P}_4)]$ (**K**, marked with *) and 0.5 equiv. $[(\text{Lc})_4\text{P}_4][\text{OTf}]_4$ (**G**[OTf] $_4$) at 260 K.^[2,7] $^1J_{\text{PP}}$ coupling is highlighted in *blue* (AA'MXX' spin system, compound **5b**) and *red* (AA'XX' spin system, *meso-7*[OTf] $_2$).

[K(18c-6)][(Ar*BIAN)Co(CN)(η^3 -P₃)] (I) + 0.5 [(L_C)₄P₄][OTf]₄ (G[OTf]₄)

A cold (-35 °C) solution of [K(18c-6)][(Ar*BIAN)Co(CN)(η^3 -P₃)] (17.6 mg, 0.01 mmol, 1.0 equiv) in thf-*d*₈ was added to solid G[OTf]₄ (7.7 mg, 0.005 mmol, 0.5 equiv) in a J. Young NMR tube.

The first measurements were conducted at 260 K, showing the formation of [(Ar*BIAN)Co(η^3 -P₄L_C)] (*exo-3b*, marked in orange) as elucidated by a ³¹P-³¹P COSY NMR experiment and simulation of the characteristic A₂MX spin system (*vide infra*). Other species arising at 260 K are an AM₂X spin system, assigned to *endo-3b* (marked in green), and *meso-7*[OTf]₂ (marked in red, Figure S54). Upon warming to room temperature, the characteristic signals of [(Ar*BIAN)Co(η^3 -P₅(L_C)₂)] [OTf] (**4b**, marked in blue) arise as a ABMXY spin system in a 1:1:1:1:1 signal ratio, which is facilitated by warming the solution to 320 K overnight.

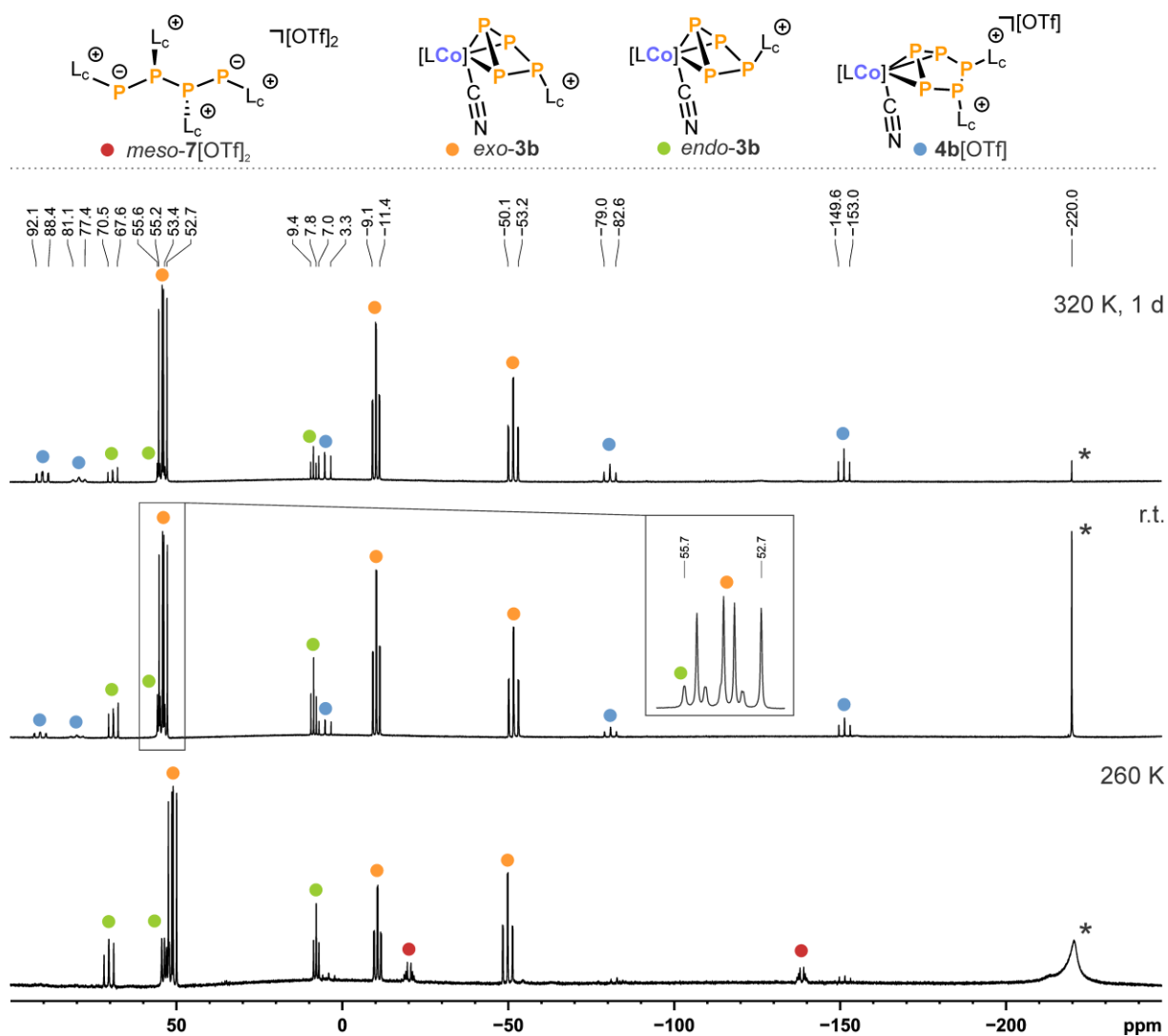


Figure S55. ³¹P{¹H} NMR monitoring (202.46 MHz, thf-*d*₈) of the reaction between [K(18c-6)][(Ar*BIAN)Co(CN)(η^3 -P₃)] (I, marked with *) + 0.5 [(L_C)₄P₄][OTf]₄ (G[OTf]₄).^[2,7] Products are marked in orange (A₂XY spin system, compound **3b**), green (AM₂X spin system), red (AA'XX' spin system, *meso-7*[OTf]₂) and blue (ABMXY spin system, compound **4b**[OTf]); [LCo] = (Ar*BIAN)Co.

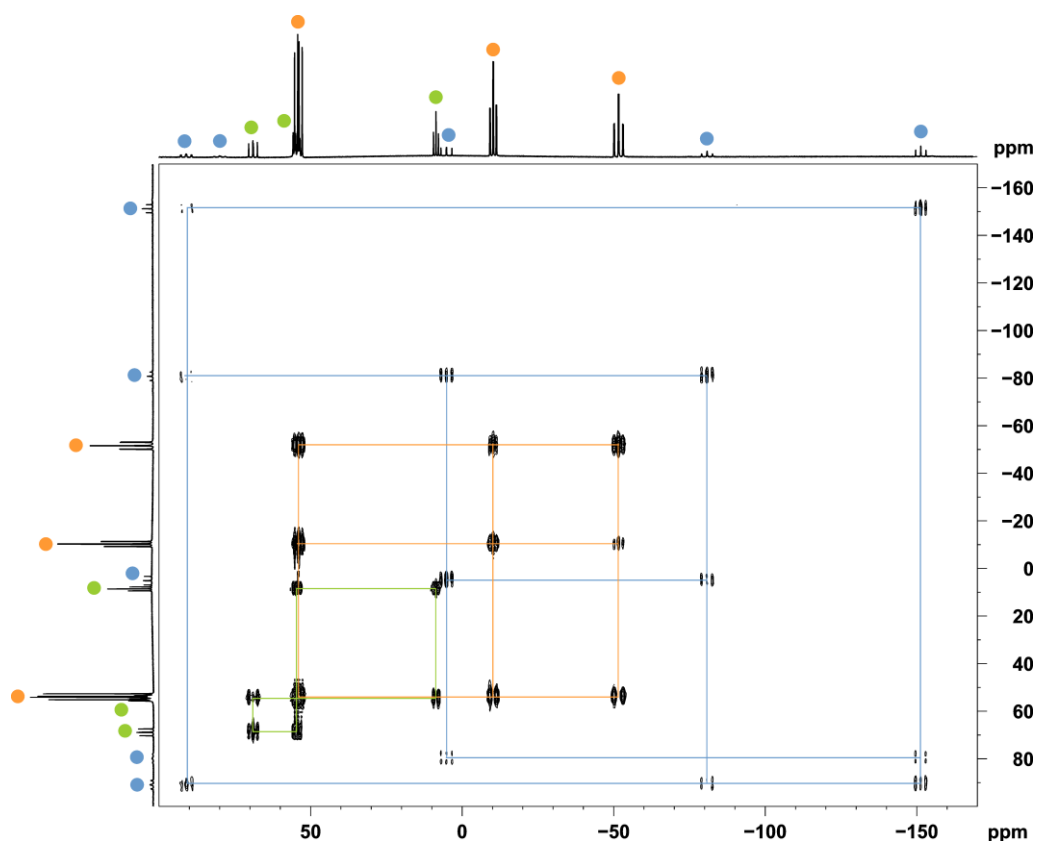


Figure S56. ^{31}P - ^{31}P -COSY NMR spectrum recorded at room temperature of the reaction between $[\text{K}(18\text{c}-6)][(\text{Ar}^*\text{BIAN})\text{Co}(\text{CN})(\eta^3\text{-P}_3)]$ (**1**) + 0.5 $[(\text{Lc})_4\text{P}_4][\text{OTf}]_4$ (**G** $[\text{OTf}]_4$).^[2,7] Products are marked in *orange* (A_2XY spin system, compound *exo-3b*), *green* (AM_2X spin system, compound *endo-3b*) and *blue* (ABMX_Y spin system, compound **4b** $[\text{OTf}]$).

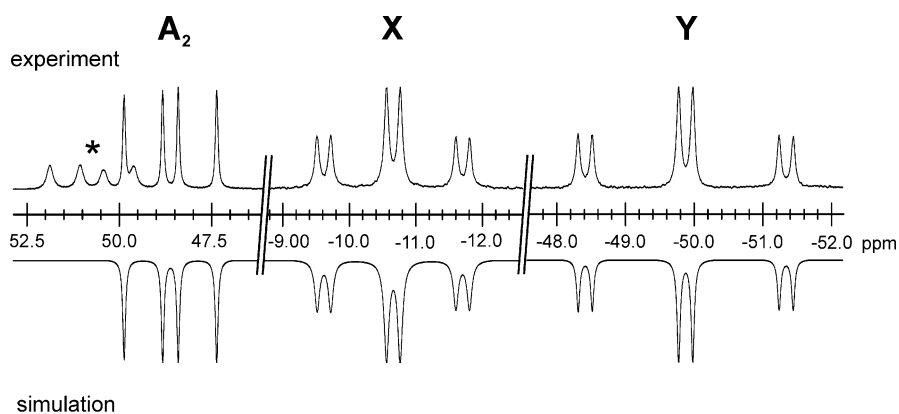


Figure S57. Section of the $^{31}\text{P}\{^1\text{H}\}$ NMR spectrum (202.46 MHz, 260 K, $\text{thf-}d_8$) of $[(\text{Ar}^*\text{BIAN})\text{Co}(\text{CN})(\eta^3\text{-P}_4\text{Lc})]$ (*exo-3b*) from the reaction mixture at 260 K; experimental (upwards) and simulation (downwards).

Table S11. Coupling constant from the iterative fit of the A_2XY spin system and schematic representation of the $\text{CoP}_4(\text{Lc})$ core of $[(\text{Ar}^*\text{BIAN})\text{Co}(\text{CN})(\eta^3\text{-P}_4\text{Lc})]$ (*exo-3b*); $\delta(\text{P}_\text{A}) = 51.11$ ppm, $\delta(\text{P}_\text{X}) = -10.65$ ppm, $\delta(\text{P}_\text{Y}) = -49.87$ ppm.



3. Additional experiments

Reduction of $[(\text{Lc})_4\text{P}_4][\text{OTf}]_4$: Reaction screening

A cold ($-35\text{ }^\circ\text{C}$) solution of $[\text{K}(\text{THF})][^{\text{Mes}}\text{BIANCo}(\text{COD})]$ ($\text{COD} = 1,5\text{-cyclooctadiene}$) (52 mg, 0.069 mmol) in THF was slowly added to a cold ($-35\text{ }^\circ\text{C}$) suspension of $\text{G}[\text{OTf}]_4$ (100 mg, 0.069 mmol) in THF. The deeply green reaction mixture was stirred for 1 h and was slowly brought to ambient temperature. The ^{31}P NMR spectrum of this mixture shows the formation of *rac/meso*-**7** $[\text{OTf}]_2$ (Figure S57). After 5 h the ^{31}P NMR spectrum shows a significant amount of compound Lc-P-Lc^+ being formed in solution (Figure S58).^[7]

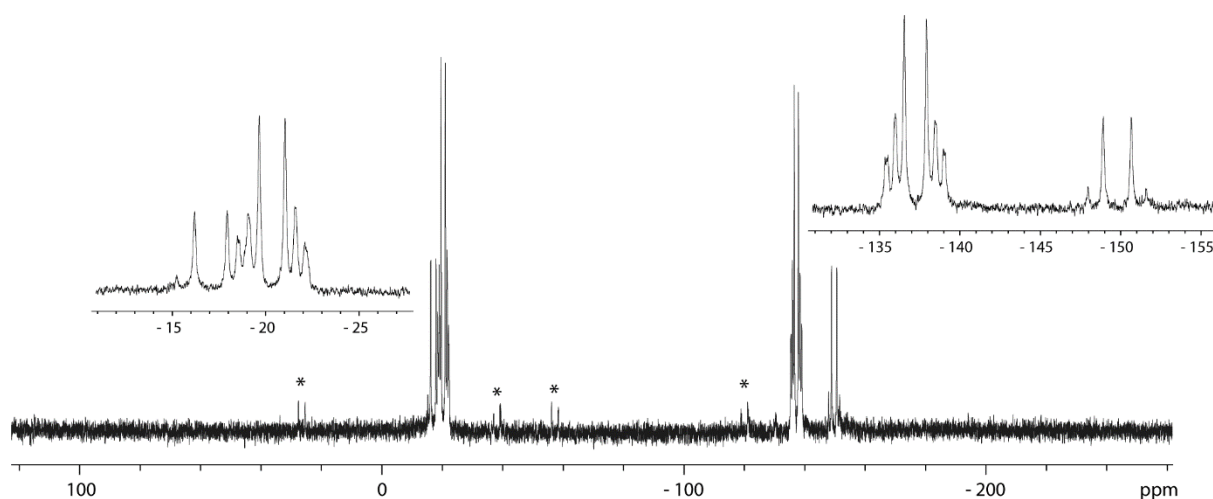


Figure S58. ^{31}P NMR spectrum from the reaction of $[\text{K}(\text{THF})][^{\text{Mes}}\text{BIANCo}(\text{COD})]$ with $\text{G}[\text{OTf}]_4$ in THF (C_6D_6 -capillary, 300 K).

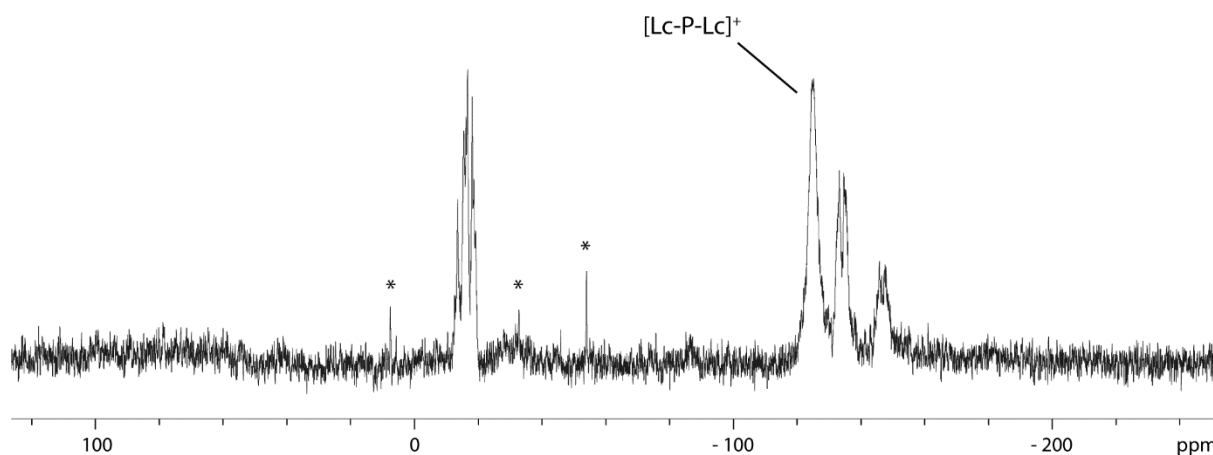


Figure S59. ^{31}P NMR spectrum from the reaction of $[\text{K}(\text{THF})][^{\text{Mes}}\text{BIANCo}(\text{COD})]$ with $\text{G}[\text{OTf}]_4$ in THF after 5 h (C_6D_6 -capillary, 300 K).

A cold ($-35\text{ }^{\circ}\text{C}$) solution of $[\text{K}(\text{DME})_2][\text{Co}(\text{anthracene})_2]$ (44 mg, 0.069 mmol) in THF was slowly added to a cold ($-35\text{ }^{\circ}\text{C}$) suspension of $\mathbf{G}[\text{OTf}]_4$ (100 mg, 0.069 mmol) in THF. The black reaction mixture was stirred for 1 h and was slowly brought to ambient temperature. The ^{31}P NMR spectrum of this mixture shows the formation of *rac/meso*-**7** $[\text{OTf}]_2$ and small amounts of unassigned side products (Figure S59).

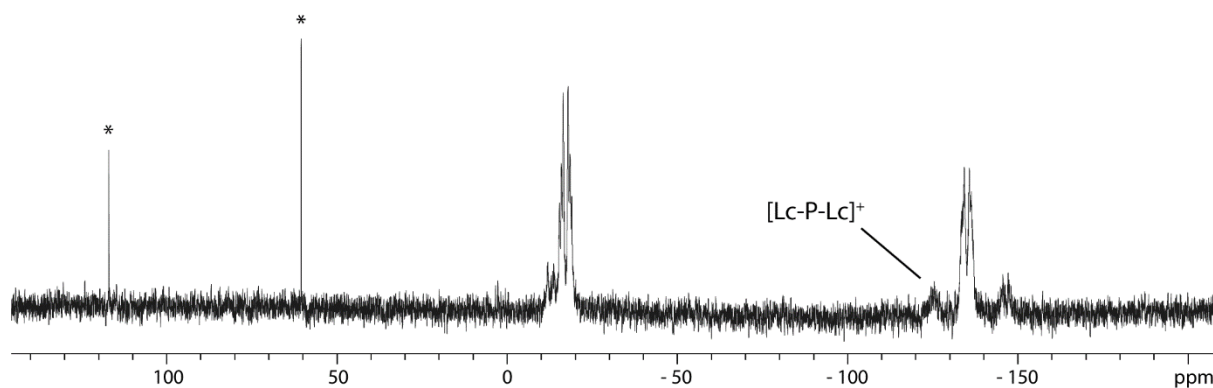


Figure S60. ^{31}P NMR spectrum from the reaction of $[\text{K}(\text{DME})_2][\text{Co}(\text{anthracene})_2]$ with $\mathbf{G}[\text{OTf}]_4$ in THF (C_6D_6 -capillary, 300 K); unassigned side products are marked with asterisks (*).

A cold ($-35\text{ }^{\circ}\text{C}$) solution of $[\text{K}(18\text{c-}6)][\text{Fe}(\text{anthracene})_2]$ (109 mg, 0.15 mmol) in THF was slowly added to a cold ($-35\text{ }^{\circ}\text{C}$) suspension of $\mathbf{G}[\text{OTf}]_4$ (220 mg, 0.069 mmol) in THF. The black reaction mixture was stirred for 1 h and was slowly brought to ambient temperature. The ^{31}P NMR spectrum of this mixture shows the formation of *rac/meso*-**7** $[\text{OTf}]_2$ (Figure S60). The reaction mixture was filtered and *n*-hexane was added to the filtrate whereupon a pale yellow solid was formed. The dried material was again dissolved in PhF and layered with *n*-hexane. After one day crystals suitable for X-ray diffraction were obtained (for SCXRD data, see section 'X-ray Crystallography', *vide infra*).

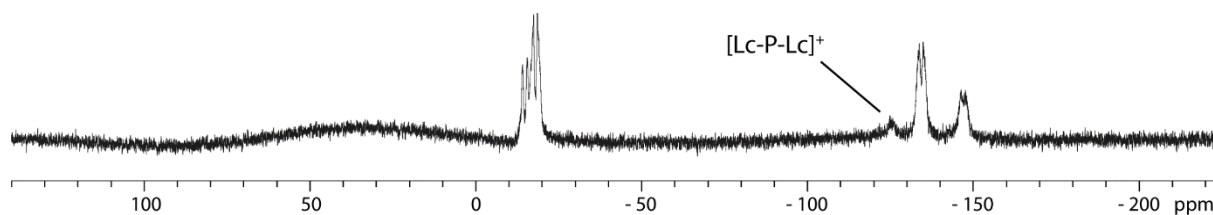


Figure S61. ^{31}P NMR spectrum from the reaction of $[\text{K}(18\text{c-}6)][\text{Fe}(\text{anthracene})_2]$ with $\mathbf{G}[\text{OTf}]_4$ in THF (C_6D_6 -capillary, 300 K).

Reaction of $[K(18c-6)][(PHDI)Co(\eta^4-P_4)]$ (**J**) with 0.25, 0.5 and 1.0 equivalents $[(Lc)_4P_4][OTf]_4$ (**G[OTf]₄**)

Solid **J** (18.9 mg, 0.018 mmol, 1.0 equiv.) and **G[OTf]₄** (6.6 mg, 0.005 mmol, 0.25 equiv.) were dissolved in 0.4 mL *thf-d₈* in a J. Young valve NMR tube resulting in a dark green solution. The $^{31}P\{^1H\}$ NMR spectrum shows unreacted starting material **J** (marked *) as well as the formation of $[(PHDI)Co(\eta^4-P_5Lc)]$ (**5a**, AA'MXX' spin system, marked *blue*) and $[(PHDI)Co(\eta^2:\eta^2-P_7Lc)]$ (**6a**, AMM'XX'YY' spin system, marked *orange*) in a 2:1 ratio (Figure S62).

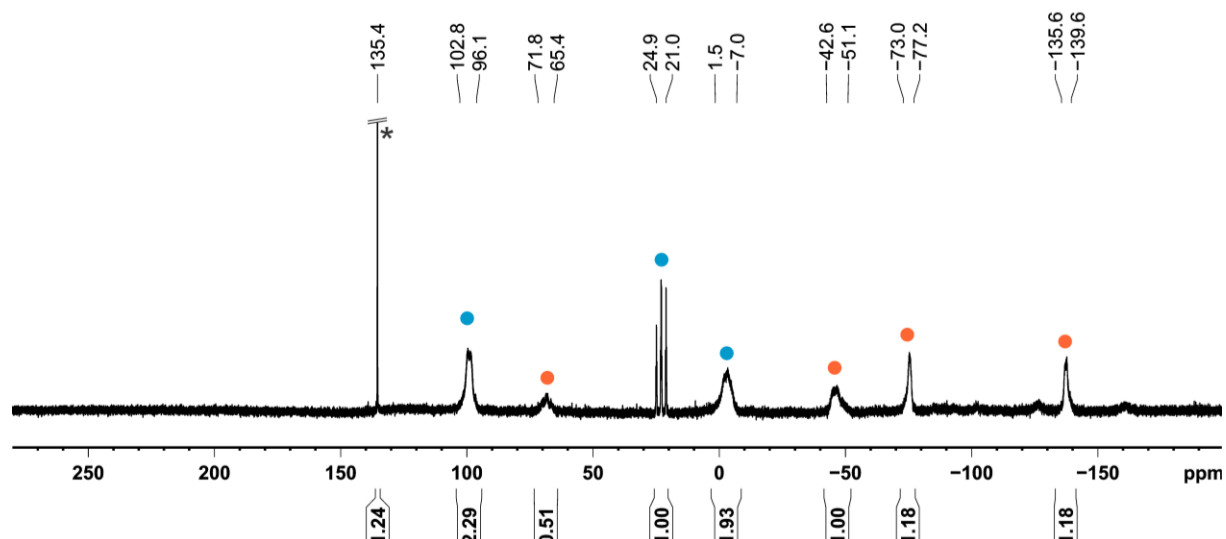


Figure S62. $^{31}P\{^1H\}$ NMR spectrum (202.46 MHz, 300 K, *thf-d₈*) of the reaction between $[K(18c-6)][(PHDI)Co(\eta^4-P_4)]$ (**J**) and 0.25 equivalents $[(Lc)_4P_4][OTf]_4$ (**G[OTf]₄**).

Solid **J** (18.9 mg, 0.018 mmol, 1.0 equiv.) and **G[OTf]₄** (13.1 mg, 0.009 mmol, 0.5 equiv.) were dissolved in 0.4 mL *thf-d₈* in a J. Young valve NMR tube. The $^{31}P\{^1H\}$ NMR spectrum (Figure S63) shows the formation of $[(PHDI)Co(\eta^4-P_5Lc)]$ (**5a**, AA'MXX' spin system, marked *blue*) and $[(PHDI)Co(\eta^2:\eta^2-P_7Lc)]$ (**6a**, AMM'XX'YY' spin system, marked *orange*) in a 2:1 ratio as well as oxidation product $[(PHDI)Co]_2(\mu,\eta^4:\eta^4-P_4)$ (marked o), *rac/meso-7*[OTf]₂ $[(Lc)_4P_4][OTf]_2$ (marked *) and $Lc-P-Lc^+$.^[7]

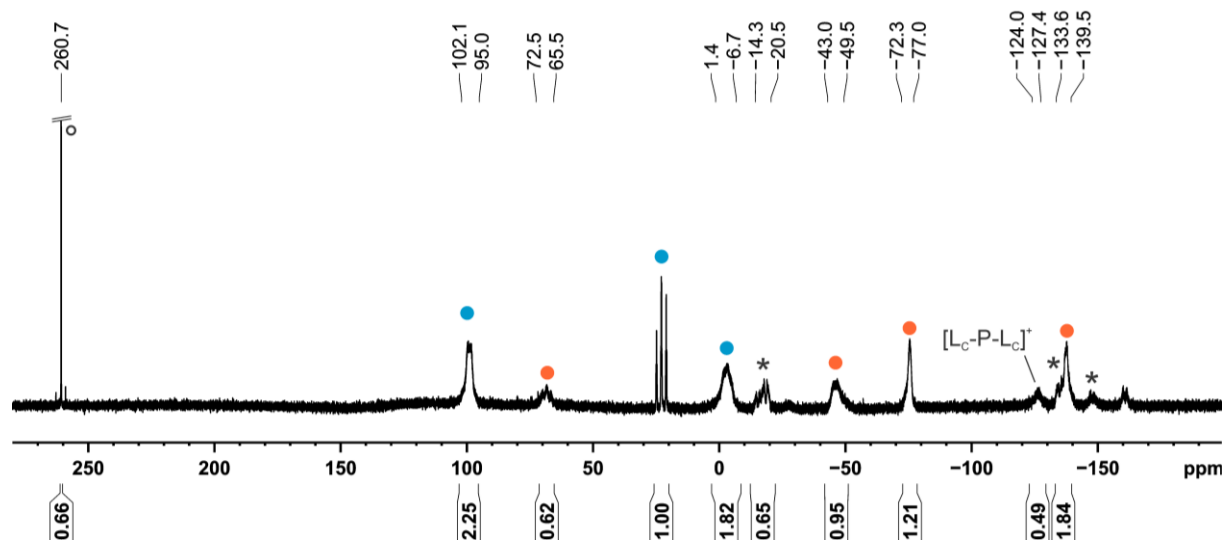


Figure S63. $^{31}P\{^1H\}$ NMR spectrum (202.46 MHz, 300 K, *thf-d₈*) of the reaction between $[K(18c-6)][(PHDI)Co(\eta^4-P_4)]$ (**J**) and 0.5 equivalents $[(Lc)_4P_4][OTf]_4$ (**G[OTf]₄**).

Solid **J** (18.9 mg, 0.018 mmol, 1.0 equiv.) and **G**[OTf]₄ (26.2 mg, 0.018 mmol, 1.0 equiv.) were dissolved in 0.4 mL thf-*d*₈ in a J. Young valve NMR tube resulting in a dark green suspension due to unreacted and undissolved **G**[OTf]₄. The ³¹P{¹H} NMR spectrum (Figure S64) shows the formation of [(PHDI)Co(η⁴-P₅L_C)] (**5a**, AA'MXX' spin system, marked in *blue*) and [(PHDI)Co(η²:η²-P₇L_C)] (**6a**, AMM'XX'YY' spin system, marked in *orange*) in a 2:1 ratio as well as oxidation product [{"(PHDI)Co}₂(μ,η⁴:η⁴-P₄)] (marked o), *rac/meso*- [(L_C)₄P₄][OTf]₂ (marked *) and L_C-P-L_C⁺.^[7]

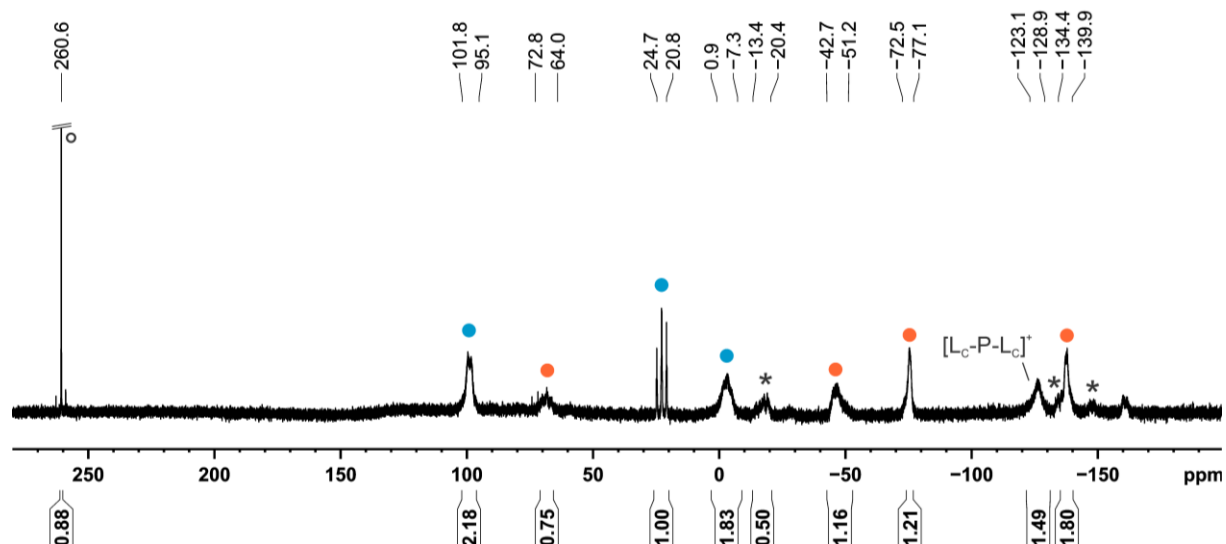


Figure S64. ³¹P{¹H} NMR spectrum (202.46 MHz, 300 K, thf-*d*₈) of the reaction between [K(18c-6)][(PHDI)Co(η⁴-P₄)] (**J**) and 1.0 equivalent [(L_C)₄P₄][OTf]₄ (**G**[OTf]₄).

Reaction of $\{[(\text{PHDI})\text{Co}]_2(\mu, \eta^4:\eta^4\text{-P}_4)\}$ and $\text{G}[\text{OTf}]_4$ or $7[\text{OTf}]_2$

To a solution of **J** (22.5 mg, 0.02 mmol, 1.0 equiv.) in 1,2-difluorobenzene (*o*-DFB, 0.2 mL) was added a dark blue solution of $[\text{Fe}(\text{C}_5\text{H}_5)_2][\text{BAR}^{\text{F}}_4]$ ($\text{BAR}^{\text{F}}_4^- = [\{3,5\text{-}(\text{CF}_3)_2\text{C}_6\text{H}_3\}_4\text{B}]^-$, 21.6 mg, 0.02 mmol, 1.0 equiv.) in *o*-DFB (0.6 mL). The selective formation of $\{[(\text{PHDI})\text{Co}]_2(\mu, \eta^4:\eta^4\text{-P}_4)\}$ was confirmed by $^{31}\text{P}\{^1\text{H}\}$ NMR spectroscopy. Solid $\text{G}[\text{OTf}]_4$ (14.8 mg, 0.005 mmol, 0.5 equiv.) was added to the in situ generated $\{[(\text{PHDI})\text{Co}]_2(\mu, \eta^4:\eta^4\text{-P}_4)\}$. A $^{31}\text{P}\{^1\text{H}\}$ NMR spectrum (Figure S65) was recorded after 15 h, which shows unreacted $\{[(\text{PHDI})\text{Co}]_2(\mu, \eta^4:\eta^4\text{-P}_4)\}$ (marked \circ), $\text{G}[\text{OTf}]_4$ (marked $*$) as well as the formation of a singlet of unknown composition (marked \square).

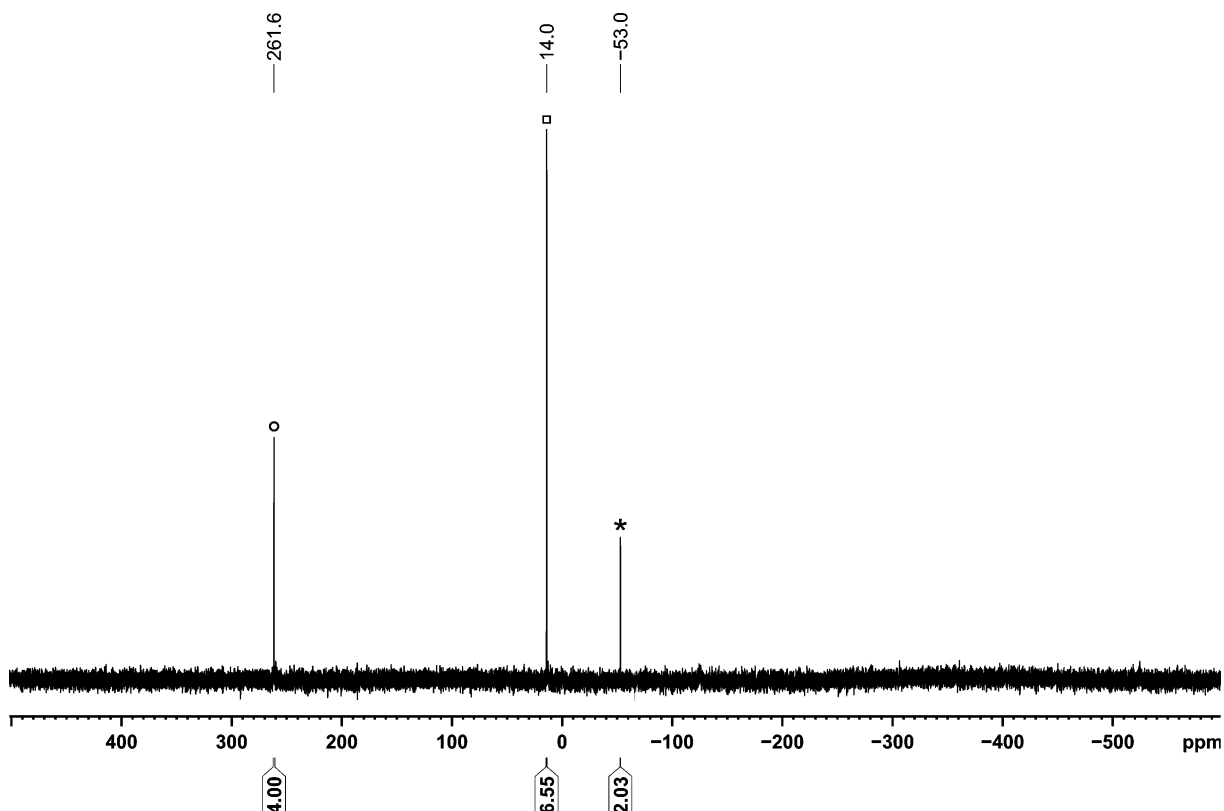


Figure S65. $^{31}\text{P}\{^1\text{H}\}$ NMR spectrum (202.46 MHz, 300 K, *o*-DFB/ C_6D_6 -capillary) of the reaction between $\{[(\text{PHDI})\text{Co}]_2(\mu, \eta^4:\eta^4\text{-P}_4)\}$ and 0.5 equivalents $[(\text{Lc})_4\text{P}_4][\text{OTf}]_4$ ($\text{G}[\text{OTf}]_4$).

$\{[(\text{PHDI})\text{Co}]_2(\mu, \eta^4:\eta^4\text{-P}_4)\}$ and $7[\text{OTf}]_2$ were prepared in situ: To a dark green solution of **J** (15.7 mg, 0.014 mmol, 1.0 equiv.) in THF (0.5 mL) was added a dark blue solution of $[\text{Fe}(\text{C}_5\text{H}_5)_2][\text{BAR}^{\text{F}}_4]$ (15.1 mg, 0.014 mmol, 1.0 equiv.) in THF (0.5 mL) resulting in a dark purple colored solution. A dark red solution of $[\text{K}(18\text{c-6})][\text{Fe}(\text{anth})_2]$ (10.3 mg, 0.014 mmol, 1.0 equiv.) in THF (0.5 mL) was added to an off-white suspension of $\text{G}[\text{OTf}]_4$ (20.7 mg, 0.014 mmol, 1.0 equiv.) in THF (0.5 mL). The resulting dark yellow solution which contained $7[\text{OTf}]_2$ was filtered and added dropwise to the dark purple solution which contained in situ generated $\{[(\text{PHDI})\text{Co}]_2(\mu, \eta^4:\eta^4\text{-P}_4)\}$. The $^{31}\text{P}\{^1\text{H}\}$ NMR spectrum shows unreacted $\{[(\text{PHDI})\text{Co}]_2(\mu, \eta^4:\eta^4\text{-P}_4)\}$ (marked \circ), $7[\text{OTf}]_2$ (marked $*$) and the release of P_4 (singlet at $\delta = -527.2$ ppm).

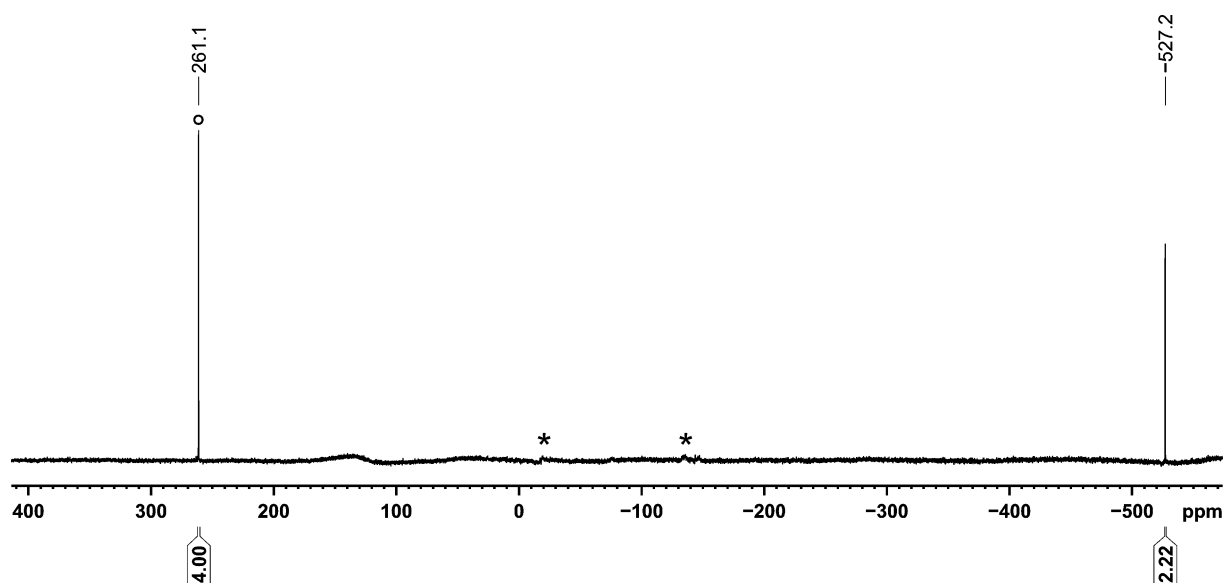


Figure S66. $^{31}\text{P}\{^1\text{H}\}$ NMR spectrum (202.46 MHz, 300 K, THF/ C_6D_6 -capillary) of the reaction between $[\{(\text{PHDI})\text{Co}\}_2(\mu, \eta^4: \eta^4\text{-P}_4)]$ and $[(\text{Lc})_4\text{P}_4][\text{OTf}]_2$ (**7**)[OTf] $_2$.

Reaction of [(PHDI)Co(μ : η^4 , κ^1 -P₅Lc){W(CO)₅}] (**5a-W(CO)₅**) with excess [W(CO)₅(THF)]

A stirred and colourless solution of [W(CO)₆] (11.6 mg, 0.033 mmol, 3.3 equiv.) in THF (1.5 mL) was irradiated with UV-light (365 nm) for 1 h. The resulting deep yellow solution was added dropwise to solid [(PHDI)Co(μ : η^4 , κ^1 -P₅Lc){W(CO)₅}] (16.0 mg, 0.010 mmol, 1.0 equiv.). The resulting dark green solution was stirred over night at room temperature. ¹H, ³¹P, ³¹P{¹H} and ³¹P-³¹P COSY NMR experiments were performed at room temperature.

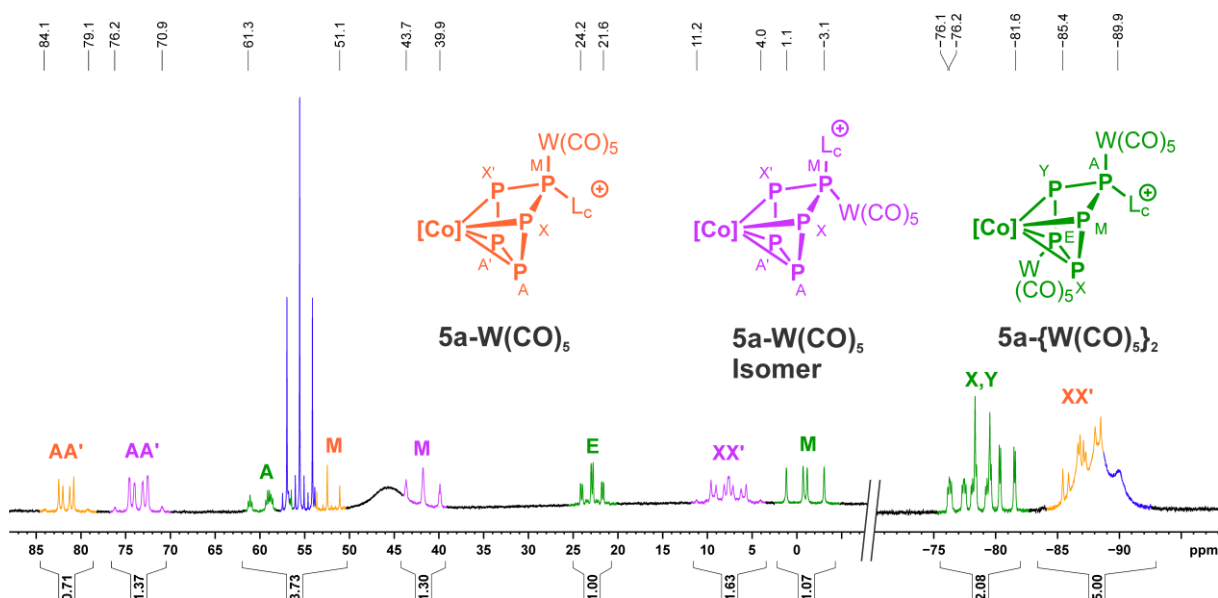


Figure S67. ³¹P{¹H} NMR spectrum (202.46 MHz, 300 K, C₆D₆) of the reaction between [(PHDI)Co(μ : η^4 , κ^1 -P₅Lc){W(CO)₅}] (**5a-W(CO)₅**) and 3.3 equiv. [W(CO)₅(THF)] exhibiting four sets of signals attributed to four spin systems marked in orange (AA'MXX', compound **5a-W(CO)₅**), purple (AA'MXX'), green (AEMXY), blue (unknown spin system).

The ratio of the resulting product mixture does not significantly change when adding more [W(CO)₅(THF)]. In total, four products are observed: marked in orange is the AA'MXX' spin system of compound **5a-W(CO)₅**. Marked in purple is a second AA'MXX' spin system, which is proposed to be an isomer of compound **5a-W(CO)₅**, presumably entailing a positional exchange of the L_c and {W(CO)₅} substituents at the apical P-atom. Marked in green is an AEMXY spin system, which is assigned to [(PHDI)Co(μ : η^4 , κ^2 -P₅Lc){W(CO)₅}]₂ (**5a-{W(CO)₅}₂**, Figure S95, *vide infra*). The remaining signals marked in blue were not assigned to a characteristic spin system, nevertheless are proposed to arise from a *cyclo*-P₅ compound substituted by at least three {W(CO)₅} fragments involved in dynamic processes at room temperature.

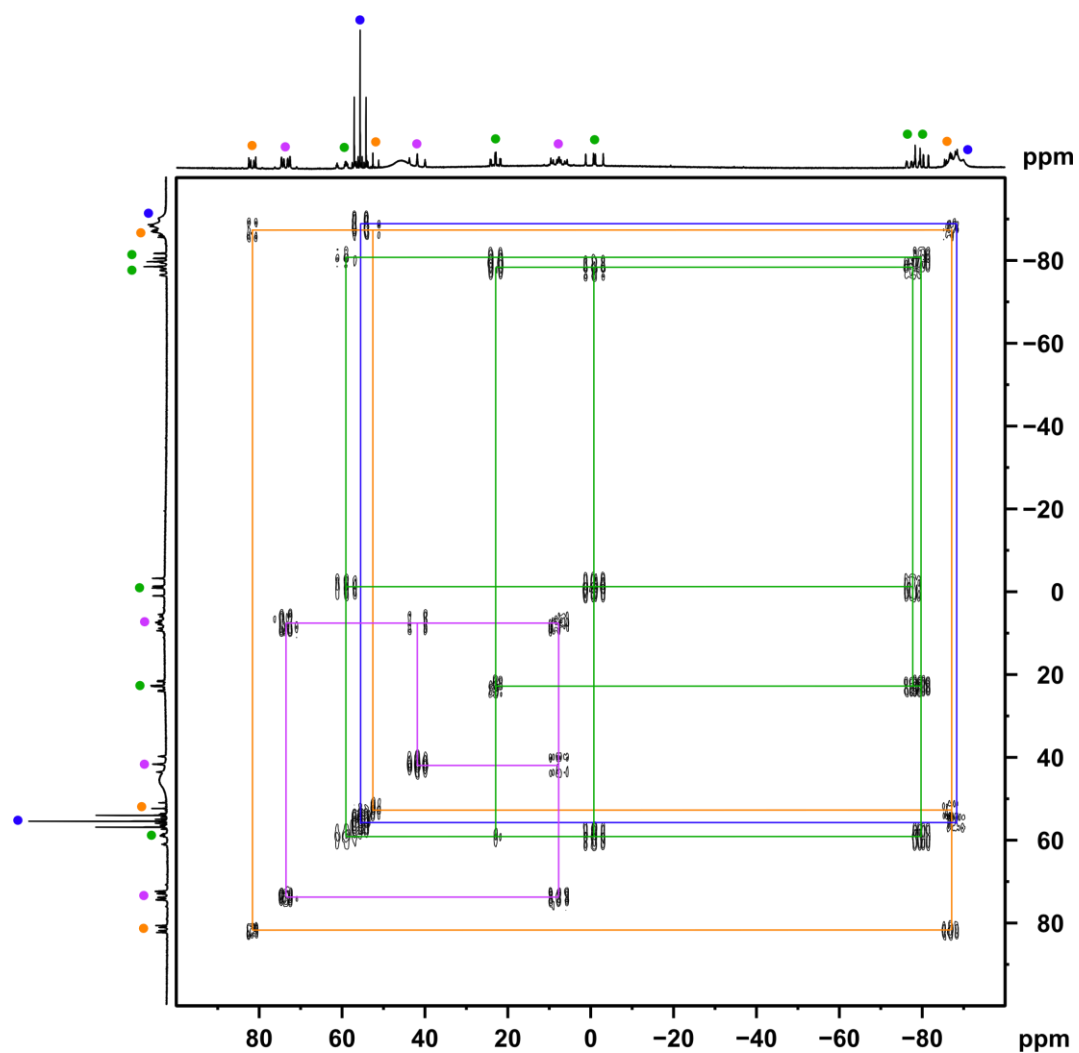


Figure S68. ^{31}P - ^{31}P -COSY NMR spectrum of the reaction between $[(\text{PHDI})\text{Co}(\mu:\eta^4, \kappa^1\text{-P}_5\text{Lc})\{\text{W}(\text{CO})_5\}]$ (**5a**- $\text{W}(\text{CO})_5$) and 3.3 equiv. $[\text{W}(\text{CO})_5(\text{THF})]$. $^1J_{\text{PP}}$ coupling is highlighted in *orange* (AA'MXX' spin system, compound **5a**- $\text{W}(\text{CO})_5$), *purple* (AA'MXX' spin system), *green* (AEMXY spin system, compound **5a**- $\{\text{W}(\text{CO})_5\}_2$), *blue* (unknown spin system).

4. UV/Vis spectra

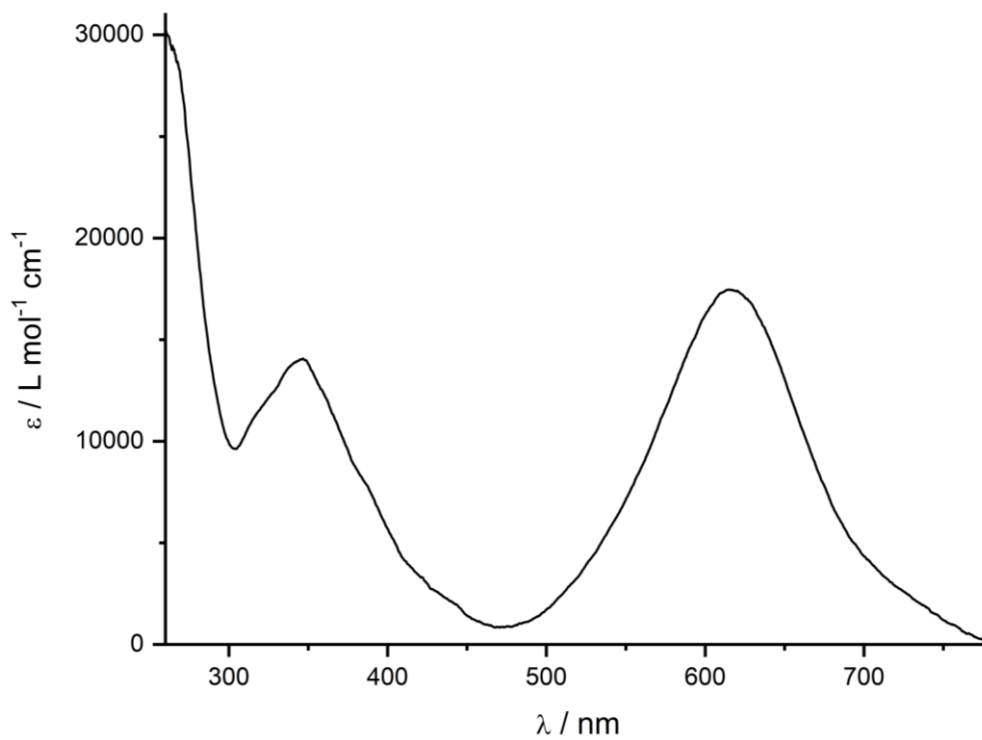


Figure S69. UV/Vis spectrum of $[(\text{PHDI})\text{Co}(\text{CN})(\eta^3\text{-P}_4\text{Cy}_2)]$ (**1a-Cy**) in THF.

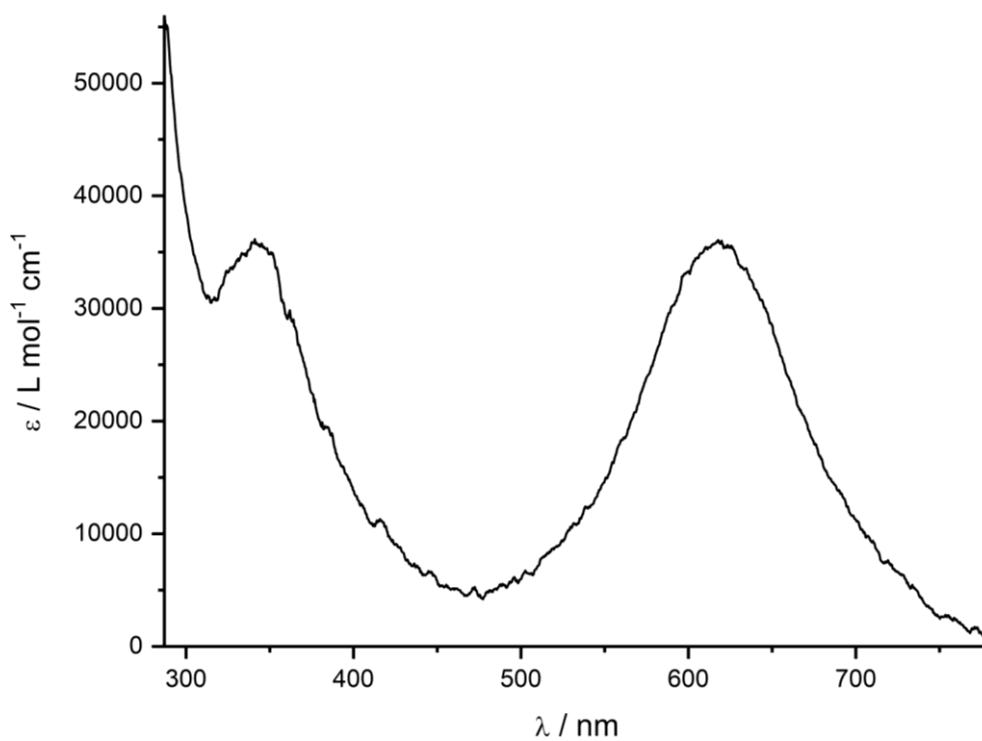


Figure S70. UV/Vis spectrum of $[(\text{PHDI})\text{Co}(\text{CN})(\eta^3\text{-P}_4\text{Ph}_2)]$ (**1a-Ph**) in THF.

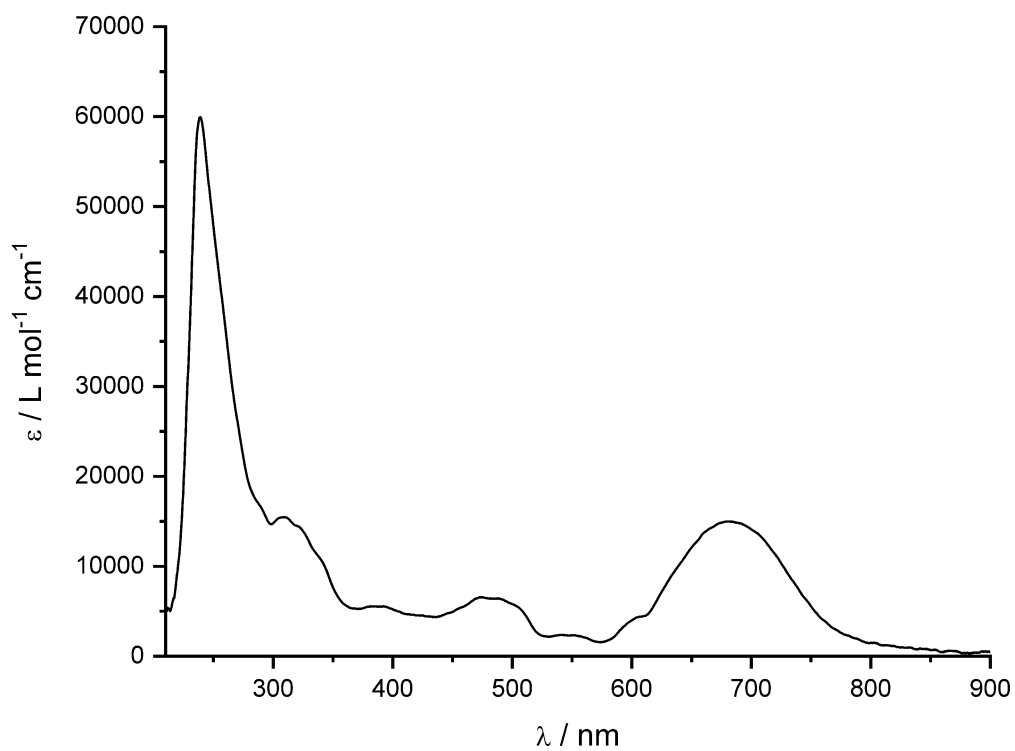


Figure S71. UV/Vis spectrum of $[(Ar^*BIAN)Co(CN)(\eta^3-P_4Cy_2)]$ (**1b-Cy**) in THF.

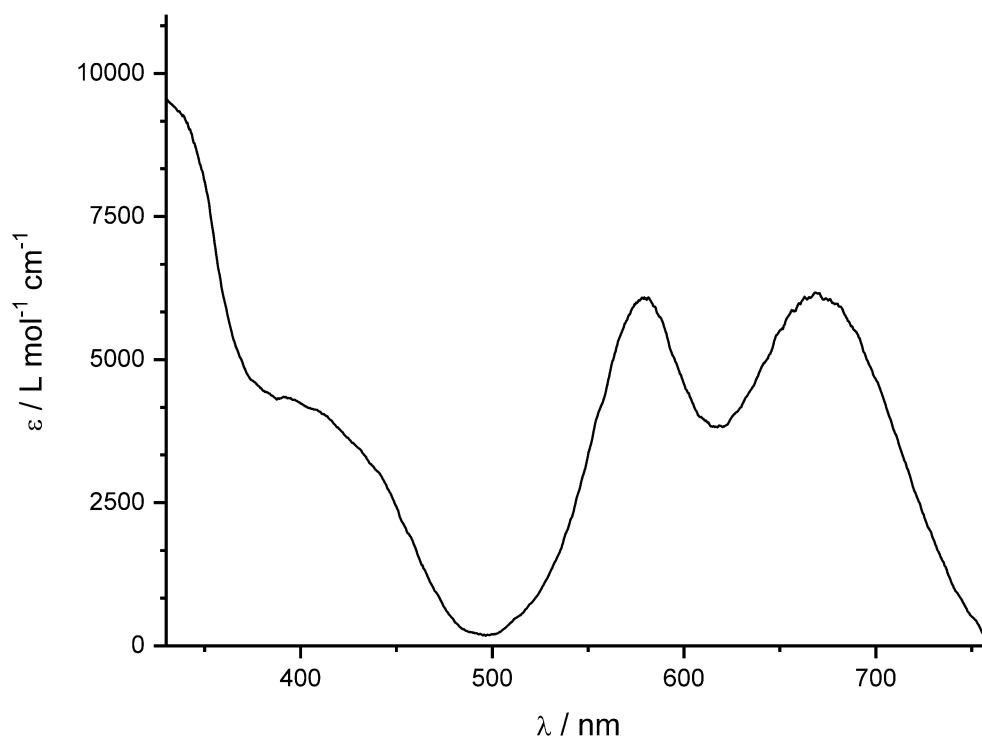


Figure S72. UV/Vis spectrum of $[(Ar^*BIAN)Co(\eta^4-P_5tBu_2)]$ (**2b-tBu**) in toluene.

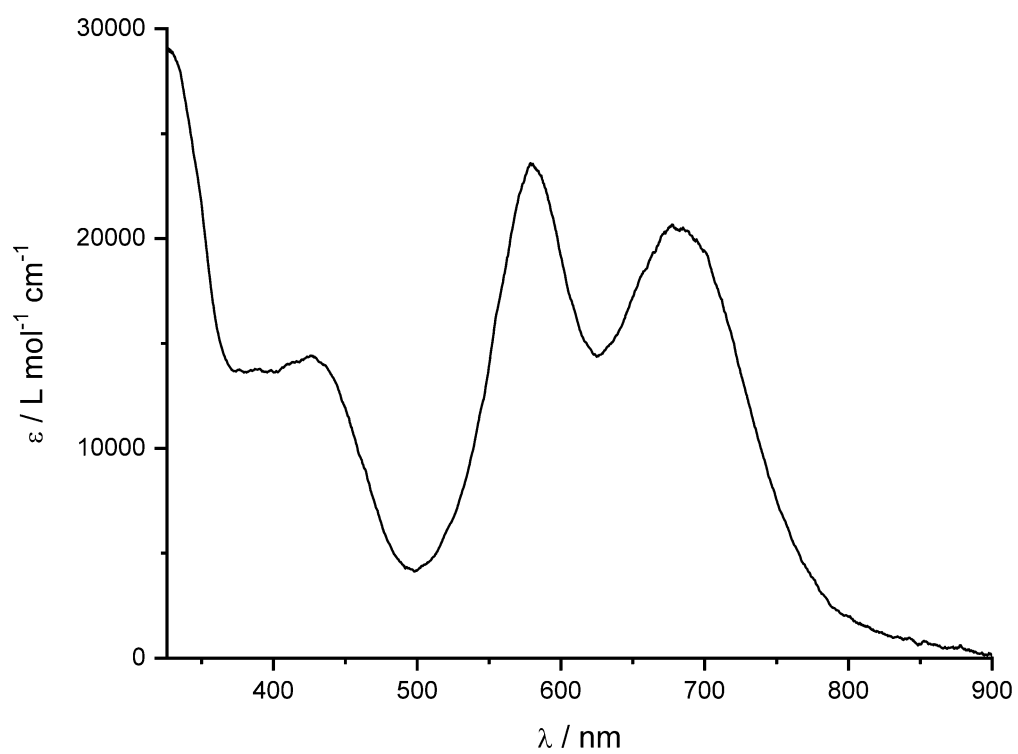


Figure S73. UV/Vis spectrum of $[(Ar^*BIAN)Co(\eta^4-P_5(N(iPr_2)_2))] (2b-N(iPr_2))$ in toluene.

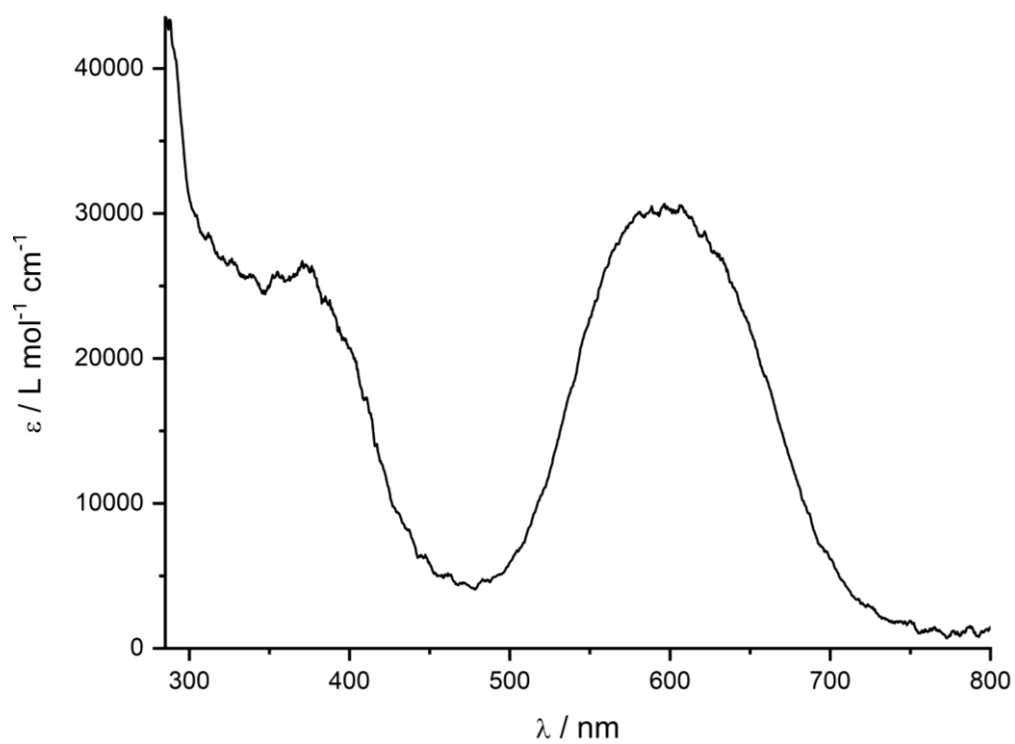


Figure S74. UV/Vis spectrum of $[(PHDI)Co(CN)(\eta^3-P_4Lc)] (3a)$ in THF.

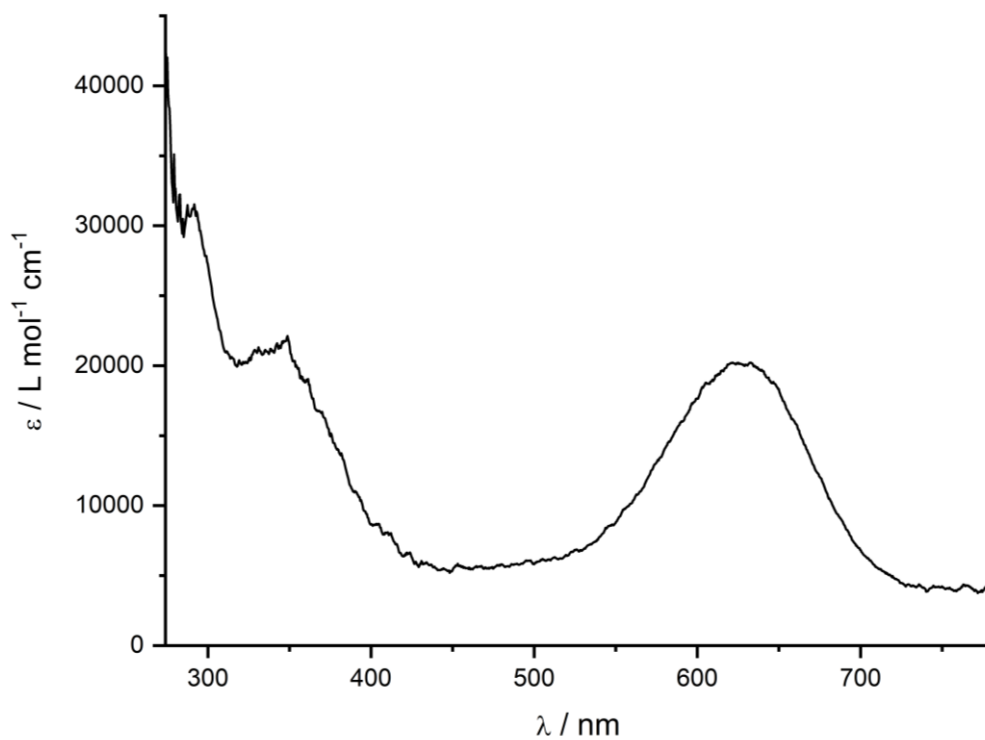


Figure S75. UV/Vis spectrum of $[(\text{PHDI})\text{Co}(\text{CN})(\eta^3\text{-P}_5(\text{Lc})_2)][\text{OTf}]$ (**4a**) in THF.

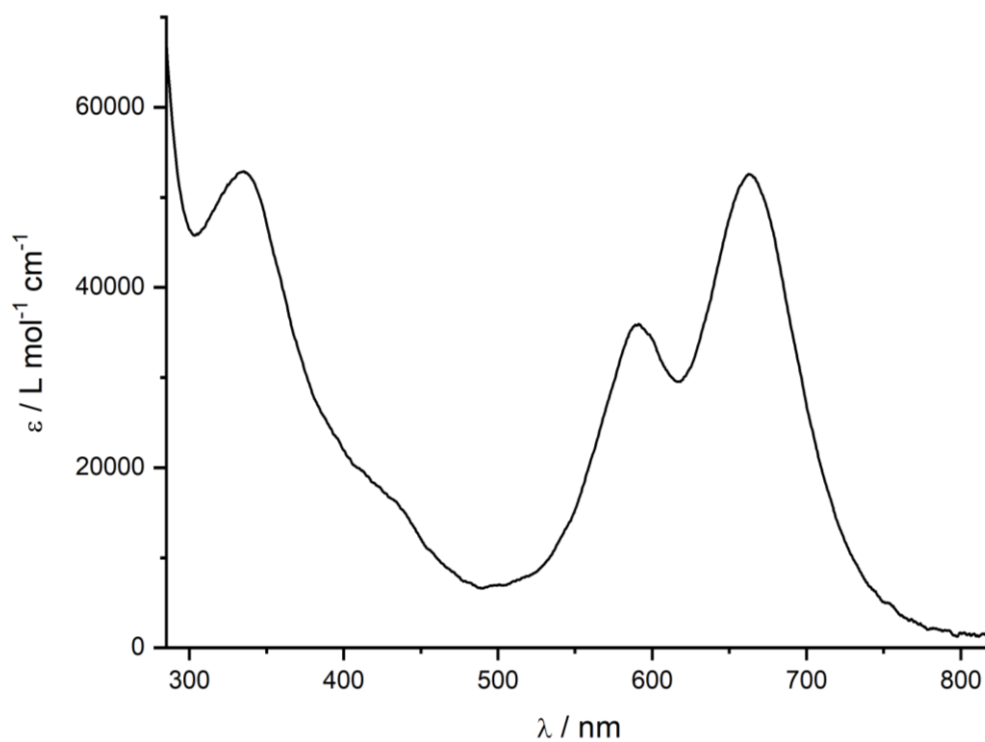


Figure S76. UV/Vis spectrum of $[(\text{PHDI})\text{Co}(\mu:\eta^4,\kappa^1\text{-P}_5\text{Lc})\{\text{W}(\text{CO})_5\}]$ (**5a-W(CO)₅**) in THF.

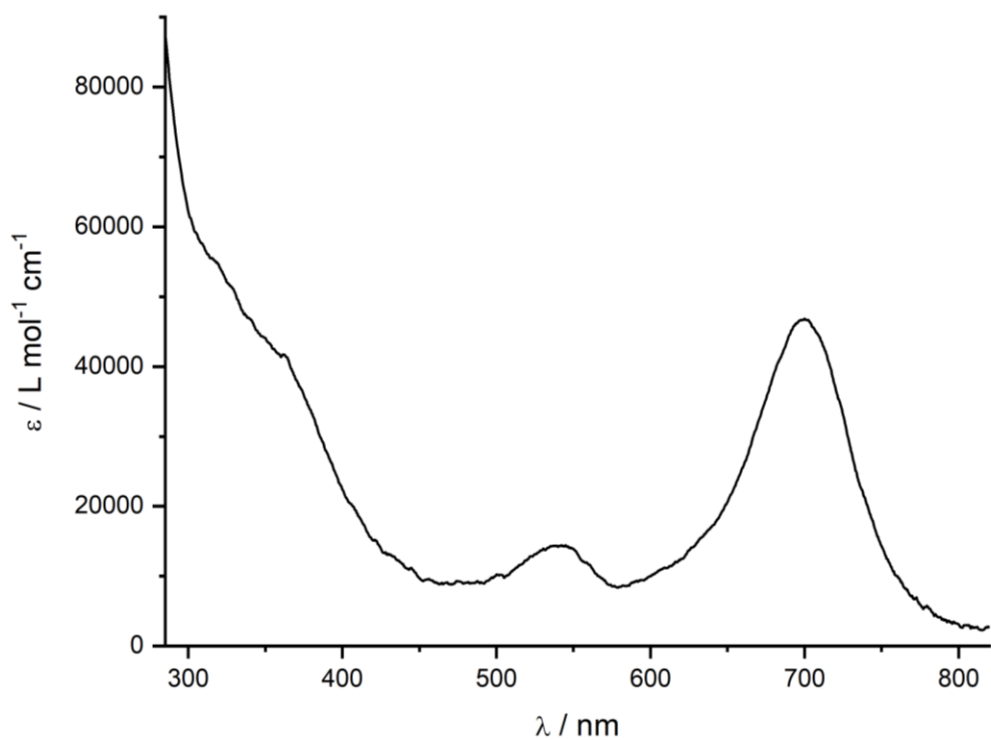


Figure 77. UV/Vis spectrum of $[(\text{PHDI})\text{Co}(\mu^3\text{:}\eta^4, \eta^1, \eta^1\text{-P}_7\text{Lc})\{\text{W}(\text{CO})_5\}_2]$ (**6a-W(CO)₅**)₂ in THF.

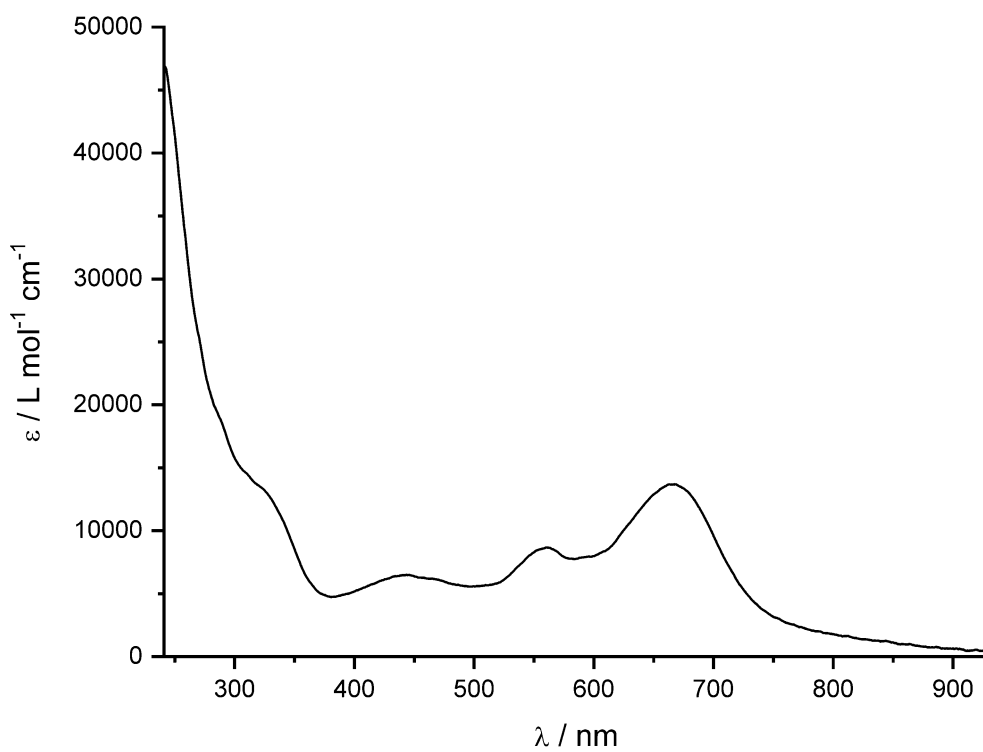


Figure S78. UV/Vis spectrum of $[(\text{Ar}^*\text{BIAN})\text{Co}(\eta^4\text{-P}_7\text{Lc})]$ (**6b**) in THF.

5. IR spectra

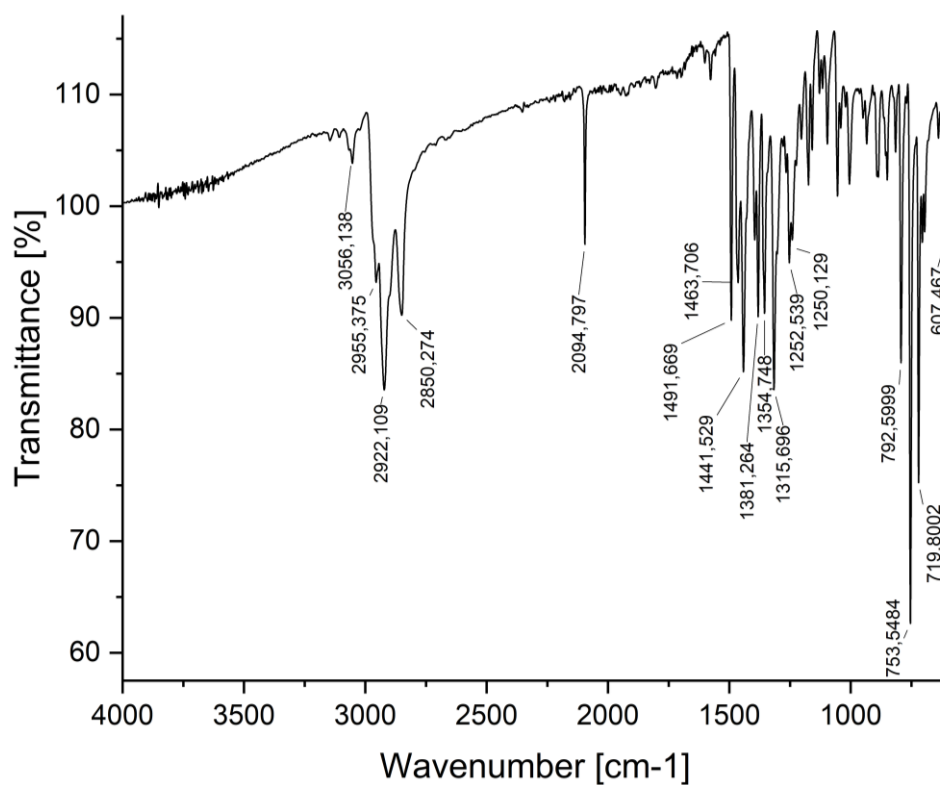


Figure S79. Solid state ATR-IR spectrum of $[(\text{PHDI})\text{Co}(\text{CN})(\eta^3\text{-P}_4\text{Cy}_2)]$ (**1a-Cy**).

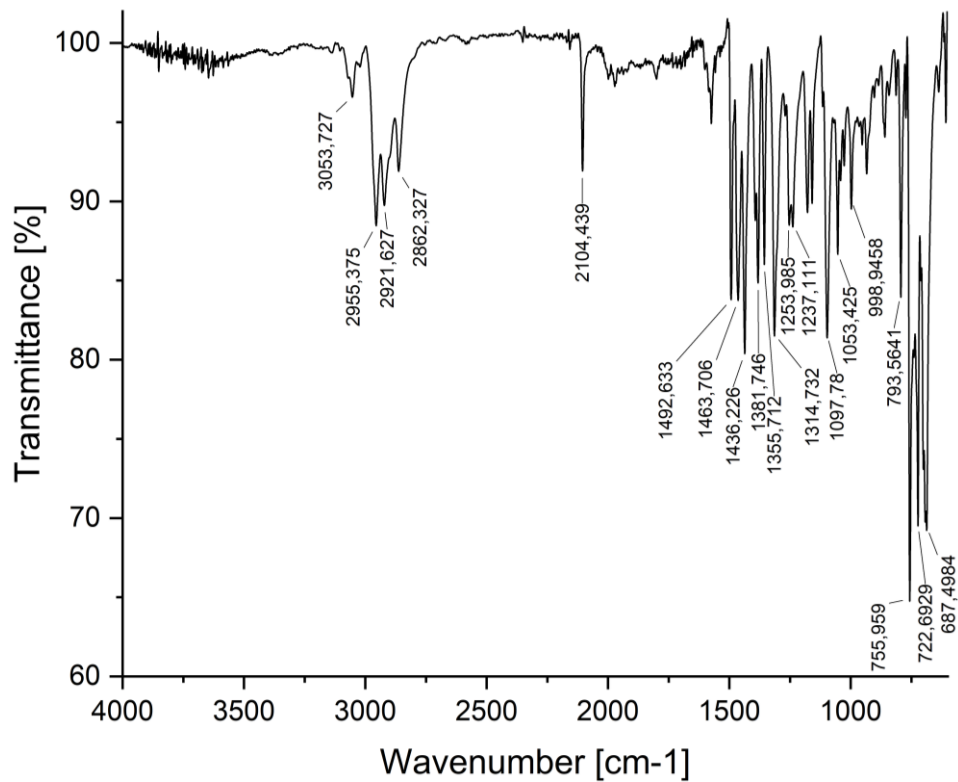


Figure S80. Solid state ATR-IR spectrum of $[(\text{PHDI})\text{Co}(\text{CN})(\eta^3\text{-P}_4\text{Ph}_2)]$ (**1a-Ph**).

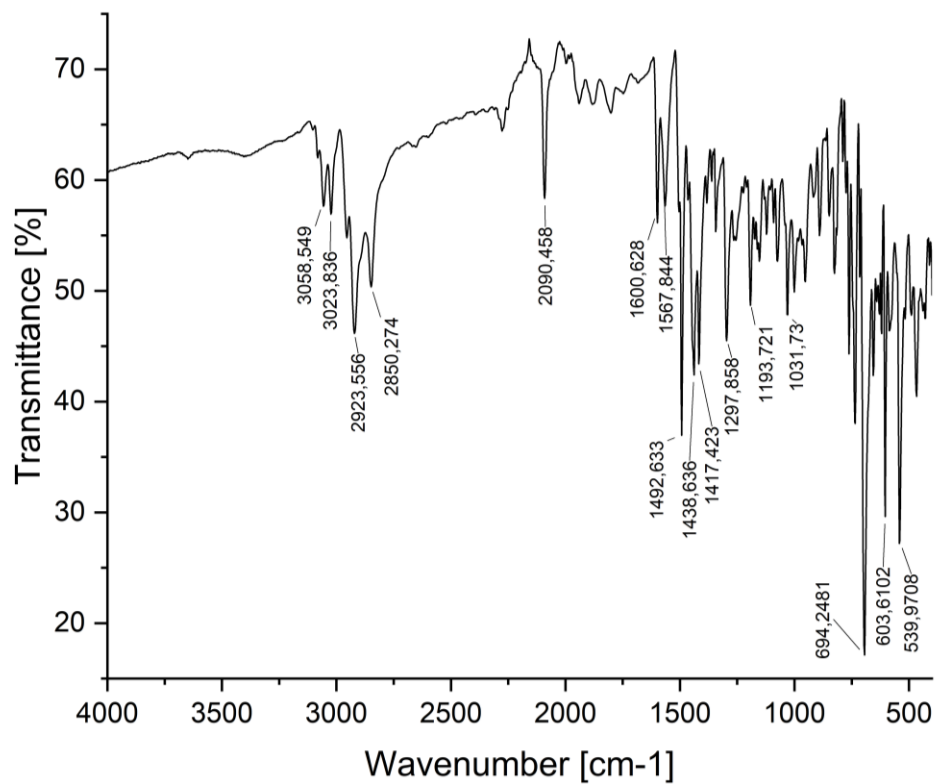


Figure S81. Solid state ATR-IR spectrum of $[(Ar^*BIAN)Co(CN)(\eta^3-P_4Cy_2)]$ (**1b-Cy**).

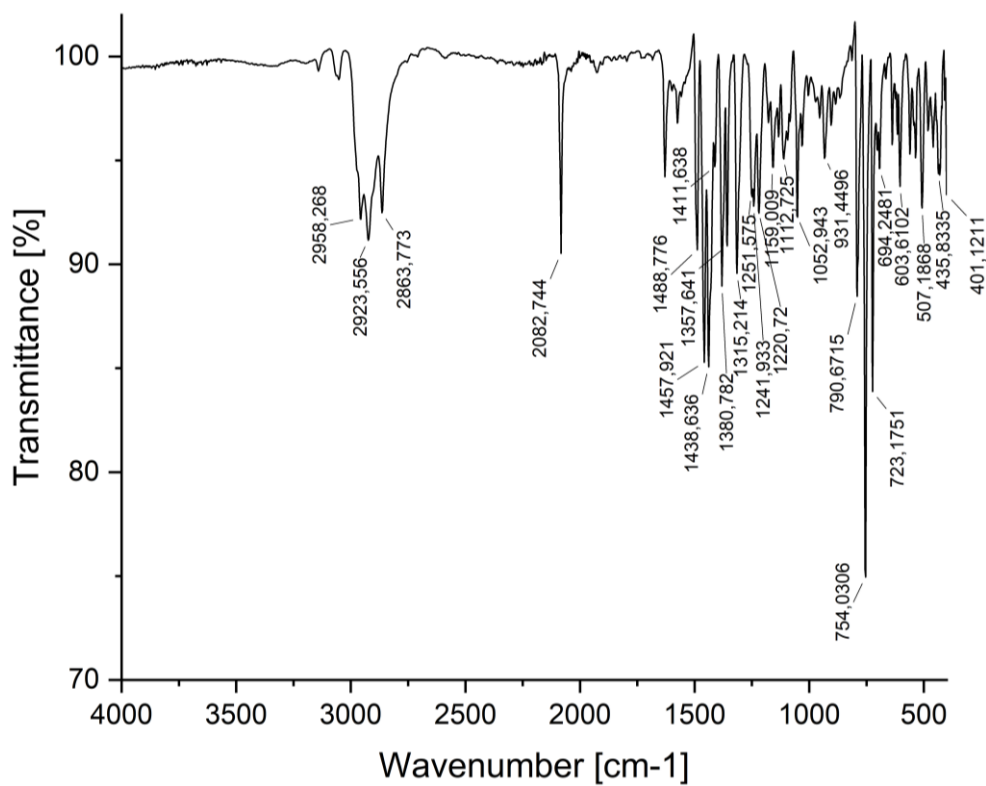


Figure S82. Solid state ATR-IR spectrum of $[(PHDI)Co(CN)(\eta^3-P_4Lc)]$ (**3a**).

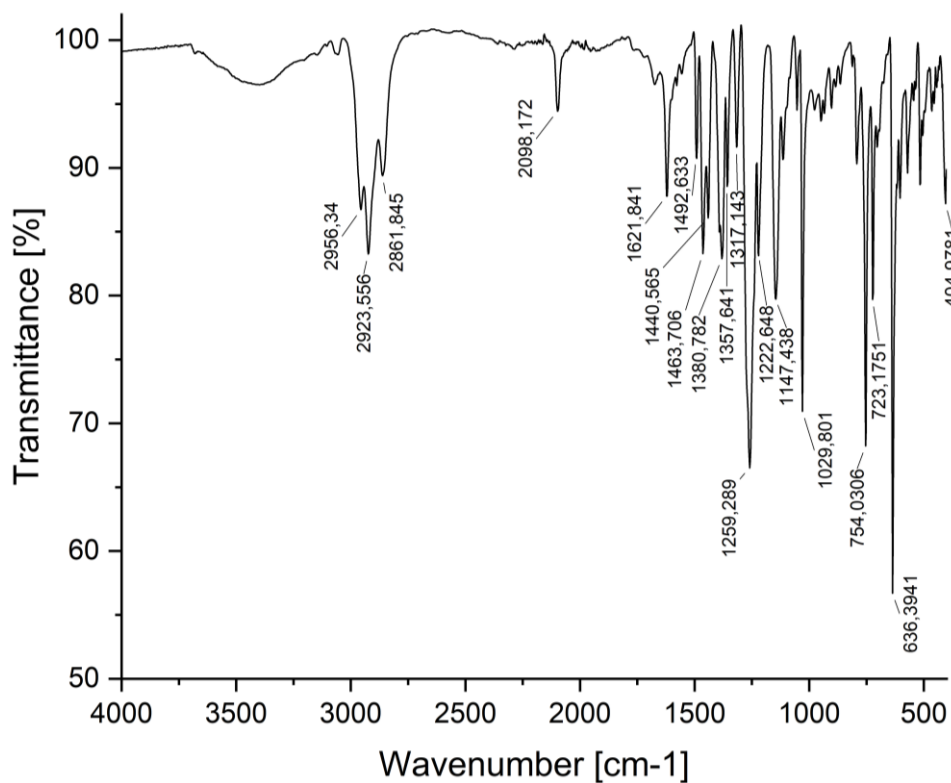


Figure S83. Solid state ATR-IR spectrum of $[(\text{PHDI})\text{Co}(\text{CN})(\eta^3\text{-P}_5(\text{Lc})_2)][\text{OTf}]$ (**4a**).

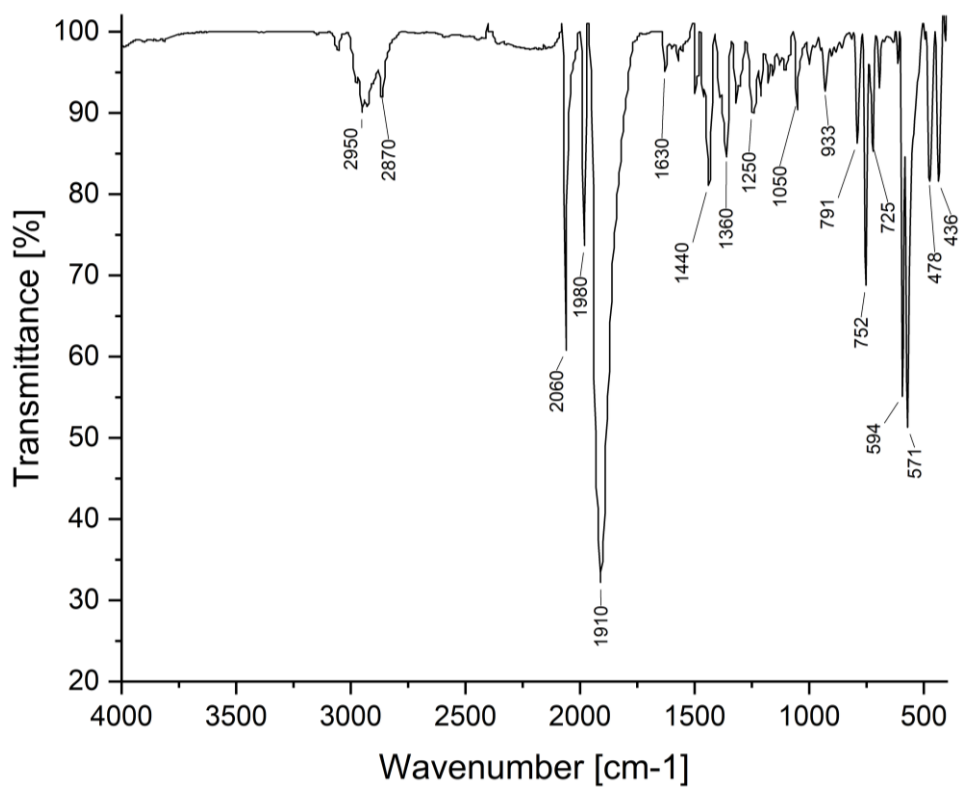


Figure S84. Solid state ATR-IR spectrum $[(\text{PHDI})\text{Co}(\mu:\eta^4,\kappa^1\text{-P}_5\text{Lc})\{\text{W}(\text{CO})_5\}]$ (**5a-W(CO)₅**).

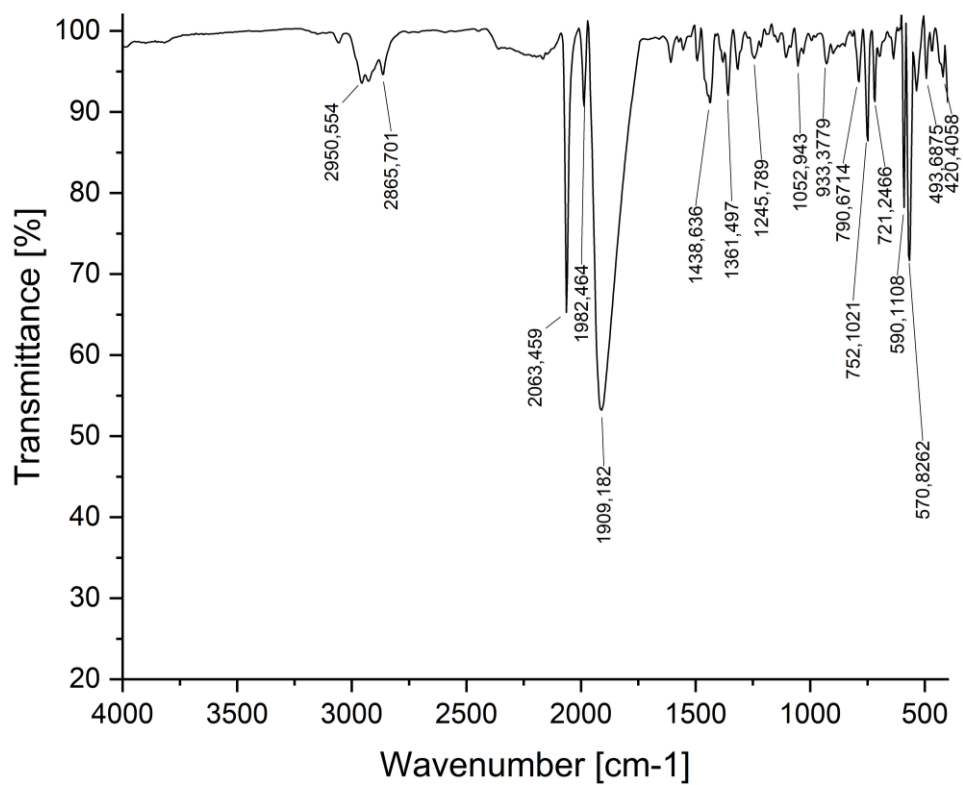


Figure S85. Solid state ATR-IR spectrum of of [(PHDI)Co(μ^3 : η^4 , η^1 , η^1 -P₇Lc){W(CO)₅}₂ (**6a**-{W(CO)₅}₂).

6. X-ray Crystallography

The single-crystal X-ray diffraction data were recorded on a GV1000 diffractometer with a TitanS2 detector, a Xcalibur Gemini ultra diffractometer with an AtlasS2 detector, a SuperNova, Dual, Cu at zero, AtlasS2 diffractometer and a XtaLAB Synergy R, DW system diffractometer with a HyPix-Arc 150 detector. In all cases, Cu-K α radiation ($\lambda = 1.54184 \text{ \AA}$) was used except for **1a-Cy** which was measured using Cu-K β radiation ($\lambda = 1.39222 \text{ \AA}$). Crystals were selected under mineral oil, mounted on micro mount loops and quench-cooled to 123 K using an Oxford Cryosystems open flow N $_2$ cooling device, except for **1a-Ph** which was measured at 293 K. The diffraction pattern was indexed and the total number of runs and images was based on the strategy calculation from the program CrysAlisPro (Rigaku, Version 1.171.42.53a, Rigaku Oxford Diffraction, 2023). The unit cell was refined using the same program. Either semi-empirical multi-scan absorption corrections^[20,21] or analytical^[22] ones were applied to the data. Using Olex2,^[23] the structures were solved with SHELXT^[24] using intrinsic phasing and refined with SHELXL^[25] using least squares refinement on F^2 . The hydrogen atoms were located in idealized positions and refined isotropically with a riding model.

[(PHDI)Co(CN)(η^3 -P $_4$ Cy $_2$)] (**1a-Cy**): Crystals were obtained from a saturated Et $_2$ O solution of **1a-Cy**.

[(PHDI)Co(CN)(η^3 -P $_4$ Ph $_2$)] (**1a-Ph**): Crystals were obtained from a saturated Et $_2$ O solution of **1a-Ph**.

[(Ar*BIAN)Co(CN)(η^3 -P $_4$ Cy $_2$)] (**1b-Cy**): Crystals were obtained by slow diffusion of *n*-hexane into a saturated toluene solution of **1b-Cy**. The crystal structure of **1b-Cy** contained two severely disordered *n*-hexane molecules per asymmetric unit. One molecule of *n*-hexane was modelled for disorder in a 55:45 ratio, while the other, which did not lend itself to effective modeling, was accounted for by use of a solvent mask. The solvent mask was calculated, and 102 electrons were found in a volume of 462 \AA^3 in one void per unit cell. This is consistent with the presence of 1.0 *n*-hexane per Formula Unit which account for 100 electrons per unit cell.

[(Ar*BIAN)Co(η^4 -P $_5$ tBu $_2$)] (**2b-tBu**): Crystals were obtained by slow diffusion of *n*-pentane into a saturated toluene solution of **2b-tBu**. The crystal structure of **2b-tBu** contained two times half a molecule of *n*-pentane and two toluene molecules each per asymmetric unit. One toluene molecule was modeled without disorder and the other one was modelled for disorder in a 55:45 ratio. The half *n*-pentane molecules were severely disordered and refined by using the solvent mask command: A solvent mask was calculated, and 93 electrons were found in a volume of 500 \AA^3 in two voids per unit cell. This is consistent with the presence of 2 \times 0.5 *n*-pentane per Formula Unit which account for 84 electrons per unit cell.

[(Ar*BIAN)Co(η^4 -P $_5$ N(*i*Pr) $_2$)] (**2b-N(*i*Pr) $_2$**): Crystals were obtained from a saturated *n*-hexane solution of **2b-N(*i*Pr) $_2$** .

[(PHDI)Co(CN)(η^3 -P $_4$ Lc)] (**3a**): Crystals were obtained from a saturated *n*-hexane solution of **3a**. Twinning of the crystal of **3a** was refined with a HKLF 5 BASF [0.305(6)] command. The disorder within the *cyclo*-P $_4$ moiety was modelled in a 59:41 ratio.

[(PHDI)Co(CN)(η^3 -P $_5$ (Lc) $_2$)] [OTf] (**4a**[OTf]): Crystals were obtained by slow diffusion of *n*-hexane into a saturated benzene solution of **4a**[OTf]. The crystal structure of **4a**[OTf] contained one severely disordered molecule of benzene and half a severely disordered molecule of *n*-hexane which were refined using the solvent mask command: A solvent mask was calculated, and 524 electrons were found in a volume of 3664 \AA^3 in one void per unit cell. This is consistent with the presence of 1.0 benzene and 0.5 *n*-hexane per Asymmetric Unit which account for 536 electrons per unit cell (1.0 benzene and 0.5 *n*-hexane: 67 e $^-$, found: 66 e $^-$ for each void).

[(PHDI)Co(μ : η^4 , κ^1 -P $_5$ Lc){W(CO) $_5$ }] (**5a-W(CO) $_5$**): Crystals were obtained from a saturated Et $_2$ O solution of **5a-W(CO) $_5$** . Twinning of the crystal of **5a-W(CO) $_5$** was refined with a HKLF 5 BASF [0.444(5)] command. The crystal structure of **5a-W(CO) $_5$** contained one disordered molecule of diethylether per

asymmetric unit, which modelled for disorder in a 57:43 ratio. Additionally, the crystal contained 0.2 severely disordered molecules of diethylether which were refined using the solvent mask command: A solvent mask was calculated, and 32 electrons were found in a volume of 392 Å³ in one void per unit cell. This is consistent with the presence of 0.2 diethylether per Asymmetric Unit which account for 34 electrons per unit cell (0.2 diethylether: 8 e⁻, found: 8 e⁻ for each void).

[(PHDI)Co(μ³:η⁴,η¹,η¹-P₇Lc){W(CO)₅}₂] (**6a**-{W(CO)₅}₂): Crystals were obtained by slow-diffusion of *n*-hexane into a saturated toluene solution of **6a**-{W(CO)₅}₂. The crystal structure of **6a**-{W(CO)₅}₂ contained one disordered toluene molecule per asymmetric unit and one toluene molecule over a symmetry axis. This is consistent with 1.5 molecules of toluene per asymmetric unit.

[(Ar*BIAN)Co(η²:η²-P₇Lc)] (**6b**): Crystals were obtained by slow diffusion of *n*-hexane into a saturated toluene solution of **6b**. The crystal structure of **6b** contained one full and additional 0.75 severely disordered 1,4-dioxane molecules per asymmetric unit. A solvent mask was calculated which found 153 electrons in a volume of 697 Å³ in one void per unit cell. This is consistent with the presence of 1.75 1,4-dioxanes per Formula Unit which account for 168 electrons per unit cell.

[(Lc)₄P₄][OTf]₂ (*meso*-**7**[OTf]₂): Crystals were obtained by layering a concentrated PhF solution of **7**[OTf]₂ with *n*-hexane. The crystal structure of **7**[OTf]₂ contained two molecules of PhF and one disordered molecule of PhF per asymmetric unit and one molecule of PhF over a symmetry axis. This is consistent with 3.5 molecules PhF per asymmetric unit.

Table S12. Crystallographic data and structure refinement for compounds **1a-Cy**, **1a-Ph**, **1b-Cy** and **2b-tBu**.

Compound	1a-Cy	1a-Ph	1b-Cy	2b-tBu
Empirical formula	C ₅₅ H ₇₄ CoN ₃ OP ₄	C ₅₅ H ₆₂ CoN ₃ OP ₄	C ₁₀₁ H ₁₀₄ CoN ₃ P ₄	C ₁₉₄ H ₁₈₈ Co ₂ N ₄ P ₁₀
Formula Weight	975.98 g/mol	963.88 g/mol	1628.85	3003.03
Temperature [K]	123(1)	293(2)	123.0(1)	100.0(1)
Crystal System	monoclinic	monoclinic	monoclinic	triclinic
Space Group	<i>P2₁/n</i>	<i>P2₁/n</i>	<i>P2₁</i>	<i>P-1</i>
<i>a</i> [Å]	16.9323(5)	16.9361(2)	15.2435(2)	13.60598(10)
<i>b</i> [Å]	15.6792(4)	15.5637(1)	18.9554(2)	23.98531(15)
<i>c</i> [Å]	21.1165(6)	20.5295(2)	15.8508(2)	26.39734(19)
α [°]	90	90	90	98.3571(6)
β [°]	111.501(3)	110.820(1)	102.2540(10)	104.1729(6)
γ [°]	90	90	90	91.1376(6)
Volume [Å ³]	5216.0(3)	5057.99(9)	4475.68(10)	8249.88(10)
<i>Z</i>	4	4	2	2
ρ_{calc} [g/cm ³]	1.243	1.266	1.209	1.209
μ [mm ⁻¹]	3.034	4.170	2.553	2.906
<i>F</i> (000)	2080.0	2032.0	1736.0	3168.0
Crystal Size [mm ³]	0.264 × 0.076 × 0.063	0.278 × 0.15 × 0.094	0.251 × 0.107 × 0.079	0.221 × 0.162 × 0.103
Diffractometer	GV1000, TitanS2	Xcalibur Gemini ultra, AtlasS2	SuperNova, Dualflex, TitanS2	XtaLAB Synergy R, DW system, HyPix- Arc 150
Radiation	Cu K β (λ = 1.39222)	Cu K α (λ = 1.54184)	Cu K α (λ = 1.54184)	CuK α (λ = 1.54184)
2 θ range for data collection [°]	5.202 to 125.322	7.314 to 143.794	7.37 to 133.918	3.73 to 148.554
Index ranges	-21 ≤ <i>h</i> ≤ 21, -19 ≤ <i>k</i> ≤ 18, -26 ≤ <i>l</i> ≤ 26	-20 ≤ <i>h</i> ≤ 20, -18 ≤ <i>k</i> ≤ 18, -23 ≤ <i>l</i> ≤ 24	-17 ≤ <i>h</i> ≤ 17, -22 ≤ <i>k</i> ≤ 20, -18 ≤ <i>l</i> ≤ 17	-16 ≤ <i>h</i> ≤ 16, -26 ≤ <i>k</i> ≤ 29, -32 ≤ <i>l</i> ≤ 32
Reflections collected	32319	18778	36708	127795
Independent reflections	11008 [R _{int} = 0.0509, R _{sigma} = 0.0685]	9592 [R _{int} = 0.0229, R _{sigma} = 0.0330]	13451 [R _{int} = 0.0733, R _{sigma} = 0.0601]	31983 [R _{int} = 0.0301, R _{sigma} = 0.0269]
Data / restraints / parameters	11008/222/642	9592/156/630	13451/26/999	31983/269/2010
Goodness-of-fit on <i>F</i> ²	1.028	1.042	1.024	1.034
Final R indexes [I >= 2 σ (I)]	R ₁ = 0.0465, wR ₂ = 0.0947	R ₁ = 0.0343, wR ₂ = 0.0833	R ₁ = 0.0599, wR ₂ = 0.1525	R ₁ = 0.0574, wR ₂ = 0.1517
Final R indexes [all data]	R ₁ = 0.0734, wR ₂ = 0.1078	R ₁ = 0.0378, wR ₂ = 0.0855	R ₁ = 0.0627, wR ₂ = 0.1559	R ₁ = 0.0626, wR ₂ = 0.1550
Largest diff. peak/hole [e Å ⁻³]	0.42/-0.34	0.36/-0.31	0.40/-0.74	1.09/-0.86
Flack parameter	-	-	-0.036(3)	-

Table S 13 Crystallographic data and structure refinement for **2b-N(*i*Pr)₂**, **3a**, **4a[OTf]**, **5a-W(CO)₅**.

Compound	2b-N(<i>i</i>Pr)₂	3a	4a[OTf]	5a-W(CO)₅
Empirical formula	C ₉₄ H ₉₆ CoN ₄ P ₅	C ₅₀ H ₆₂ CoN ₅ P ₄	C ₆₂ H ₈₂ CoF ₃ N ₇ O ₃ P ₅ S	C ₅₈ H ₇₂ CoN ₄ O ₆ P ₅ W
Formula Weight	1495.52	915.85 g/mol	1276.18 g/mol	1318.82
Temperature [K]	123.0(1)	123(1)	123(1)	122.96(14)
Crystal System	orthorhombic	tetragonal	orthorhombic	orthorhombic
Space Group	<i>Pna</i> 2 ₁	<i>P</i> 4 ₁ 2 ₁ 2	<i>Pbca</i>	<i>P</i> 2 ₁ 2 ₁ 2 ₁
<i>a</i> [Å]	30.9069(4)	21.6656(2)	14.5541(2)	17.35880(10)
<i>b</i> [Å]	19.5965(3)	21.6656(2)	18.2358(2)	18.65900(10)
<i>c</i> [Å]	13.02160(10)	19.8986(2)	56.4931(10)	18.82150(10)
α [°]	90	90	90	90
β [°]	90	90	90	90
γ [°]	90	90	90	90
Volume [Å ³]	7886.76(17)	9340.4(2)	14993.6(4)	6096.24(6)
<i>Z</i>	4	8	8	4
ρ_{calc} [g/cm ³]	1.260	1.303	1.131	1.437
μ [mm ⁻¹]	3.044	4.481	3.469	7.210
<i>F</i> (000)	3160.0	3872.0	5376.0	2688.0
Crystal Size [mm ³]	0.204 × 0.072 × 0.051	0.187 × 0.08 × 0.046	0.174 × 0.048 × 0.04	0.246 × 0.206 × 0.122
Diffractometer	XtaLAB Synergy R, DW system, HyPix-Arc 150	XtaLAB Synergy R, DW system, HyPix-Arc 150	XtaLAB Synergy R, DW system, HyPix-Arc 150	XtaLAB Synergy R, DW system, HyPix-Arc 150
Radiation	Cu K α (λ = 1.54184)	Cu K α (λ = 1.54184)	Cu K α (λ = 1.54184)	Cu K α (λ = 1.54184)
2 θ range for data collection [°]	5.34 to 146.13	5.768 to 146.962	6.258 to 134.154	8.394 to 134.006
Index ranges	-37 ≤ <i>h</i> ≤ 36, -22 ≤ <i>k</i> ≤ 23, -11 ≤ <i>l</i> ≤ 15	-21 ≤ <i>h</i> ≤ 26, -26 ≤ <i>k</i> ≤ 25, -23 ≤ <i>l</i> ≤ 24	-17 ≤ <i>h</i> ≤ 17, -17 ≤ <i>k</i> ≤ 21, -67 ≤ <i>l</i> ≤ 67	-20 ≤ <i>h</i> ≤ 17, -22 ≤ <i>k</i> ≤ 22, -21 ≤ <i>l</i> ≤ 22
Reflections collected	30252	57010	49852	64643
Independent reflections	11704 [R _{int} = 0.0248, R _{sigma} = 0.0307]	9070 [R _{int} = 0.0420, R _{sigma} = 0.0299]	13260 [R _{int} = 0.0876, R _{sigma} = 0.0608]	10803 [R _{int} = 0.0482, R _{sigma} = 0.0232]
Data / restraints / parameters	11704/1/1146	9070/544/790	13260/192/839	10803/142/752
Goodness-of-fit on <i>F</i> ²	1.032	1.067	1.042	1.044
Final R indexes [<i>I</i> ≥ 2 σ (<i>I</i>)]	R ₁ = 0.0422, wR ₂ = 0.1114	R ₁ = 0.0529, wR ₂ = 0.1136	R ₁ = 0.0887, wR ₂ = 0.2482	R ₁ = 0.0255, wR ₂ = 0.0663
Final R indexes [all data]	R ₁ = 0.0477, wR ₂ = 0.1153	R ₁ = 0.0652, wR ₂ = 0.1218	R ₁ = 0.1000, wR ₂ = 0.2565	R ₁ = 0.0256, wR ₂ = 0.0665
Largest diff. peak/hole [e Å ⁻³]	0.70/-0.34	0.34/-0.32	1.12/-0.58	0.49/-0.61
Flack/Hoof parameter	-0.033(2)	0.305(6)	-	0.444(5)

Table S14. Crystallographic data and structure refinement for **5a**-{W(CO)₅}₂, **6a**-{W(CO)₅}₂, **6b**, **7**[OTf]₂.

Compound	5a -{W(CO) ₅ } ₂	6a -{W(CO) ₅ } ₂	6b	7 [OTf] ₂
Empirical formula	C ₅₉ H ₆₂ CoN ₄ O ₁₀ P ₅ W ₂	C _{69.5} H ₇₄ CoN ₄ O ₁₀ P ₇ W ₂	C ₁₀₀ H ₁₀₂ CoN ₄ O _{3.5} P ₇	C ₆₇ H _{97.5} F _{9.5} N ₈ O ₆ P ₄ S ₂
Formula Weight	1568.60	1768.74	1691.57	1479.52
Temperature [K]	123.00(10)	122.99(1)	123.00(10)	100.01(10)
Crystal System	monoclinic	triclinic	triclinic	triclinic
Space Group	P2 ₁ /n	P-1	P-1	P-1
<i>a</i> [Å]	13.10840(10)	12.23045(8)	14.31880(10)	14.1645(2)
<i>b</i> [Å]	25.7731(2)	15.87651(6)	15.61740(10)	14.1756(3)
<i>c</i> [Å]	20.6519(2)	20.32376(7)	21.9186(2)	19.9097(4)
α [°]	90	95.1122(3)	90.5700(10)	73.9941(16)
β [°]	100.1270(10)	106.5990(5)	108.1410(10)	88.7269(14)
γ [°]	90	101.5319(5)	108.5180(10)	78.7940(15)
Volume [Å ³]	6868.42(10)	3660.40(3)	4384.35(7)	3767.36(12)
<i>Z</i>	4	2	2	2
ρ_{calc} [g/cm ³]	1.517	1.605	1.281	1.304
μ [mm ⁻¹]	3.749	9.354	3.165	2.096
<i>F</i> (000)	3096.0	1758.0	1780.0	1562.0
Crystal Size [mm ³]	0.174 × 0.138 × 0.093	0.191 × 0.087 × 0.059	0.164 × 0.063 × 0.046	0.23 × 0.148 × 0.047
Diffractometer	XtaLAB Synergy R, DW system, HyPix-Arc 150	XtaLAB Synergy R, DW system, HyPix-Arc 150	XtaLAB Synergy R, DW system, HyPix-Arc 150	SuperNova, Dual, Cu at zero, AtlasS2
Radiation	Mo K α (λ = 0.71073)	Cu K α (λ = 1.54184)	Cu K α (λ = 1.54184)	Cu K α (λ = 1.54184)
2 θ range for data collection [°]	4.308 to 81.176	5.752 to 150.632	6.012 to 151.58	4.62 to 153.666
Index ranges	-23 ≤ <i>h</i> ≤ 20, -39 ≤ <i>k</i> ≤ 47, -37 ≤ <i>l</i> ≤ 35	-15 ≤ <i>h</i> ≤ 15, -17 ≤ <i>k</i> ≤ 19, -25 ≤ <i>l</i> ≤ 25	-17 ≤ <i>h</i> ≤ 17, -18 ≤ <i>k</i> ≤ 19, -27 ≤ <i>l</i> ≤ 26	-17 ≤ <i>h</i> ≤ 17, -17 ≤ <i>k</i> ≤ 15, -25 ≤ <i>l</i> ≤ 24
Reflections collected	178935	80748	86378	42325
Independent reflections	42928 [R _{int} = 0.0312, R _{sigma} = 0.0406]	14877 [R _{int} = 0.0209, R _{sigma} = 0.0136]	17859 [R _{int} = 0.0287, R _{sigma} = 0.0257]	15694 [R _{int} = 0.0277, R _{sigma} = 0.0336]
Data / restraints / parameters	42928/0/744	14877/198/912	17859/96/1014	15694/1233/1114
Goodness-of-fit on χ^2	1.024	1.060	1.080	1.014
Final R indexes [<i>I</i> ≥ 2 σ (<i>I</i>)]	R ₁ = 0.0455, wR ₂ = 0.1004	R ₁ = 0.0223, wR ₂ = 0.0584	R ₁ = 0.0404, wR ₂ = 0.1085	R ₁ = 0.0430, wR ₂ = 0.1156
Final R indexes [all data]	R ₁ = 0.0775, wR ₂ = 0.1092	R ₁ = 0.0233, wR ₂ = 0.0589	R ₁ = 0.0474, wR ₂ = 0.1122	R ₁ = 0.0475, wR ₂ = 0.1201
Largest diff. peak/hole [e Å ⁻³]	5.05/-1.44	0.82/-0.81	0.50/-0.36	0.68/-0.56

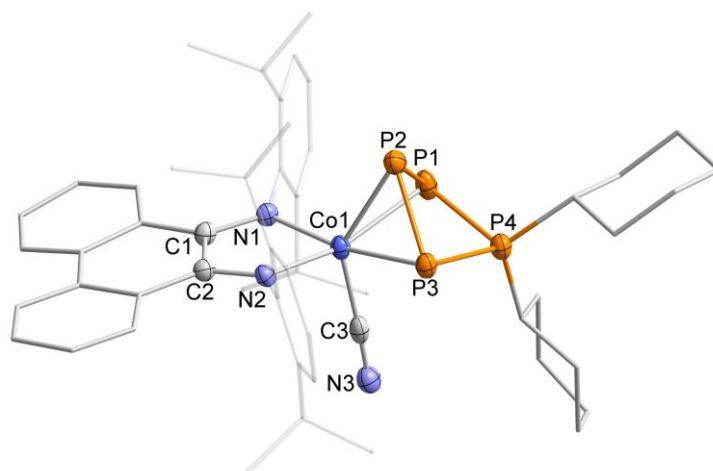


Figure S86. Solid-state molecular structure of $[(\text{PHDI})\text{Co}(\text{CN})(\eta^3\text{-P}_4\text{Cy}_2)]$ (**1a-Cy**). Hydrogen atoms and disorder are omitted for clarity. Thermal ellipsoids are drawn at the 50% probability level. The asymmetric unit of **1a-Cy** contained one molecule of Et_2O , which is not shown. Selected bond lengths [Å] and angles [°]: C1–C2 1.465(3), C1–N1 1.329(3), C2–N2 1.331(3), Co1–C3 1.920(3), Co1–N1 1.920(2), Co1–N2 1.914(2), Co1–P1 2.325(8), Co1–P2 2.258(8), Co1–P3 2.341(7), C3–N3 1.148(3), P1–P2 2.189(1), P2–P3 2.190(9), P3–P4 2.173(9), P4–P1 2.170(9), P1 P2 P3 87.470(3), P2 P3 P4 82.030(3), P3 P4 P1 88.370(3), P4 P1 P2 82.110(3), P1 P2 P3 P4 59.97(2).

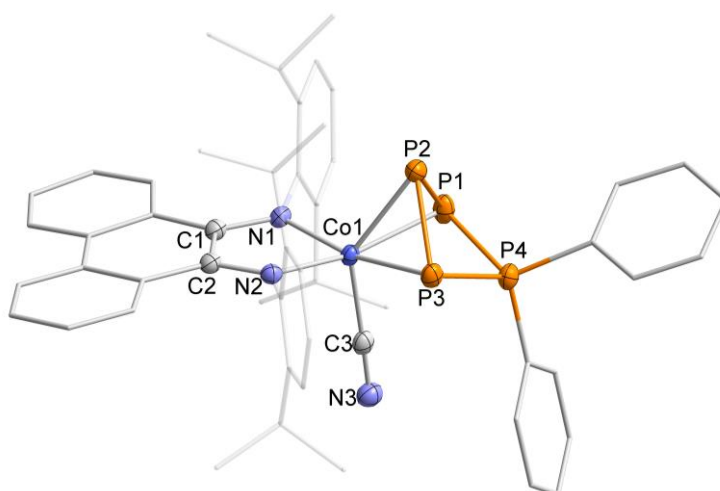


Figure S87. Solid-state molecular structure of $[(\text{PHDI})\text{Co}(\text{CN})(\eta^3\text{-P}_4\text{Ph}_2)]$ (**1a-Ph**). Hydrogen atoms and disorder are omitted for clarity. Thermal ellipsoids are drawn at the 50% probability level. The asymmetric unit of **1a-Ph** contained one molecule of Et_2O , which is not shown. Selected bond lengths [Å] and angles [°]: C1–C2 1.463(2), C1–N1 1.334(2), C2–N2 1.328(2), Co1–C3 1.915(2), Co1–N1 1.918(1), Co1–N2 1.911(1), Co1–P1 2.315(5), Co1–P2 2.265(5), Co1–P3 2.319(5), C3–N3 1.150(2), P1–P2 2.194(7), P2–P3 2.192(6), P3–P4 2.167(6), P4–P1 2.165(6), P1 P2 P3 87.74(2), P2 P3 P4 81.91(2), P3 P4 P1 89.10(2), P4 P1 P2 81.91(2), P1 P2 P3 P4 60.00(2).

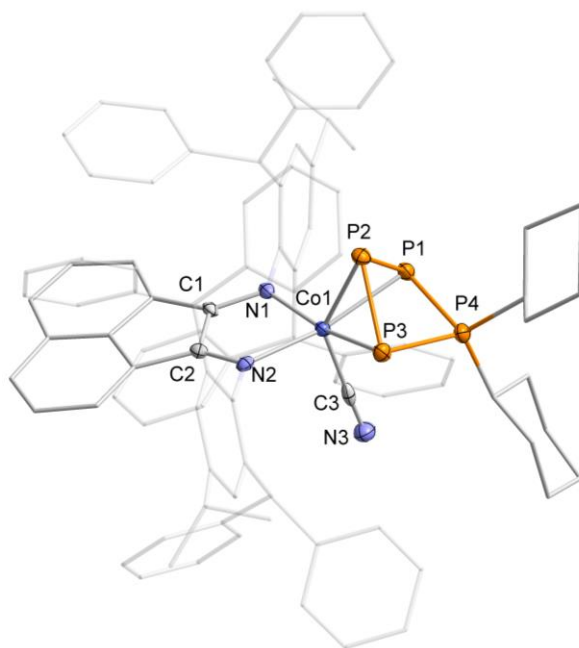


Figure S88. Solid-state molecular structure of $[(Ar^*BIAN)Co(CN)(\eta^3-P_4Cy_2)]$ (**1b-Cy**). Hydrogen atoms and non-coordinating solvent molecules are omitted for clarity. Thermal ellipsoids are drawn at the 50% probability level. Selected bond lengths [Å] and angles [°]: C1–C2 1.459(7), C1–N1 1.307(7), C2–N2 1.309(7), Co1–C3 1.901(6), Co1–N1 1.970(5), Co1–N2 2.002(4), Co1–P1 2.2922(2), Co1–P2 2.2692(2), Co1–P3 2.2933(2), C3–N3 1.135(8), P1–P2 2.202(2), P2–P3 2.2015(2), P3–P4 2.176(2), P4–P1 2.1703(2), P1 P2 P3 86.36(7), P2 P3 P4 82.60(7), P3 P4 P1 87.79(7), P4 P1 P2 82.71(7), P1 P2 P3 P4 59.93(5).

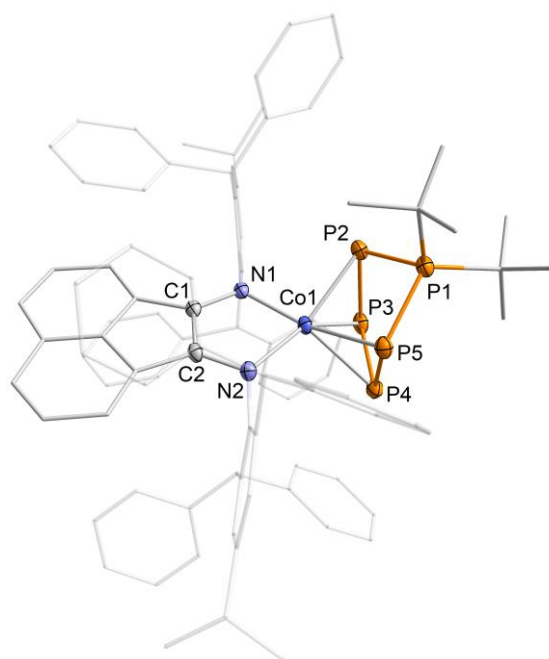


Figure S89. Solid-state molecular structure of $[(Ar^*BIAN)Co(\eta^4-P_5tBu_2)]$ (**2b-tBu**). Hydrogen atoms, disorder in the *t*Bu group and non-coordinating solvent molecules are omitted for clarity. The asymmetric unit cell of **2b-tBu** contained a second crystallographically independent molecule with very similar structural parameters; only one of these molecules is shown. Thermal ellipsoids are drawn at the 50% probability level. Selected bond lengths [Å] and angles [°]: C1–C2 1.424(4), C1–N1 1.331(3), C2–N2 1.341(3), Co1–N1 1.935(2), Co1–N2 1.945(2), Co1–P2 2.3407(8), Co1–P3 2.3193(8), Co1–P4 2.3169(9), Co1–P5 2.3510(8), P1–P2 2.158(1), P2–P3 2.1633(1), P3–P4 2.1330(1), P4–P5 2.1544(1), P5–P1 2.1632(1), P5 P1 P2 93.84(4), P1 P2 P3 101.26(4), P2 P3 P4 104.11(4), P3 P4 P5 103.29(4), P4 P5 P1 102.45(4).

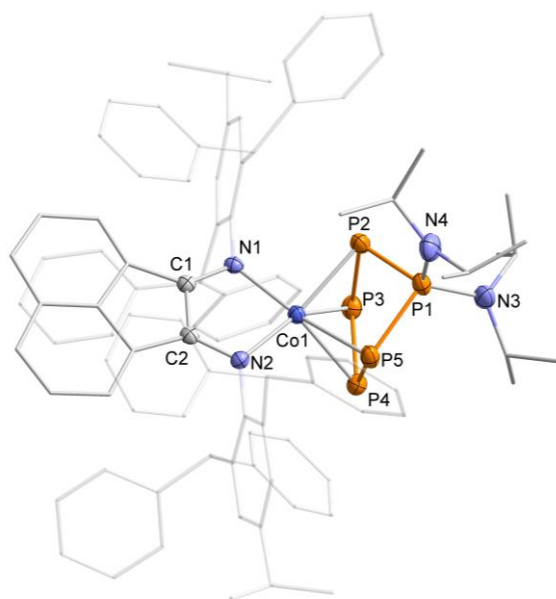


Figure S90. Solid-state molecular structure of $[(Ar^*BIAN)Co(\eta^4-P_5(N(iPr)_2))] (2b-N(iPr)_2)$. Hydrogen atoms are omitted for clarity. Thermal ellipsoids are drawn at the 50% probability level. Selected bond lengths [Å] and angles [°]: C1–C2 1.416(6), C1–N1 1.335(5), C2–N2 1.334(5), Co1–N1 1.947(3), Co1–N2 1.941(3), Co1–P2 2.3095(1), Co1–P3 2.3369(1), Co1–P4 2.3488(1), Co1–P5 2.3365(1), P1–P2 2.1613(1), P2–P3 2.1481(2), P3–P4 2.1404(2), P4–P5 2.1497(2), P5–P1 2.1613(2), P5 P1 P2 93.92(5), P1 P2 P3 98.76(6), P2 P3 P4 104.21(6), P3 P4 P5 103.00(6), P4 P5 P1 100.07(6).

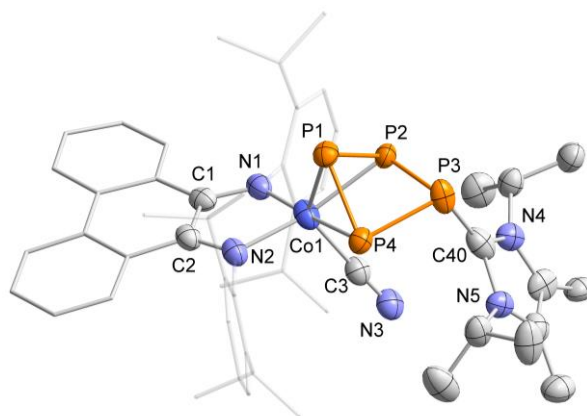


Figure S91. Solid-state molecular structure of $[(PHDI)Co(CN)(\eta^3-P_4Lc)] (3a)$. Hydrogen atoms and disorder in one of the Dipp groups, the L_c substituent as well as the P_4 moiety are omitted for clarity. Thermal ellipsoids are drawn at the 40% probability level. Selected bond lengths [Å] and angles [°]: C1–C2 1.452(7), C1–N1 1.334(6), C2–N2 1.343(7), Co1–N1 1.925(5), Co1–N2 1.926(4), Co1–P1 2.332(6)*, Co1–P2 2.333(9)*, Co1–P4 2.204(8)*, C3–N3 1.161(6), P1–P2 2.157(9)*, P2–P3 2.233(7)*, P3–P4 2.236(7)*, P4–P1 2.162(6)*, P3–C40 1.840(2)*, C40–N4 1.346(14)*, C40–N5 1.348(14)*, P1–P2–P3 84.4(3)*, P2–P3–P4 79.5(3)*, P3–P4–P1 84.2(2)*, P4–P1–P2 82.9(3)*. * Bond lengths [Å] and angles [°] result from the disordered part with the higher contribution.

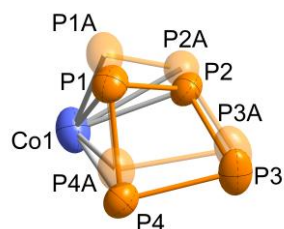


Figure S92. View of the disordered P_4 ligand in the solid-state molecular structure of $[(PHDI)Co(CN)(\eta^3-P_4Lc)] (3a)$. Part 1 is occupied 41% and part 2 is occupied 59%. Thermal ellipsoids are drawn at the 50% probability level.

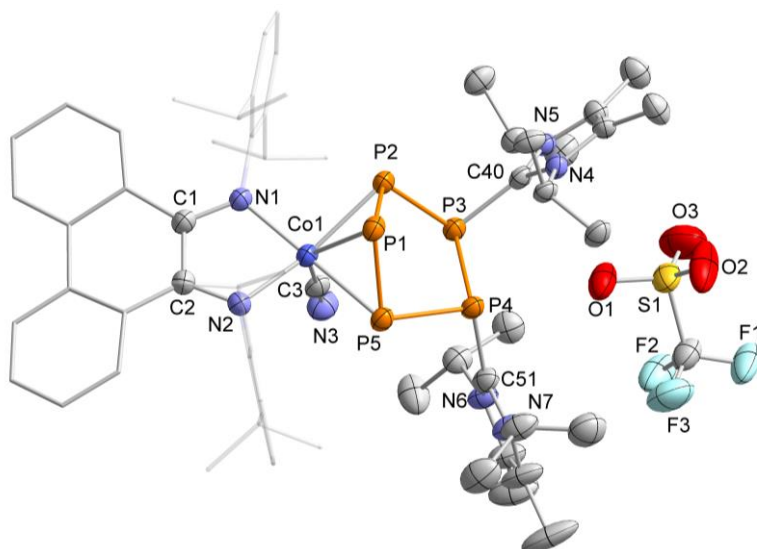


Figure S93. Solid-state molecular structure of $[(\text{PHDI})\text{Co}(\text{CN})(\eta^3\text{-P}_5(\text{Lc})_2)]$ (**4a**). Hydrogen atoms and disorder in the PHDI ligand are omitted for clarity. Thermal ellipsoids are drawn at the 50% probability level. Selected bond lengths [Å] and angles [°]: C1–C2 1.441(7), C1–N1 1.343(6), C2–N2 1.321(6), Co1–N1 1.920(4), Co1–N2 1.938(4), Co1–P1 2.3152(15), Co1–P2 2.3094(14), Co1–P5 2.3123(14), C3–N3 1.153(7), P1–P2 2.1610(18), P2–P3 2.2014(17), P3–P4 2.1970(17), P4–P5 2.2003(17), P5–P1 2.1533(18), P3–C40 1.848(5), P4–C51 1.848(5), P1–P2–P3 109.61(7), P2–P3–P4 98.89(7), P3–P4–P5 100.96(6), P4–P5–P1 97.60(7), P5–P1–P2 94.50(7), P2 P3 C40 100.46(15), P4 P3 C40 103.82(15), P5 P4 C51 104.61(16), P3 P4 C51 113.03(18).

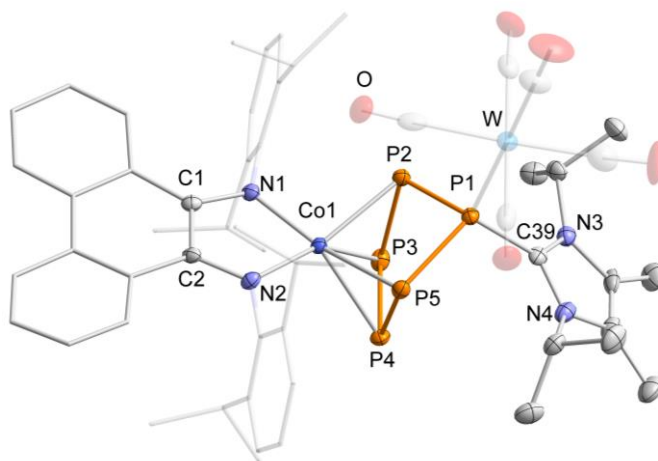


Figure S94. Solid-state molecular structure of $[(\text{PHDI})\text{Co}(\mu:\eta^4,\kappa^1\text{-P}_5\text{Lc})\{\text{W}(\text{CO})_5\}]$ (**5a-W(CO)₅**). Hydrogen atoms and solvent molecules are omitted for clarity. Thermal ellipsoids are drawn at the 50% probability level. Selected bond lengths [Å] and angles [°]: C1–C2 1.443(6), C1–N1 1.353(6), C2–N2 1.349(6), Co1–N1 1.898(4), Co1–N2 1.903(4), Co1–P2 2.3425(12), Co1–P3 2.3589(13), Co1–P4 2.3592(13), Co1–P5 2.3338(12), P1–P2 2.1874(15), P2–P3 2.1490(17), P3–P4 2.1294(17), P4–P5 2.1493(17), P5–P1 2.1815(15), P1–C39 1.860(4), C39–N3 1.339(6), C39–N4 1.348(6), C39 P1 P2 110.27(15), C39 P1 P5 108.81(15), P5 P1 P2 89.88(5), P1 P2 P3 102.64(6), P2 P3 P4 102.97(7), P3 P4 P5 102.74(7), P4 P5 P1 102.78(6).

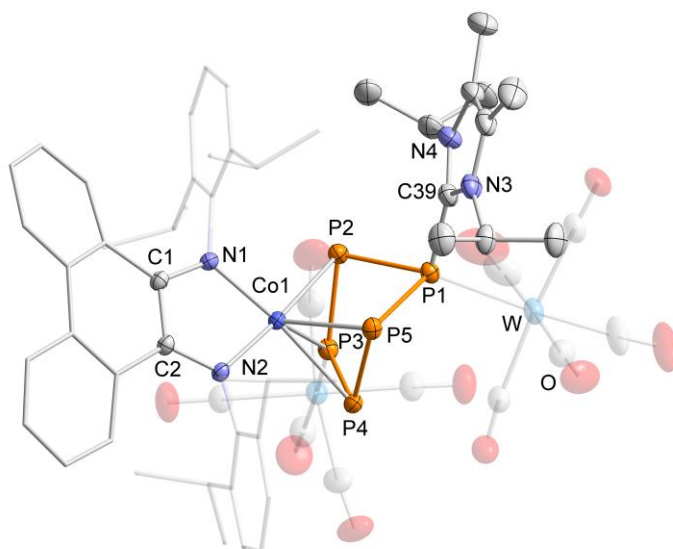


Figure S95. Solid-state molecular structure of $[(\text{PHDI})\text{Co}(\mu:\eta^4, \kappa^2\text{-P}_5\text{Lc})\{\text{W}(\text{CO})_5\}_2]$ (**5a**- $\{\text{W}(\text{CO})_5\}_2$). Hydrogen atoms and solvent molecules are omitted for clarity. Thermal ellipsoids are drawn at the 50% probability level. Selected bond lengths [Å] and angles [°]: C1–C2 1.434(3), C1–N1 1.359(3), C2–N2 1.344(3), Co1–N1 1.9080(18), Co1–N2 1.9153(18), Co1–P2 2.3286(6), Co1–P3 2.3460(6), Co1–P4 2.3834(6), Co1–P5 2.3031(7), P1–P2 2.2245(8), P2–P3 2.1186(8), P3–P4 2.1393(9), P4–P5 2.1395(9), P5–P1 2.2198(8), P1–C39 1.854(2), C39–N3 1.352(3), C39–N4 1.358(3), C39 P1 P2 103.05(8), C39 P1 P5 107.50(8), P5 P1 P2 85.34(3), P1 P2 P3 93.73(3), P2 P3 P4 103.17(3), P3 P4 P5 100.49(3), P4 P5 P1 93.96(3).

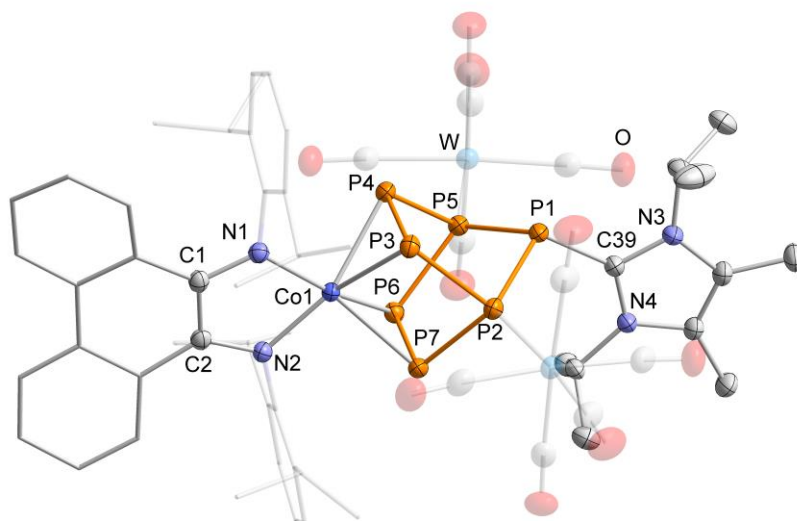


Figure S96. Solid-state molecular structure of $[(\text{PHDI})\text{Co}(\mu^3:\eta^4, \eta^1, \eta^1\text{-P}_7\text{Lc})\{\text{W}(\text{CO})_5\}_2]$ (**6a**- $\{\text{W}(\text{CO})_5\}_2$). Hydrogen atoms, solvent molecules and disorder in one of the *i*Pr groups are omitted for clarity. Thermal ellipsoids are drawn at the 50% probability level. Selected bond lengths [Å] and angles [°]: C1–C2 1.431(3), C1–N1 1.357(3), C2–N2 1.354(3), Co1–N1 1.9089(19), Co1–N2 1.9053(19), Co1–P3 2.3361(7), Co1–P4 2.3479(7), Co1–P6 2.3509(7), Co1–P7 2.3601(6), P1–P2 2.1827(8), P2–P7 2.1989(8), P7–P6 2.1277(8), P6–P5 2.2000(8), P5–P1 2.1869(8), P2–P3 2.1936(8), P3–P4 2.1636(8), P4–P5 2.2035(8), P1–C39 1.834(2), C39–N3 1.344(3), C39–N4 1.356(3), C39 P1 P2 108.83(8), C39 P1 P5 112.62(8), P5 P1 P2 96.38(3), P7 P2 P3 84.33(3), P1 P2 P7 114.52(3), P1 P2 P3 93.99(3), P2 P3 P4 104.72(3), P3 P4 P5 104.06(3), P6 P5 P1 114.12(3), P6 P5 P4 82.58(3), P4 P5 P1 94.46(3), P7 P6 P5 105.28(3), P2 P7 P6 104.45(3).

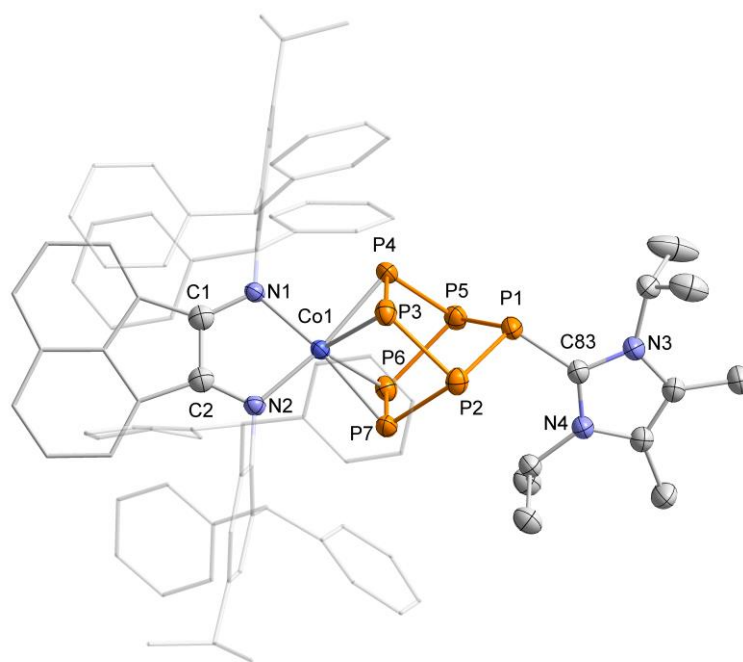


Figure S97. Solid-state molecular structure of $[(Ar^*BIAN)Co(\eta^2:\eta^2-P_7Lc)]$ (**6b**). Hydrogen atoms, solvent molecules and disorder in the Ar^*BIAN ligand are omitted for clarity. Thermal ellipsoids are drawn at the 50% probability level. Selected bond lengths [Å] and angles [°]: C1–C2 1.421(2), C1–N1 1.332(2), C2–N2 1.345(2), Co1–N1 1.9699(15), Co1–N2 1.9481(15), Co1–P3 2.3349(6), Co1–P4 2.3118(5), Co1–P6 2.3513(6), Co1–P7 2.3002(5), P1–P2 2.1789(7), P2–P7 2.2138(7), P7–P6 2.1396(7), P6–P5 2.2250(7), P5–P1 2.1758(7), P2–P3 2.2236(7), P3–P4 2.1627(7), P4–P5 2.1967(7), P1–C39 1.855(2), C39–N3 1.356(2), C39–N4 1.350(2), C39–P1–P2 109.47(7), C39–P1–P5 107.26(7), P5–P1–P2 103.21(3), P7–P2–P3 79.61(2), P1–P2–P7 108.83(3), P1–P2–P3 92.46(3), P2–P3–P4 104.49(3), P3–P4–P5 108.39(3), P6–P5–P1 110.36(3), P6–P5–P4 81.27(2), P4–P5–P1 90.90(3), P7–P6–P5 104.96(3), P2–P7–P6 108.38(3).

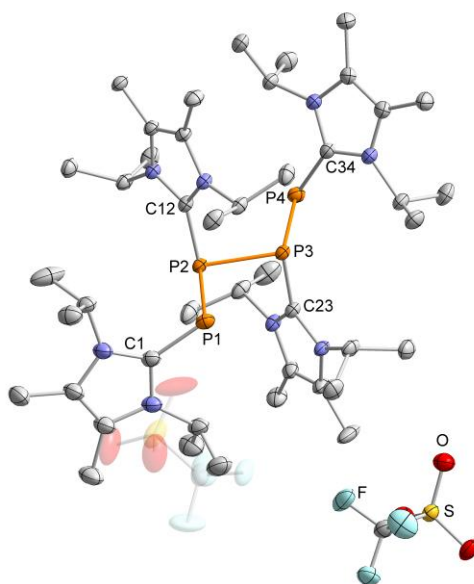


Figure S98. Solid-state molecular structure of $[(Lc)_4P_4][OTf]_2$ (**7[OTf]₂**). Hydrogen atoms and solvent molecules are omitted for clarity. Thermal ellipsoids are drawn at the 50% probability level. Selected bond lengths [Å]: P1–P2 2.1572(5), P2–P3 2.2588(5), P3–P4 2.1637(5), P1–C1 1.8311(18), P2–C12 1.8545(15), P3–C23 1.8405(15), P4–C34 1.8205(17).

7. References

- [1] C. M. Hoidn, T. M. Maier, K. Trabitsch, J. J. Weigand and R. Wolf, [3+2] Fragmentation of a Pentaphosphido Ligand by Cyanide, *Angew. Chem. Int. Ed.* 2019, **58**, 18931–18936.
- [2] S. Hauer, T. M. H. Downie, G. Balázs, K. Schwedtmann, J. J. Weigand and R. Wolf, Cobalt-Mediated [3+1] Fragmentation of White Phosphorus: Access to Acylcyanophosphanides, *Angew. Chem. Int. Ed.* 2024, **63**, e202317170.
- [3] C. G. P. Ziegler, T. M. Maier, S. Pelties, C. Taube, F. Hennersdorf, A. W. Ehlers, J. J. Weigand and R. Wolf, Construction of alkyl-substituted pentaphosphido ligands in the coordination sphere of cobalt, *Chem. Sci.* 2019, **10**, 1302–1308.
- [4] W. W. Brennessel, R. E. Jilek and J. E. Ellis, Bis(1,2,3,4- η^4 -anthracene)ferrate(1-): A Paramagnetic Homoleptic Polyarene Transition-Metal Anion, *Angew. Chem. Int. Ed.* 2007, **46**, 6132–6136.
- [5] W. W. Brennessel, V. G. Young Jr. and J. E. Ellis, Bis(1,2,3,4- η^4 -anthracene)cobaltate(1-), *Angew. Chem. Int. Ed.* 2002, **41**, 1211–1215.
- [6] P. Li, B. Lü, C. Fu and S. Ma, Zheda-Phos for General α -Monoarylation of Acetone with Aryl Chlorides, *Adv. Synth. Catal.* 2013, **355**, 1255–1259.
- [7] K. Schwedtmann, J. Haberstroh, S. Roediger, A. Bauzá, A. Frontera, F. Hennersdorf and J. J. Weigand, Formation of an imidazoliumyl-substituted [(L_C)₄P₄]⁴⁺ tetracation and transition metal mediated fragmentation and insertion reaction (L_C = NHC), *Chem. Sci.* 2019, **10**, 6868–6875.
- [8] P. H. M. Budzelaar, *IvorySoft: gNMR for Windows, NMR Simulation Program*, 2006.
- [9] S. Aime, M. Fild, E. M. McVicker and M. Fild, Multinuclear Magnetic Resonance Studies. Part 2. Diphosphanes and Dithioxodi- λ^5 -phosphanes, *J. Chem. Soc., Dalton Trans.* 1976, 2144–2153.
- [10] J. P. Albrand, H. Faucher, D. Gagnaire and J. B. Robert, Calculation of the ¹J(PP) Angular Dependence in P₂H₂, *Chem. Phys. Lett.* 1976, 521–523.
- [11] J. E. Del Bene, J. Elguero and I. Alkorta, Computed Spin-Spin Coupling Constants (¹J_{X-Y}) in Molecules H_mX-YH_n for X and Y ¹³C, ¹⁵N, and ³¹P: Comparisons with Experiment and Insights into the Signs of ¹J_{X-Y}, *J. Phys. Chem. A* 2004, **108**, 3662–3667.
- [12] E. G. Finer and R. K. Harris, N.M.R. spectra of the X_nAA'X_n' type, *Mol. Phys.* 1967, 65–75.
- [13] M. A. M. Forgeron, M. Gee and R. E. Wasylishen, A Theoretical Investigation of One-Bond Phosphorus-Phosphorus Indirect Nuclear Spin-Spin Coupling Tensors, ¹J(³¹P,³¹P), Using Density Functional Theory, *J. Phys. Chem. A* 2004, **108**, 4895–4908.
- [14] H. C. E. McFarlane, W. McFarlane and J. A. Nash, Phosphorus-Phosphorus Nuclear Spin Coupling in Tetraorganobiphosphines and Some of Their Derivatives, *J. Chem. Soc., Dalton Trans.* 1980, 240–244.
- [15] S. Pelties, T. Maier, D. Herrmann, B. de Bruin, C. Rebreyend, S. Gärtner, I. G. Shenderovich and R. Wolf, Selective P₄ Activation by a Highly Reduced Cobaltate: Synthesis of Dicobalt Tetraphosphido Complexes, *Chem. Eur. J.* 2017, **23**, 6094–6102.
- [16] M. Baudler, J. Hellmann and J. Hahn, 1,2-Dichlor-1,2-di-*tert*-butyldiphosphan, *Z. Anorg. Allg. Chem.* 1982, **489**, 11–15.
- [17] M. Baudler, Polyphosphorus Compounds—New Results and Perspectives, *Angew. Chem. Int. Ed.* 1987, **26**, 419–441.
- [18] K.-O. Feldmann and J. J. Weigand, One-Pot Syntheses of Cationic Polyphosphorus Frameworks with Two-, Three-, and Four-Coordinate Phosphorus Atoms by One-Pot Multiple P-P Bond Formations from a P₁ Source, *J. Am. Chem. Soc.* 2012, **134**, 15443–15456.
- [19] M. Cicač-Hudi, C. M. Feil, N. Birchall, M. Nieger and D. Gudat, A PH-functionalized dicationic bis(imidazolio) diphosphine, *Dalton Trans.* 2022, **51**, 998–1007.
- [20] SCALE3ABS, CrysAlisPro, Agilent Technologies Inc., Oxford, GB, 2012.
- [21] G. M. Sheldrick, SADABS, Bruker AXS, Madison, USA, 2007.
- [22] R. C. Clark and J. S. Reid, The Analytical Calculation of Absorption in Multifaceted Crystals, *Acta Cryst. A* 1995, **51**, 887–897.
- [23] O. V. Dolomanov, L. J. Bourhis, R. J. Gildea, J. A. K. Howard and H. Puschmann, OLEX2: a complete structure solution, refinement and analysis program, *J Appl Crystallogr* 2009, **42**, 339–341.

- [24] G. M. Sheldrick, SHELXT – Integrated space-group and crystal structure determination, *Acta Cryst. A* 2015, **A71**, 3–8.
- [25] G. M. Sheldrick, Crystal structure refinement with SHELXL, *Acta Cryst. C* 2015, **C71**, 3–8.